T12 Electromagnetic Ballast Modeling And Retrofit LED Tube Driver Design

A Dissertation Presented

By

Yiwen Chen

Student ID: 4310721

In Partial Fulfillment of the Requirements for the Degree of

Master of Science

In

Electrical Engineering (Microelectronics Track)

Electrical Engineering, Mathematics and Computer Science Faculty

Delft University of Technology

Delft, the Netherlands

6th, July 2015

Preface

The thesis of Yiwen Chen was approved by the following:

Responsible professor: Prof. G. Q. Zhang

Daily supervisor: Dr. Haimin Tao

MSc thesis committee members:

Prof. G. Q. Zhang	ECTM laboratory, EEMCS, TU delft
Dr. Haimin Tao	Philips Lighting
Dr. Jelena Popvic	DCE&S, EEMCS, TU delft

Electronic Components, Technology and Material Laboratory

Faculty of electrical Engineering, Mathematics and Computer Science

Delft University of Technology

LED Platform Development, Philips Lighting B.V.

An electronic version of this dissertation available at:
http://repository.tudelft.nl/

Abstract

LED lamps have become increasingly popular in the market thanks to high energy efficiency. Tubular LED lamps are widely adopted to replace conventional linear fluorescent lamps, like T8 and T12. Compared with rewiring of fixtures (remove or bypass the ballast) retrofit LED Tubes (TLED), which can be directly powered by the existing ballast, are preferred by installers. Today, T12 fluorescent tubes are still widely used in the US. A T12 electromagnetic (EM) ballast compatible retrofit TLED has great energy saving potential and commercial value. This work proposes a T12 EM ballast model and a compatible TLED driver.

In this project, T12 EM ballast structure and classification were introduced. For compatible driver design, firstly a T12 EM ballast model was built in LTspice and its corresponding modeling approach was developed and verified. Different ballast measurement results were included in this report. The proposed TLED driver uses a buck-boost topology and self-oscillation control to achieve constant output power. By using emitter switch and proportional drive techniques, the proposed driver is compatible with various T12 EM ballasts, including single-lamp, dual-lamp and three-lamp ballasts. Experimental results from the prototypes demonstrated driver compatibility with the ballasts. The driver has a power efficiency above 85%. System measurements shown that power consumption of the retrofit TLED lighting fixture is 55% lower than its fluorescence counterpart.

Key words: Ballast; Retrofit; LED Tube; Fluorescent lamp.

Acknowledgment

During my master program in Delft University of Technology, a lot of people helped me. Without their support, I cannot complete my master study on time.

To start, I would like to express my gratitude to Prof. G. Q. Zhang for offering me this precious thesis project opportunity and for his guidance during the project. His helpful advices guided my steps and kept me motivated.

My second word of thanks goes to my daily supervisor Dr. Haimin Tao and Dr. Yi Wang. As my supervisors and colleagues in Philips, their rigorous attitude of scholarship and hard work left me with a very deep impression. They not only brought me ideas for solving problems in thesis project but also guided me in research method establishing. Although they are busy with their own work, they never hesitant to share their time and opinion with me whenever I asked for help. Their supervision on this project is effective and cannot be replaced.

Furthermore, I am grateful to my colleagues in Philips. Frits de Jongh always led a helping hand to me whenever my project languished. Dijk Christiaan van is a genius engineer, and he gave me a lot brilliant ideas to solve project problems. I would also like to thank our group leader Dik Pardijs for giving me this internship position in Philips Lighting.

A great thanks also goes to my classmates and friends in TU delft. With their company and help, I can finish my master program study and enjoy my two years life in the Netherlands. I cannot forget those days we spent together in library for tough projects and moments of watching world cup together. In additional, I am also thankful to my old friends from group “unity is strength”: Shihua, Yejun and Shanpei. Although we widely dispersed around the world, your encouragement and support keep me energetic and brave to overcome any difficulty. Wish the friendship and memories never fade away.

Finally, I would like to pay tribute to my parents and girlfriend for their support not only financial but also spiritual in these two years. Words cannot describe how much I appreciate them.

Contents

1. Introduction

1.1 Background of fluorescent tube lamp

Fluorescent tube lamps are widely used in various places, such as office buildings, classrooms and stores. A typical florescent tube lamp is shown in Fig1.1. Low pressure inert gases (argon or mixture of inert gas) and mercury vapor are filled in the glass tube, while phosphor powder are coated on the inner wall of the glass tube. At each end of lamp, heating filament, as an electrode, can be heated to emit electrons. Fluorescent lamp glows by using electrons to excite mercury vapor. Electrons are released at heated filament and moved to another side by the electric field. Collision between ionized electron and mercury atom excites electron of mercury atom jump to higher energy band. Then the excited electron generates ultraviolet (UV) light through falling back to lower energy band, meanwhile the phosphor coated on the tube absorb the UV light and convert it to visible light. Because of this luminous discharge mechanism, fluorescent lamp has a special characteristic - negative dynamic resistance. When the current flow through the lamp increase, the resistance of fluorescent lamp will decrease. As a result of positive feedback, the fluorescent lamp will be destroyed by continuously increasing current when connect it to a voltage source directly. For solving this problem, ballast was employed to regulate the current flow through fluorescent lamp.

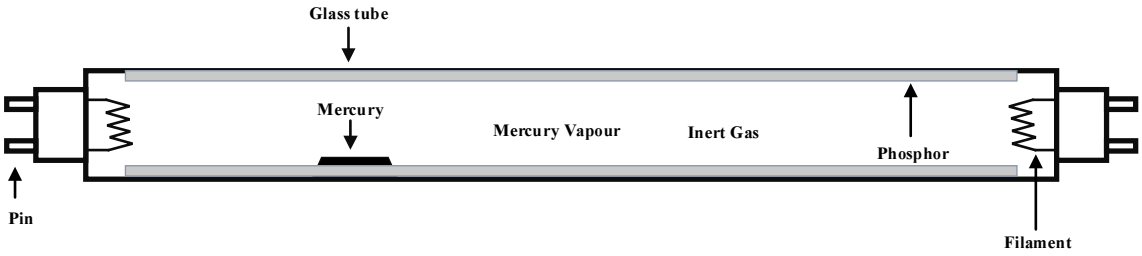

Fig1.1 Florescent lamp

1.2 Introduction to electromagnetic ballast

As previously mentioned, ballast is an essential component installed in fluorescent lighting fixture for regulating the current. Electronic and electromagnetic (EM) ballasts are two main types of fluorescent lamp ballast. Their basic configurations are illustrated in Fig1.2 [1]. Electromagnetic ballasts are basically transformers made by steel core and wire (copper or aluminum). The wire is coiled around the steel core which is made up of stacked steel laminations [2]. Electromagnetic ballast transforms mains voltage to the fluorescent lamp voltage and its leakage inductance, which works as an inductor, regulate the current flow through fluorescent lamp. Electronic ballast is realized by solid state circuitry and often based on switch mode power supply topology. Input power can be rectified and chopped by electronic ballast at high frequency, then supplied to fluorescent lamp on proper starting and operating electrical conditions [3]. Traditionally, electromagnetic ballast has a simple structure which makes it reliable, robust and cheap. Promoted as replacements for electromagnetic ballasts for the last decades, electronic ballasts have higher energy efficiency and more expensive price. Comparison

between electromagnetic ballast and electronic ballast is shown in Tab1.1 [4] [5].

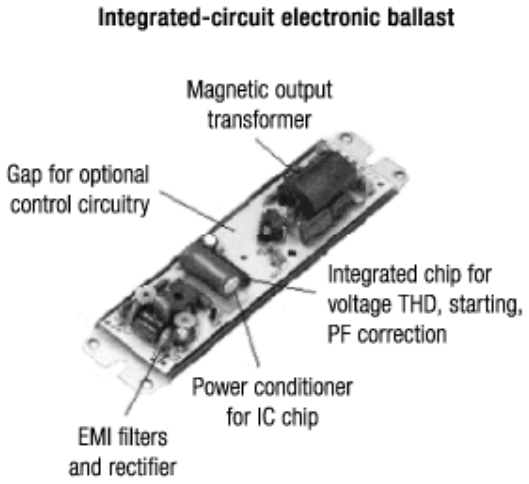

Fig1.2a configuration of electronic ballast [1]

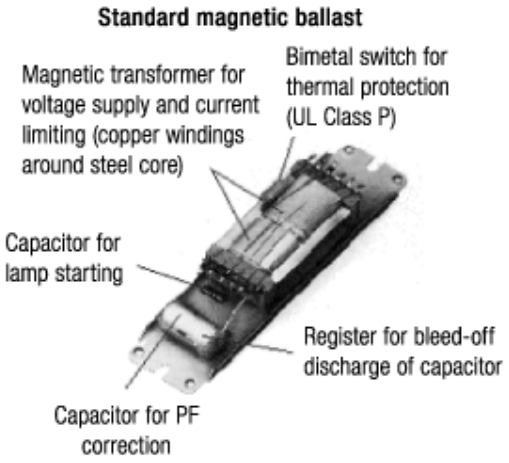

Fig1.2b configuration of electromagnetic ballast [1]

	Electromagnetic ballast	**Electronic ballast**
Cost	Low cost	Relatively expensive
Lifetime	Long lifetime (> 30years at 105˚C)	Short lifetime (typically one to five years)
Dimmability	Not dimmable (in the past)	Dimmable
Operating weather condition	Suitable for extreme weather conditions such as high humidity, wide temperature variation, and lightning	Relatively poor immunity against extreme weather conditions such as high humidity, wide temperature variation, and lighting
Environment friendly	Environment friendly (magnetic chokes are recyclable)	Not environment friendly (toxic and/or nonbiodegradable electronic waste that is not recyclable)
Self-recovery	Self-recovery feature (when the ac mains voltage recovers after a disturbance)	No self-recovery feature
Maintenance cost	Very low maintenance costs	High maintenance and repair costs
Energy efficiency	Not energy saving (in the past)	Energy saving (up to 13%)
Flickering	Flickering effect	No flickering effect
Noise	Acoustic resonance phenomenon	Low audible noise
Size and weigh	Large size and heavy weigh	Relatively small size and light weigh
History	Proven record of over 50 years	Proven record of more than one decade

Tab1.1 Comparison between electromagnetic ballast and electronic ballast [4] [5]

According to ballast starting mode, ballasts can be classified into four types [3] [6],

Instant start: Without preheating the electrodes, ballast provides a sufficiently high starting voltage to initiate the discharge arc, so it has the shortest start delay time (less than 0.1s). As a result of elimination of electrode heating, this type ballast can typically save 2 watts per lamp compared to

rapid start ballast. It is best suited for applications with long duty cycles because of its fewest lamp-start cycles (typically 10000-15000).

Rapid start: Rapid start ballast's delay time is longer than instant start ballast (about 0.5-1s). It heats the lamp electrodes and applies voltage simultaneously. Because of heated electrodes, applied voltage produced by rapid start ballast can be little lower than the instant start ballast. Electrode heating continue to consume energy as the lamp operates (typically 2 watts per lamp) result in this type ballast more energy consumption. Lamp-start cycles of this type ballast increases to 15000-20000 compare to instant ballast.

Programmed start: Programmed start ballast applies voltage on lamp after precisely preheating the electrodes. By using this method, it maximizes lamp life time (up to 50000 or more lamp-start cycles) while has a longer start delay time (about 1-1.5s). So programmed start ballast is preferred for application with very frequent power cycling and electronic dimming systems to provide proper starting of dimmed mode lamps.

Hybrid: Hybrid ballast consists of an electronic switch for the electrode heating circuit, a magnetic core and coil transformer. Similar to magnetic ballast, it operates at line power frequency. After starting the lamp, electrode heating circuit can be disconnected by electronic switch. So this type ballast is also called "cathode-disconnect ballast".

1.3 Principles and advantages of Light-Emitting Diode (LED)

Essentially, light-Emitting diode (LED) is a P-N junction, which consists of two types semiconducting material doped with different impurities respectively. A semiconducting material doped with acceptor impurity atoms (group III or group II elements) have fewer valence electrons, so it is called P-type semiconductor (positive charge of the hole). Oppositely, N- type semiconductor (negative charge of the electron) have more valence electrons due to doping with donor impurity atoms (group V or group VI elements). The holes in P-type semiconductor and the electrons in N-type semiconductor are called majority carriers. Without forward voltage applied, majority carriers cannot pass through the junction region because of potential barrier. When forward bias voltage is applied on the P-N junction, the potential barrier is lowered and depletion zone become thin enough for carriers pass through it. Then current will flow from P-type to N-type semiconductor and electrons will recombine with holes. Their recombination process will produce photons because electrons fall into a lower energy level and release energy in the form of photon as shown in Fig1.3. In this way, the P-N junction emits light. [7] [8] [9]

For indirect bandgap materials (like Si or Ge), combination between holes and electrons is non-radiative transition. So only direct bandgap materials (like GaAs) can be used in high brightness LEDs [7] [9]. An LED is intrinsically monochromatic and its color depends on the band gap energy (E_g) of semiconductor material, which is the difference between conduction band energy (E_c) and valence band energy (E_v). For a photon emitted by a recombination process between an electron located on the minimum of the conduction band and a hole located at the maximum of the valence band, its frequency and wavelength is determined by the band gap energy:

$$hv = E_g = E_c - E_v \qquad [1.1]$$

, where v is frequency of photon and h is Plank constant.

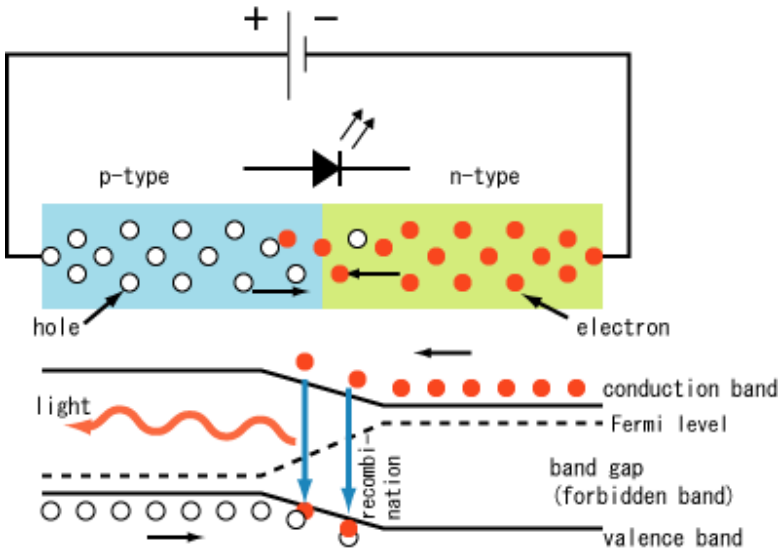

Fig1.3 Forward biased light-emitting diode and its band diagram [7]

	Incandescent GLS	**Incadescent TH**	**Fluorescent T12**	**Fluorescent T8**	**LEDs**
Output range (lm)	5-12000	40-50000	1000-10500	650-6200	20-220
Power range (W)	1-1000	4-2000	25-140	13-70	1-5
Efficiency (lm/W)	8-14	15-25	50-80	50-96	30-230
Control gear	No	No	Yes	Yes	Yes
Color temp (K)	2500-2700	2700-3200	3000-6500	2700-17000	2685-6500
Color rendering (Ra)	100	100	50-90	50-98	40-85
Run-up time	Instant	Instant	30sec	30sec	Instant
Dimming	Easy to 0%	Easy to 0%	Limited to 25%	Easy to 2%	Easy to 0%
Life (h)	1000	1500-5000	8000-12000	8000-17000	15000-60000

Tab1.2 characteristics comparison [11]

By using multiple LEDs and controlling their output power respectively, it is possible that LED lamp produce light in variety of colors. As for producing white light, the dominated method is using a blue or ultraviolet LED to generate a short wavelength and covered phosphor which absorbs part of short wavelength photons to convert them into a long wavelength photons. For example, using a blue diode (InGaN) combined with a yellow phosphor (YAG-Ce) can generate high power white light. The other methods are by using multiple diodes to produce complementary wavelength photons which arriving human eyes simultaneously cause a white light sensation, such as assembling three fundamental color (red, blue and green) LEDs together. [9]

Due to this luminous mechanism, LED lamps have many advantages and promising future in solid lighting market. A characteristics comparison among Incandescent lamps, fluorescent lamps and LED lamps is list in Tab1.2. [11] Compared with traditional light sources, LED lamps generally have benefits

in lifetime, energy efficiency, run-up time and dimmability. Life time of LED lamp is dozens times longer than incandescent lamp and several times longer than fluorescent lamp. As a result, low maintenance cost of LED lamp can counteract its initial high cost in long-term use. High energy efficiency make LED lamp be environment friendly and show potential in replacing conventional lamps for reducing energy consumption and carbon emission. Besides, as for the run-up time, which means the time a lamp takes to reach 80% of its full light output, performance of LED lamps is much better than fluorescent lamp.

1.4 Retrofit Tube LED (TLED) lamp

Due to those advantages mentioned previously, LED lamps are widely used to replace conventional lamps, such as screw-in incandescent bulbs, halogen lamps and fluorescent tube lamps. To make these retrofit LED lamps be compatible with conventional lighting fixture, they have standard light shapes (like bulb or tube) and driver circuitries which rectify the supply power and make LED lamps be compatible with former stage. [10]

The T12 fluorescent tubes are still widely used in the US. A vast majority of the T12 lamps runs off a rapid start electromagnetic ballast. For replacing existing traditional fluorescent lamp, there are two solutions. The first one is rewiring of fixtures (remove or bypass the ballast). Most of existing retrofit TLED lamp in market belong to this one. This solution is not so convenient for customers, however, they have to hire an electrician to rewire the lighting fixture. Another solution is using retrofit TLED lamp which is compatible with the ballast and work with existing lighting fixture directly. In this way, customers can simply remove the old fluorescent tube lamp and install the new TLED. Advantage of this solution is saving replacement cost and time. While the power efficiency of lighting fixture may be lowered because of the power loss in the ballast. Additionally, it is technically challenging to design a TLED driver compatible with various ballast, including electronic ballast and electromagnetic ballast. As for EM ballast compatible TLED driver design, the first challenge is to determine operating points of different types of EM ballasts, such as single-lamp, multi-lamp, compensated and uncompensated ballasts. The second challenge is to design a TLED driver and guarantee retrofit TLED compatible with various application circuitries. Supplied by different EM ballasts, driver should be able to output same power to LEDs. Meanwhile system performance parameters like efficiency and power factor must be maintained to comply with standards while not compromising safety and reliability of the ballast.

1.5 Project objective and research procedure

This master project is a part of Philips T12 retrofit TLED project. Its main objective is designing a T12 EM ballast compatible TLED driver to replace traditional fluorescence lamp for energy saving. To reach the goal, it is essential first to study T12 EM ballast operating principle and input-output characteristics. So this project is divided into two parts: ballast modeling and driver design. The work stream of these two parts are as follows.

Ballast modeling part:

1. Study T12 EM ballast operating principle and classification;

2. Develop a modeling approach for T12 EM ballast;

3. Build T12 EM ballast model in LTspice for simulation and verification;

4. Measure different ballasts input-output characteristics.

T12 retrofit TLED driver design part:

1. Determine proper ballast operating points based on product specifications;

2. Select DC-DC converter topology;

3. Design DC-DC converter switch control circuit;

4. Driver simulation and optimization;

5. Driver Prototype test.

1.6 Thesis report outline

This thesis report consists of 5 chapters.

Chapter 1 reviews backgrounds of fluorescence lamp, EM ballast and LED. Concept of retrofit TLED lamp is also mentioned in this chapter.

Chapter 2 introduces T12 EM ballast modeling and measurement. Fundamental magnetic laws are reviewed in this chapter. Hysteresis characteristic and magnetic circuit model are explained. Based on T12 EM ballast physical structure, a magnetic circuit model can be built and its corresponding equivalent circuit is simulated in LTspice. According to comparison, this T12 EM ballast model and modeling approach are verified. Various T12 EM ballasts input and output characteristics are measured and illustrated in this chapter.

Chapter 3 presents the procedure of T12 EM ballast compatible driver design. Different ballasts operating points are determined firstly. Then DC-DC converter topology is selected based on product specification. Problems and solutions in driver design are explained. Driver circuit model and simulation results in LTspice are shown at the end of this chapter.

Chapter 4 contains measurement result of the driver prototype. Each functional module and whole driver circuit test results are illustrated in this chapter. System performance and a comparison with traditional fluorescence lamp system performance are described.

Chapter 5 is the conclusion of this thesis project work. Achievements in this master project are summarized and presented.

2. Ballast modeling and measurement

The goal of this project is to develop a retrofit TLED and make it be compatible with T12 EM rapid start ballasts, which are widely used in the US market. For the sake of compatibility, it is essential to study principles and characteristics of T12 EM rapid start ballast.

In this chapter, types and structures of T12 EM rapid start ballasts will be introduced and discussed. R140-1-TP T12 EM ballast model will be built in LTspice, and its simulation results will be compared with measurement results. Various T12 EM ballasts input and output characteristics also will be measured and illustrated in this chapter.

2.1 T12 EM ballast structure

Previous chapter has discussed the classification of ballast. Majority of the T12 EM ballast in US market belong to rapid start type ballasts. A simplified configuration of rapid start EM ballast with fluorescent tube lamp is shown in Fig2.1.

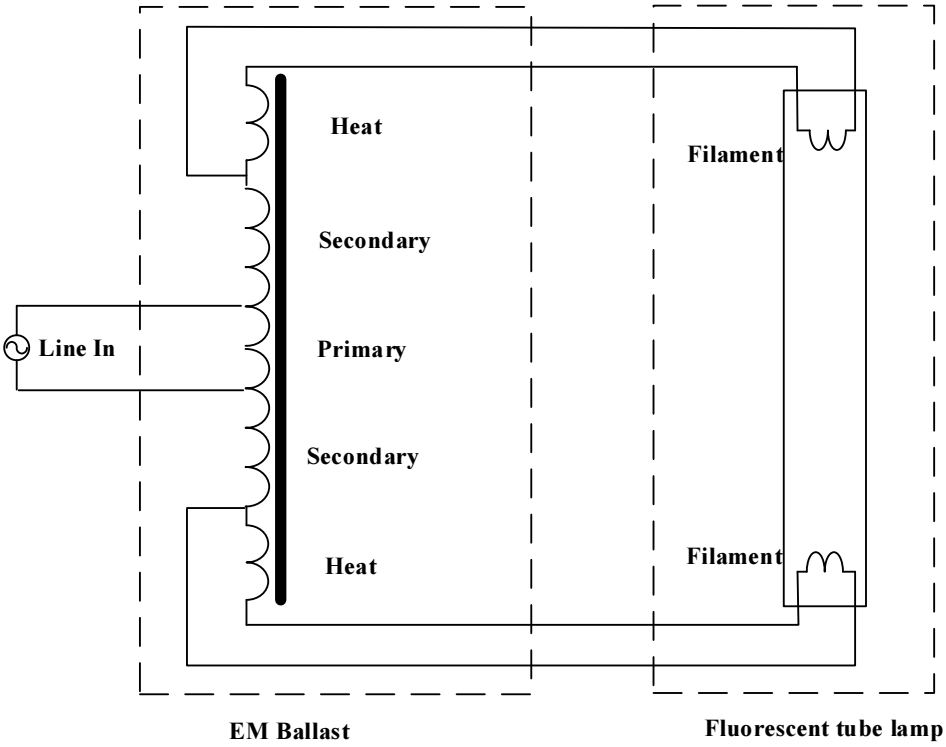

Fig2.1 Simplified rapid start EM ballast with fluorescent tube lamp

The US T12 EM ballast can be treated as a transformer and its leakage inductance acts as an inductor to regulate the lamp current. It has one common magnetic core, which is constructed by stacked carbide steel dies, with several windings. Annealed wires are coiled around the magnetic core to form windings. These windings can share one coil or use isolated coils separately. The primary winding is connected to power supply and magnetizes the core. According to the law of electromagnetic induction, induction electromotive force is produced in the secondary winding as a result of the current flowing in the primary winding. Meanwhile, a small voltage (approximately 3.5V) produced by heating winding is applied to the filament of the fluorescent tube lamp for heating and rapid start. The

primary winding is not perfectly coupled with the secondary winding, so its leakage inductance can work as an inductor to regulate lamp current.

Based on lighting fixture, T12 EM rapid start ballasts can be divided into several categories. Classified by number of lamps, ballasts have three types: single-lamp, dual-lamp and three-lamp; according to power factor, there are two types: compensated and uncompensated ballast. Fig2.1 shows the configuration of uncompensated rapid start single lamp ballast. Compensated rapid start dual lamp ballast is shown in Fig2.2 below. Compared with single lamp ballast, dual-lamp ballast has one more heating winding for connecting lamps in series and heating filaments. Similarly, three-lamp ballast has two more auxiliary heating windings to connect three lamps in series. In compensated ballast, as shown in Fig2.2, a capacitor is used to correct ballast input power factor. This compensation capacitor corrects the lagging current caused by ballast leakage inductance. As a result, total power factor is close to unity. While an uncompensated ballast, as shown in Fig2.1, doesn't have this compensation capacitor, which leads to lower power factor.

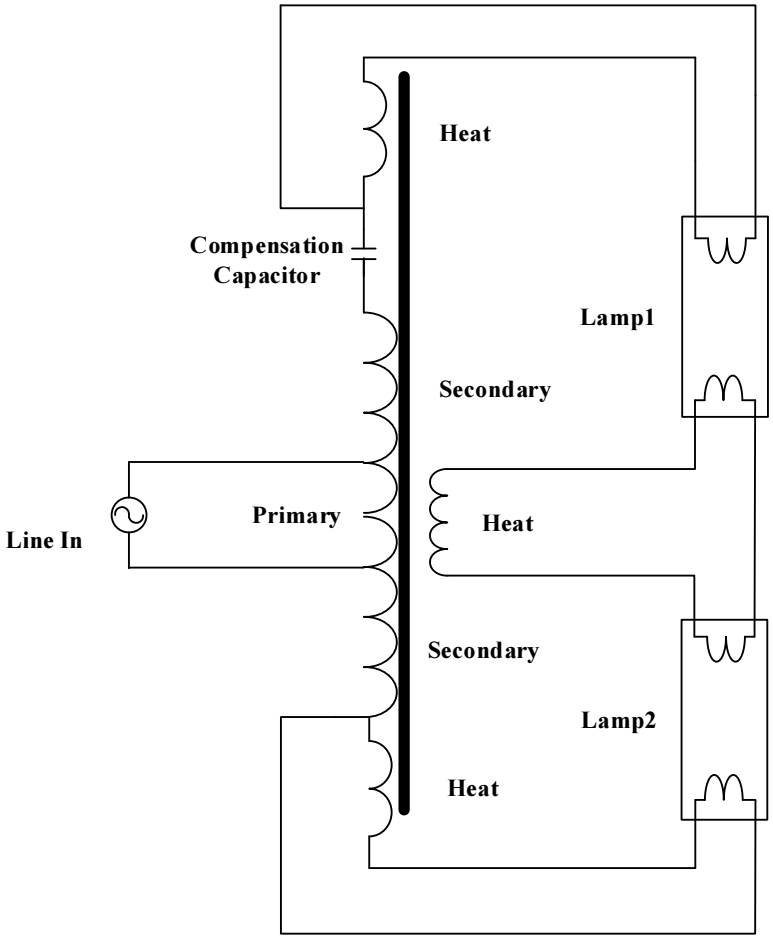

Fig2.2 Compensated rapid start dual lamp ballast with two lamps

In this project, modeling of R-140-1-TP ballast, which is a typical single-lamp ballast with compensation capacitor as shown in Fig2.3, is illustrated in following section. This modeling helps us to understand working principle of the T12 EM ballast and to find out TLED driver operating points.

Fig2.3 R-140-1-TP T12 EM ballast

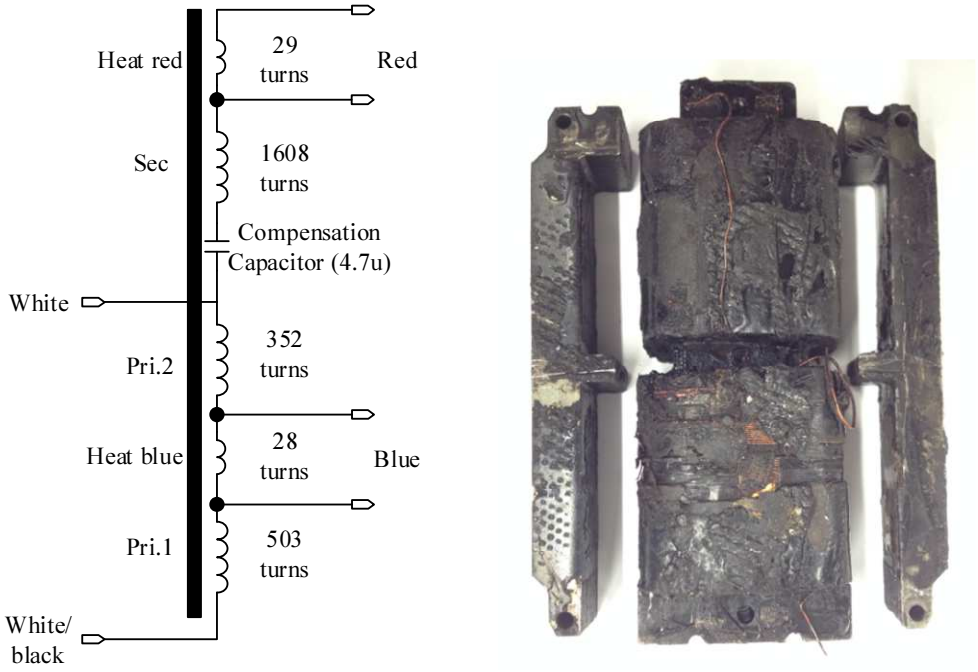

Fig2.4 Circuit configuration and magnetic core picture of R-140-1-TP T12 EM ballast

Circuit configuration of R-140-1-TP EM ballast is shown in Fig2.4. It has six wires: the white wire and white/black wire are for input voltage and connected to primary winding; two red wires and other two blue wires are separately connected to each filament of the fluorescent tube lamp. A compensation capacitor (4.7uF) is added in series with the primary winding and the secondary winding. Input mains voltage (120V, 60Hz) is applied on the lower winding, which has three segments: primary winding 1 (503turns), primary winding 2 (352turns) and blue heating winding (28turns). Two heating windings, 29 turns for rea and 28 turns for blue respectively, generate a low voltage (approximately 3.5V) to heat up filament for rapid start up. Between those two heating windings, induced voltage on the turns (1608+352 turns) is the output voltage and applied on the fluorescent tube lamp. This ballast can be seen as an autotransformer, as its input and output share the turns of primary winding 2.

2.2 Ballast Modeling

In this section, fundamental electromagnetic laws, hysteresis characteristic of magnetic core and magnetic circuit model are reviewed firstly. Then a magnetic circuit model of T12 EM ballast is derived from its physical model. Based on this magnetic circuit model, a T12 ballast model can be built in LTspice with a hysteretic core model for simulation. [12] [13] [14]

2.2.1 Fundamental electromagnetic laws review

Faraday's law, Lenz' law, Ampere's law and Gauss' law are four fundamental laws which are primarily used in magnetic analysis. Any magnetic structure is governed and described by these three laws. For building a magnetic structure model, such as T12 EM ballast model, magnetic circuit model is a good choice to simplify these general laws and to make analysis simpler.

Faraday's law describes relationship between voltage induced in a conductor and magnetic flux. For uniform flux distribution, it is given by

$$v(t) = N \cdot \frac{d\Phi}{dt} = N \cdot A_c \cdot \frac{d\vec{B}}{dt} \qquad [2.1]$$

, where N is number of conductor turns, A_c is interior surface area of enclosed conductor, $\vec{B}$ is magnetic flux density, and magnetic flux Φ is equal to magnetic flux multiply by interior surface area. This formula indicates that occurrence of conductor voltage is related to changing magnetic flux in the inductor and this voltage is proportional to the number of inductor turns and rate of change of the magnetic flux passing through the inductor. As shown in Fig2.5 and Fig2.6, changing magnetic flux $\vec{B}$ generates electric field $\vec{E}$ in a plane perpendicular to the direction of the magnetic flux, then electrons in this coil are moved by this electric field to one end of the coil. As a result, potential difference is induced in ends of the coil.

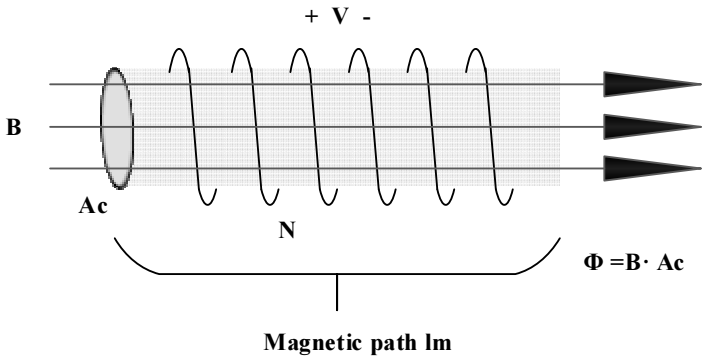

Fig2.5 Magnetic flux and induced voltage in Faraday's law

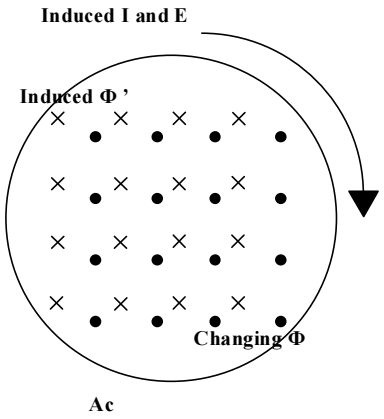

Fig2.6 Induce current and electric field direction in Lenz's law

Lenz's law states that voltage $v(t)$ generated by changing flux tends to drive a current in the direction which can counteract the flux change, as shown in Fig2.6. The changing Φ generates electronic field and current flow around the closed loop. This current induces an opposite direction magnetic flux Φ' to counteract the flux change.

Ampere's law gives the relationship between current and magnetic field intensity. It is given by

$$\oint_l \vec{H} d\vec{l} = I \qquad [2.2]$$

, where $\vec{H}$ is the magnetic field intensity, $d\vec{l}$ is an increment of closed path and I is the total current passing through the interior of the path. According to ampere's law, the magneto motive force (MMF), which is the line integral of the magnetic field intensity $\vec{H}$ around a closed path, is equal to the total current passing through the interior of the path. As shown in Fig2.7, a current I flow through a closed circle. For uniform magnetic field, the line integral of $\vec{H}$ around this circle is

$$2\pi \mathrm{r} \cdot \mathrm{H} = \mathrm{I} \qquad [2.3]$$

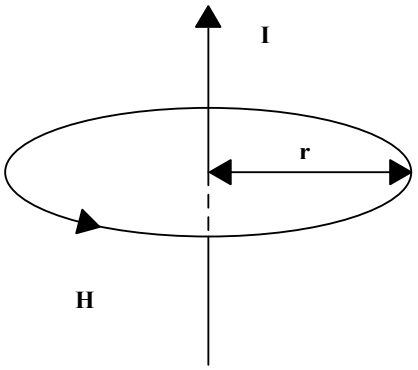

Fig2.7 Relationship between H and I in Ampere's law

, while the direction of $\vec{H}$ and I obey the right-hand rule.

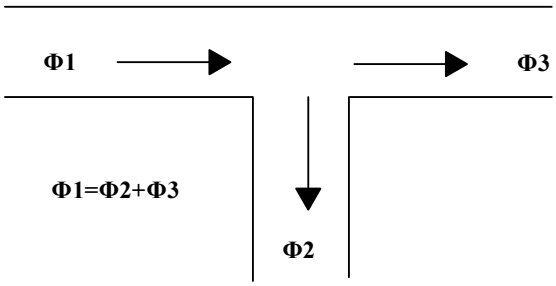

Fig2.8 Magnetic flux entering and leaving a node stated in Gauss' law

Gauss's law for the magnetic fields states that the magnetic flux passing through any three-dimensional body with surface S_G is zero. It is given by

$$\oint_{S_G} \vec{B} d\vec{s} = 0 \qquad [2.4]$$

In another words, the total flux entering a node is equal to the magnetic flux leaving this node. As shown in Fig2.8, the magnetic flux entering the node Φ_1 can be expressed by the equation below,

$$\Phi_1 = \Phi_2 + \Phi_3 \qquad [2.5]$$

, where Φ_2 and Φ_3 are the magnetic flux leaving the node. [12] [13]

2.2.2 Hysteresis characteristic of magnetic core

In free space, the magnetic field intensity $\vec{H}$ and magnetic flux density $\vec{B}$ are proportional to each other, and their relationship is given by

$$\vec{B} = \mu_0 \cdot \vec{H} \qquad [2.6]$$

, where μ_0 is the permeability of free space and equal to $4\pi \cdot 10^{-7} H/m$. The B-H characteristics curve in free space is shown in Fig2.9, and the slope of this cure is the permeability of free space.

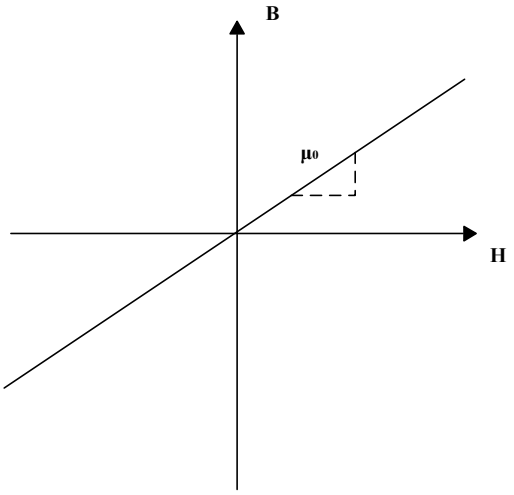

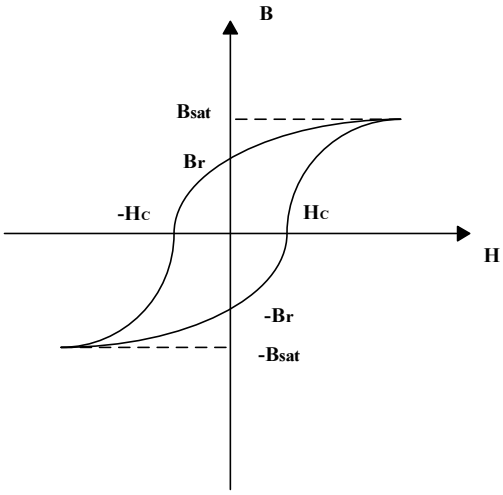

Fig2.9 B-H characteristics in free space Fig2.10 Magnetic hysteresis loop of a ferromagnetic material

When magnetic field is applied to a magnetic material, the magnetic flux density is determined by the relative permeability μ_r of this material. Typical value of μ_r lie in the range 10^3 to 10^5.

$$\vec{B} = \mu \cdot \vec{H} = \mu_r \mu_0 \cdot \vec{H} \qquad [2.7]$$

Because μ_r is not a constant value, $\vec{B}$ is a nonlinear function of $\vec{H}$ and will be saturate at B_{sat}. When $\vec{B}$ has reached the saturation point B_{sat}, increasing magnetic field intensity will increase the magnetization of the material as in free space, and the μ_r decrease to 1. This phenomenon can be explained by the concept of magnetic domains. Magnetic materials are composed of magnetic domains which can be magnetized in different directions. External applied magnetic field forces these magnetic domains align with the field. Before saturation, larger magnetic field intensity $\vec{H}$ results in more domains aligned and larger flux density $\vec{B}$. So the flux density nonlinearly increase with magnetic field intensity. When all the magnetic domains have been aligned, further increase magnetic field intensity can't align more domains. Then slope of B-H curve decrease to μ_0.

Besides saturation, magnetic hysteresis is another characteristic of magnetic material which results in nonlinear B-H curve. As mentioned, magnetic domains are aligned by external magnetic field. This process is not simultaneous with the magnetizing field but lags behind. When the imposed magnetizing field is reduced or removed, part of these domains will still keep their direction and demagnetization of these domains is also not simultaneous with the decreasing magnetic field. No matter magnetic field intensity $\vec{H}$ increase or decrease, flux density $\vec{B}$ always lag behind its change.

If a sinusoidal steady-state excitation applied on a magnetic core material, its B-H curve is as shown in Fig2.10. Magnetic flux density $\vec{B}$ nonlinearly increase with magnetic field intensity $\vec{H}$ to saturation point B_{sat}, then it is saturated. When driving magnetic field drops to zero, part of magnetic domains still retain magnetization, and the remnant flux density is B_r. After $\vec{H}$ decrease to a negative value, which means the magnetic field in the opposite direction, magnetic material will gradually demagnetize. At the point where $\vec{B}$ drops to zero, $\vec{H}$ has a negative value and this value is called coercive force H_c. Similarly, the opposite direction $\vec{H}$ also results in $\vec{B}$ saturation at the point $-B_{sat}$. Vice versa, $\vec{H}$ increases from negative value to positive value has similar hysteresis process. That's why the B-H curve shown in Fig2.10 is a hysteresis loop.

For simulating this hysteresis, a hysteretic core model is employed to simulate the hysteresis loop in LTspice simulation. In this proposed hysteretic core model, the major hysteresis loop is composed of two branches: increasing field $\vec{H}$ curve is described by a lower branch and another upper branch is account for the decreasing field $\vec{H}$ curve. This model defines the hysteresis loop with only three parameters: coercive force H_c, remnant flux density B_r and saturation flux density B_{sat}. The upper and lower branches are given by [14]

$$\text{Upper:} \quad B_u(H) = B_{sat} \cdot \frac{H+H_c}{|H+H_c|+H_c\cdot\left(\frac{B_{sat}}{B_r}-1\right)} + \mu_0 \cdot H \qquad [2.8a]$$

$$\text{Lower:} \quad B_l(H) = B_{sat} \cdot \frac{H-H_c}{|H-H_c|+H_c\cdot\left(\frac{B_{sat}}{B_r}-1\right)} + \mu_0 \cdot H \qquad [2.8b]$$

These two branches are inversely symmetric through zero point and can be given by

$$B_u(H) = -B_l(-H) \qquad [2.9]$$

If the B-H curve starts from zero point of the B-H plane and increase or decrease the field without reversals. Then the B-H curve is the average of upper branch and lower branch,

$$B(H) = \frac{B_u(H)+B_l(H)}{2} \qquad [2.10]$$

For minor loops, the core's absolute and differential permeability are a function of $\vec{H}$ and the history value of $\vec{H}$.

2.2.3 Magnetic circuit model

To simplify those electromagnetic law, magnetic circuit model is introduced. Fig2.5 illustrates uniform magnetic field in a magnetic material which has magnetic path length l_m, cross-sectional area A_c and permeability μ. Coil turns number of coil is N and the current flow through it is i. When $\vec{H}$ is constant and aligned with the path, the magnetomotive force (MMF) can be expressed by

$$\mathcal{F} = H \cdot l_m = N \cdot i \qquad [2.11]$$

Since $\vec{B} = \mu \cdot \vec{H}$ and $\Phi = B \cdot A_c$, $\mathcal{F}$ can be expressed by

$$\mathcal{F} = \Phi \cdot \frac{l_m}{\mu A_c} = \Phi \cdot \mathcal{R} \qquad [2.12]$$

, where $\mathcal{R}$ is defined to as the reluctance of the path l_m and equal to $\frac{l_m}{\mu A_c}$. Equation [2.12] resembles Ohm's law. According to this equation, magnetic circuit can be constructed and similar to electric circuit model as shown in Fig2.11. Magnetic flux is linearly proportional to MMF, voltage and current can be replaced by MMF and magnetic flux. Meanwhile, the reluctance is analogous to the resistance

of electric circuit model. Analogous parameters in magnetic circuit model and electric circuit model are list in Tab2.1 below.

Magnetic circuit model	Electric circuit model
Voltage - **V**	Magnetomotive force- $\boldsymbol{\mathcal{F}}$
Current - **I**	Magnetic flux- $\boldsymbol{\Phi}$
Current density - **J**	Magnetic flux density - $\boldsymbol{\vec{B}}$
Resistance - **R**	Reluctance - $\boldsymbol{\mathcal{R}}$

Tab2.1 Analogous Parameters in magnetic circuit model and electric circuit model

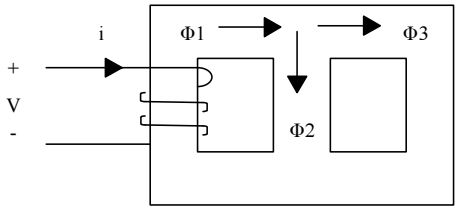

Fig2.11a physical model

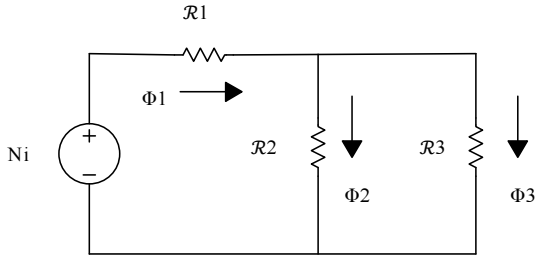

Fig2.11b magnetic circuit model

It is possible to solve flux and MMF of magnetic circuit model by using conventional circuit analysis. Followed from gauss' law in equation [2.4], magnetic flux entering a node is equal to the magnetic flux leaving this node and magnetic flux lines are continuous. This property of magnetic circuit model, as given by equation [2.13], is analogous to Kirchhoff's current law.

$$\sum_{i=1}^{k} \Phi_i = 0 \qquad [2.13]$$

Followed from Ampere's law in equation [2.2], magnetic also have a property which is analogous to Kirchhoff's voltage law, as given by equation [2.14]. The right side in equation [2.14] is the integral of all MMFs across reluctance around the closed path, while the left side is the integral of all MMF sources induced by current in windings.

$$\sum_{i}^{n} \mathcal{F}_i = \sum_{i}^{m} \Phi \cdot \mathcal{R}_i \qquad [2.14]$$

The magnetic circuit model can be linked with electric circuit model. For example, inductor value has different expressions in magnetic circuit model and electric circuit model respectively. According to Faraday's law, equation [2.11] and [2.12], induced voltage can be given by

$$v(t) = N \cdot \frac{d\Phi}{dt} = N \cdot \frac{N}{\mathcal{R}} \cdot \frac{di}{dt} = \frac{N^2}{\mathcal{R}} \cdot \frac{di}{dt} = L \cdot \frac{di}{dt} \qquad [2.15]$$

In this way, the inductor value in magnetic circuit model is

$$L = \frac{N^2}{\mathcal{R}} \qquad [2.16]$$

Transformation from magnetic circuit model to electric circuit model is very useful in the ballast modeling, which will be illustrated in following section. [12] [13]

2.2.4 Ballast physical model and magnetic circuit model

The magnetic circuit model of ballast R-140-1-TP can be derived from its physical configuration as shown in Fig2.12. Due to symmetrical structure of magnetic core, magnetic flux path flowing in left side and right side are equal. Mean magnetic flux paths of left side are analyzed and shown in Fig2.13.

Currents flowing in the primary winding and secondary winding are the MMF sources in the magnetic circuit model. The mutual magnetic flux Φ_M links the primary winding and the secondary winding. The mean paths of leakage magnetic flux are Φ_{pl} for the primary winding and Φ_{sl} for the secondary winding respectively. Besides, there is an air gap designed in this magnetic core. The magnetic flux paths Φ_P and Φ_S flow through this air gap, so there will be a reluctance caused by this air gap.

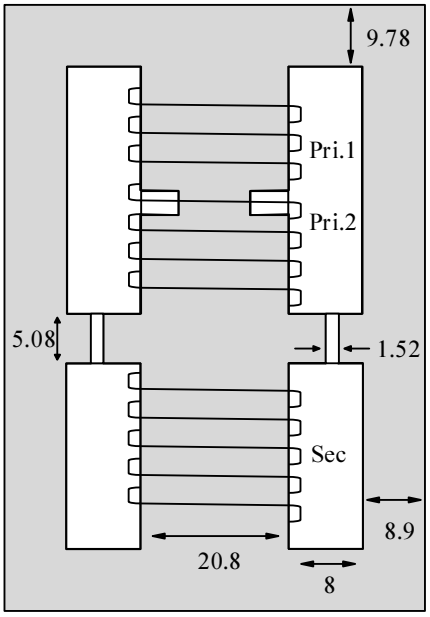

Fig2.12 Physical configuration of ballast R-140-1-TP

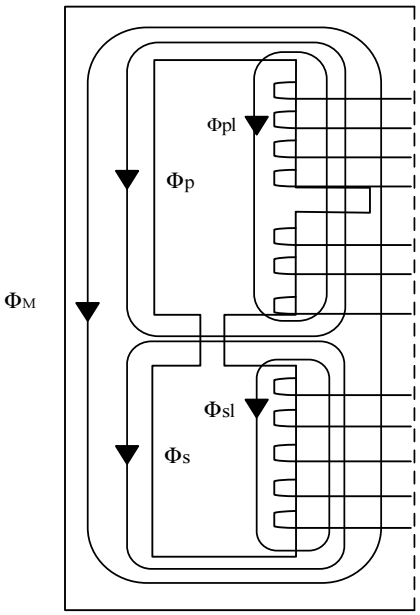

2.13 Mean magnetic flux paths of left side

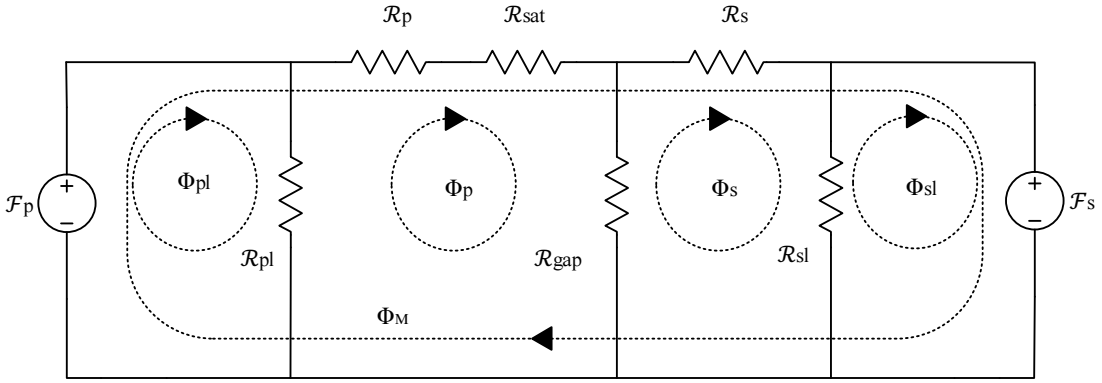

Fig2.14 Magnetic circuit model of ballast R-140-1-TP

Because of non-linear B-H curve, permeability of magnetic core varies with the flux density. It is essential to divide this magnetic core into several sections each of which has a substantially uniform flux density. According to the physical dimension shown in Fig2.12, cross-sectional area A_c of all sections are approximately equal except the air-gap section and the narrow section in primary winding. As a result, the magnetic core can be divided into four sections each of which has a uniform flux. The schematic magnetic circuit of ballast R-140-1-TP is shown in Fig2.14. Reluctance $\mathcal{R}_P$ presents primary winding section except the narrow part and carries magnetic flux density $\Phi_M + \Phi_P$; reluctance $\mathcal{R}_S$ presents secondary section and carries magnetic flux density $\Phi_M + \Phi_S$. The narrow section saturates more easily because of its smaller cross-sectional area. Reluctance $\mathcal{R}_{sat}$ corresponds to this narrow section and carries the same magnetic flux density as $\mathcal{R}_P$. The primary winding and the secondary

winding have leakage fluxes Φ_{pl} and Φ_{sl}. They are carried by the reluctance $\mathcal{R}_{pl}$ and $\mathcal{R}_{sl}$, which are the air portion reluctance of their paths respectively. For the air gap, its reluctance is $\mathcal{R}_{gap}$ and magnetic fluxes Φ_P and Φ_S flow through it.

2.2.5 Ballast equivalent electric circuit model and LTspice model

The equivalent electric circuit model of magnetic core, as shown in Fig2.15, can be derived directly from the magnetic circuit model by using topological principle of duality. The magnetic circuit model form and electric circuit model form are dual to each other. Each reluctance in the magnetic flux is connected to corresponding node in electric circuit mode through an inductor. For the reluctance which is common to two magnetic flux paths, an inductor interconnects the corresponding nodes in electric circuit model. The driving current in electric circuit model corresponds to magnetomotive force in magnetic circuit model and voltage between nodes corresponds to magnetic flux. [15]

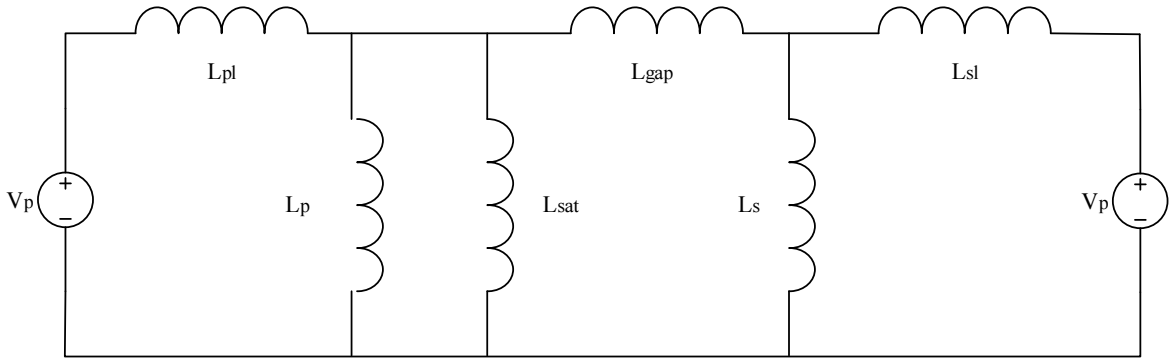

Fig2.15 Equivalent electric circuit model of magnetic core

Based on this magnetic circuit model, the model of ballast R-140-1-TP can be built in LTspice. As input winding and output winding share the primary winding 2 with a series capacitor, it is too complicate to calculate the output voltage by using this magnetic circuit model directly. For simplification, the output voltage is generated by an ideal transformer whose primary winding is connected to the equivalent electric circuit model and secondary winding is the output with compensation capacitor and output resistor. Because of the narrow part of the primary winding, magnetic saturation is mainly determined by this section. The turns ratio of the ideal transformer is the turns of primary winding 2 divided by the turns of the secondary winding.

AS for the leakage inductance L_{pl} and L_{sl}, they are simplified in the magnetic circuit model by using a mean magnetic flux path in air portion while can be directly measured in the real ballast. According to the measurement result, both of them have the same inductance value of 100mH. The inductance of an air gap inductor is determined by the dimension of air gap, because the flux density flow through it is linearly proportional to magnetic field intensity with instant slope μ_0. The other three inductors, L_p, L_{sat} and L_s, have nonlinear permeability which are affected by the B-H curve of magnetic core material. Nonlinearity of these three inductors result in waveform distortion and saturation. For simulating nonlinear characteristic, aforementioned hysteretic core model is employed in LTspice simulation. Parameters of these three nonlinear inductors are measured and list in Tab2.2 below.

	$\mathbf{L}_p$	$\mathbf{L}_{sat}$	$\mathbf{L}_s$
coercive force $\boldsymbol{H_c}$ (A/m)		100	
remnant flux density $\boldsymbol{B_r}$ (T)		1.4	
saturation flux density $\boldsymbol{B_{sat}}$ (T)		1.5	
Magnetic Length $\mathbf{L}_m$ (m)	0.209	0.00508	0.209
Length of gap $\mathbf{L}_g$ (m)		0	
Cross sectional area **A** ($\boldsymbol{m^2}$)	0.00033	0.000144	0.00033
Number of turns **N**		855	

Tab2.2 Parameters of three nonlinear inductor used in LTspice simulation

Besides, input and output winding resistance are not mentioned in the magnetic circuit model and can be directly measured. For ballast R-140-1-TP, the input resistance is 18Ω and output resistance is 68Ω. The 4.2uF value compensation capacitor is at the output of the ideal transformer. However, some non-ideal factors, such as core loss, are still not considered in this model. These non-ideal effects can be simulated by adjusting inductor L_{mod} and resistor R_2 in LTspice modulation. The R-140-1-TP T12 EM ballast model used in LTspice for simulation is shown in Fig2.16 below.

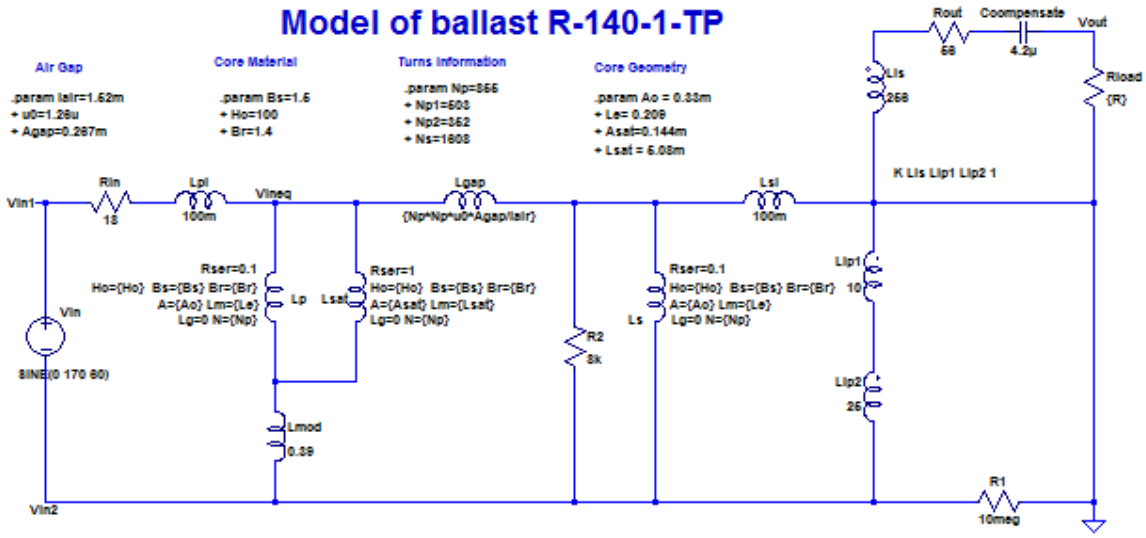

Fig2.16 LTspice model of ballast R-140-1-TP

2.2.6 LTspice model validation

To verify this LTspice model built in last section, some output parameters, namely output voltage, output power, power factor (PF), efficiency and total harmonic distortion (THD), are simulated in LTspice and measured in practical experiment with different load resistors. Tab 2.3 shows the results.

Load resistance (Ω)	Output voltage (V)		Output power (W)		Power factor		Efficiency		THD	
	simu	meas	simu	meas	simu	meas	simu	meas	simu	meas
3091	209	201.2	14.2	13.1	0.466	0.47	30.0%	31%	22.0%	23.7%
2737	207	199.8	15.8	14.6	0.5	0.5	33.0%	34%	21.0%	23.5%
2336	205.4	197.9	18.3	16.7	0.536	0.54	37.3%	38%	20.0%	22.7%
2004	203.1	197	20.7	19.4	0.576	0.59	41.1%	43%	18.4%	21.2%
1683	200.3	194.3	24.0	22.4	0.622	0.65	45.9%	48%	16.5%	20.1%
1199	192.5	188.2	31.0	29.6	0.706	0.75	54.3%	57%	12.8%	17.4%
881	181.7	181.7	37.6	37.5	0.774	0.84	60.5%	64%	9.9%	14.3%
685	170.3	172	45	43.2	0.821	0.88	64.0%	67%	8.3%	13.7%
194	87.6	90.4	40.0	42.1	0.968	0.94	65.4%	60%	13.2%	18.8%

Tab 2.3 Output parameters in LTspice simulation and practical measurement

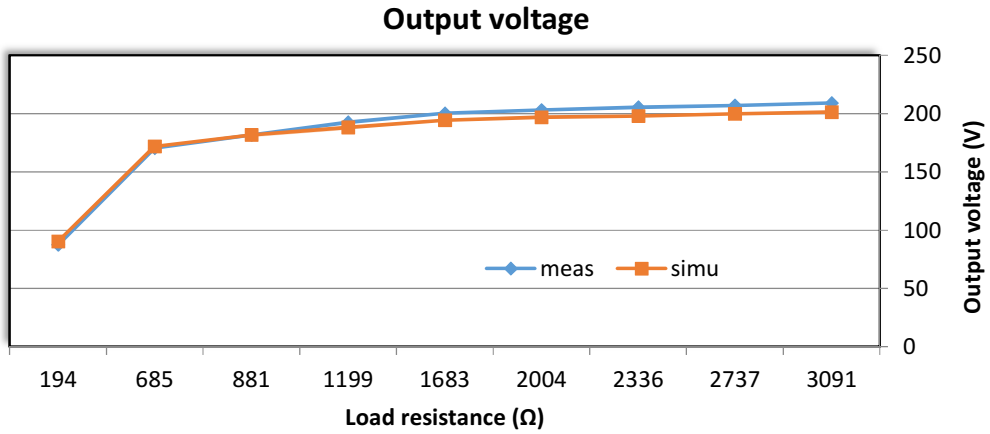

(a)

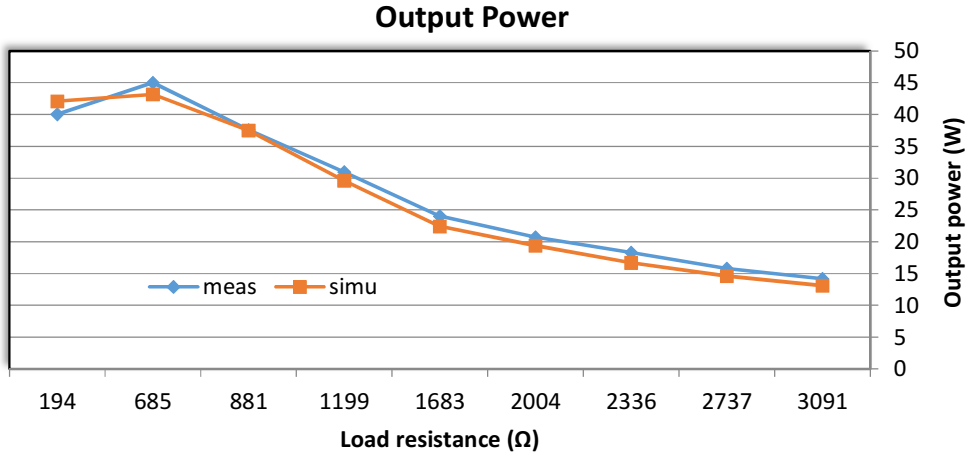

(b)

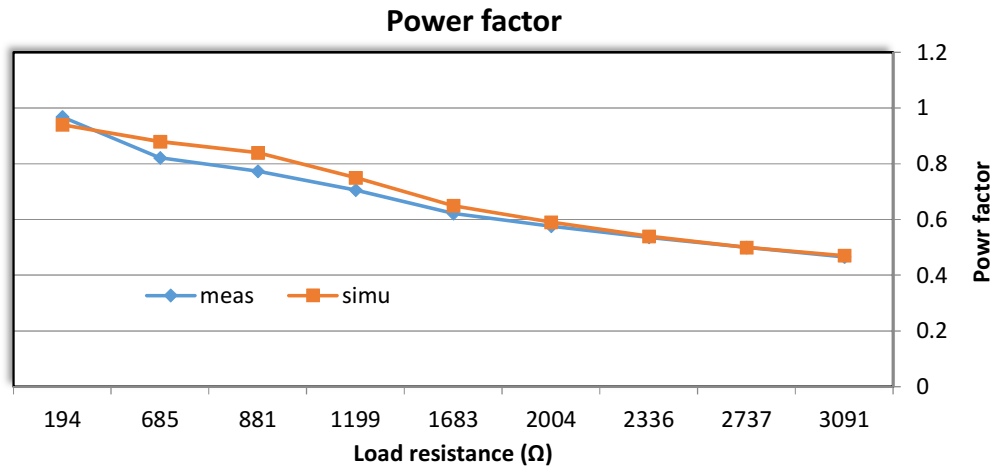

(c)

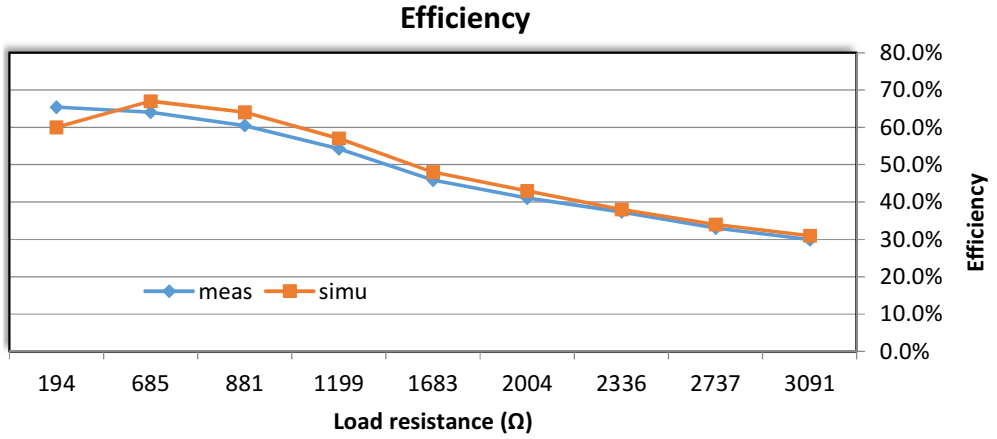

(d)

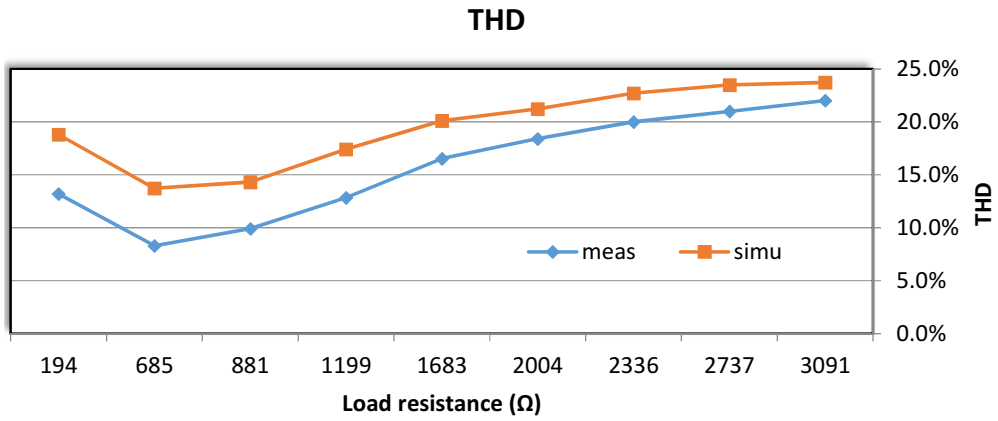

(e)

Fig 2.17 Ballast output parameters in measurements (blue) and simulation (red) comparison:

(a) output voltage; (b) output power; (c) power factor; (d) efficiency (e) THD.

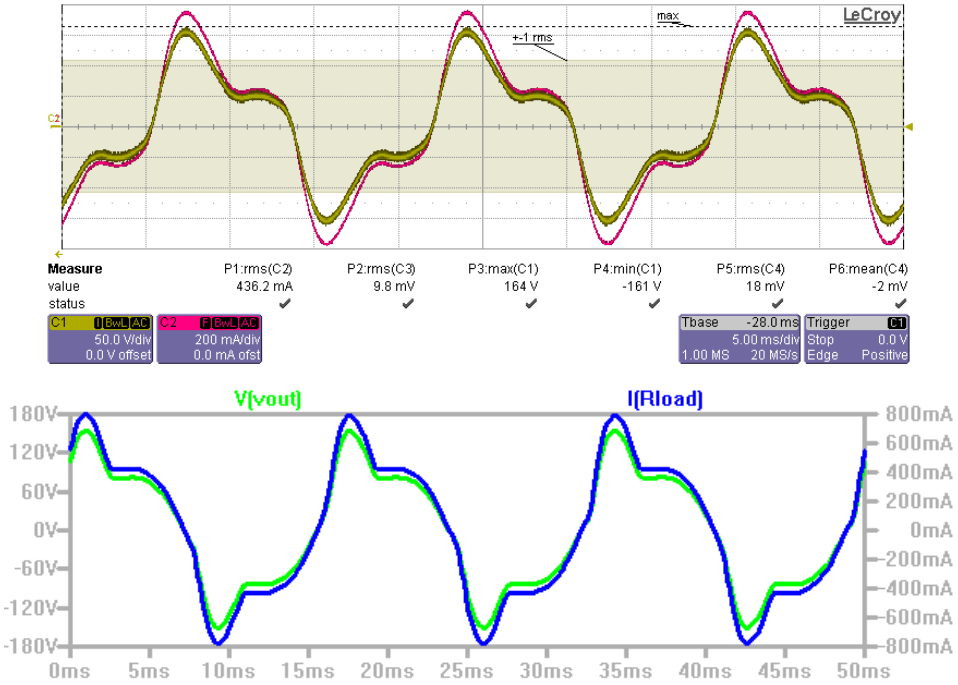

(a)

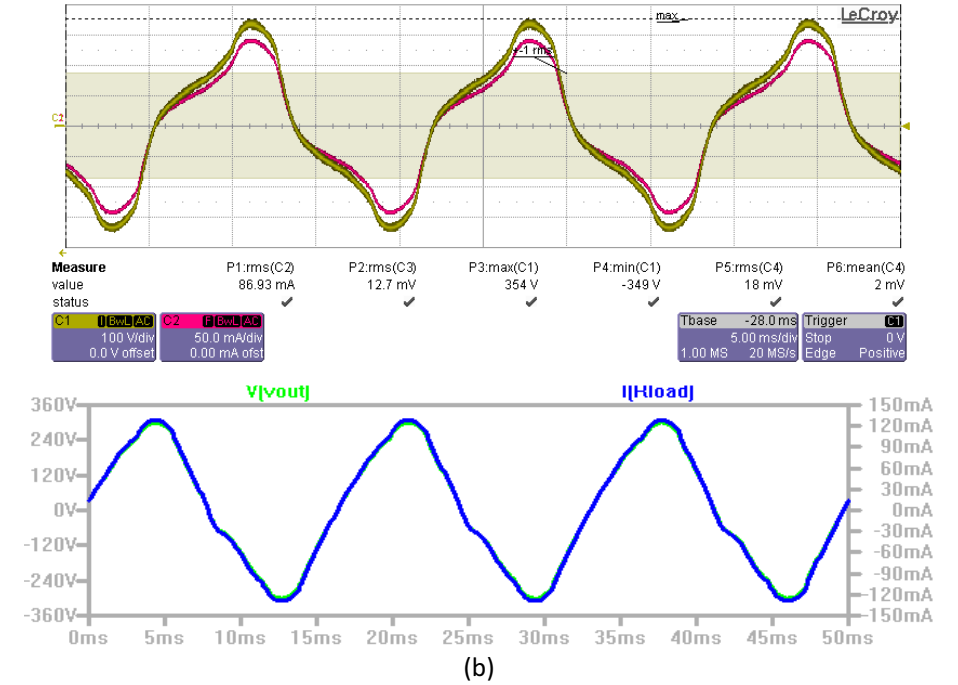

(b)

Fig2.18 Ballast output current and voltage waveforms with 196 Ω (a) and 2336 Ω (b) in practical measurement (upper) and LTspice simulation (low), respectively

For the convenience of examining model fitting, output parameters are plotted in Fig2.17. According to these charts, simulation results are basically according to the measurement results. Although the THD in LTspice simulation is a little higher than that in practical measurement, which may be caused by some non-ideal factors not considered in LTspice model, this deviation is acceptable and will not cause serious problem in driver design. As for other four parameters, simulation results match

measurement results very well, especially the perfectly matching output power which is crucial for the operating point setting in driver design. Furthermore, Fig 2.18 shows ballast output current and voltage waveforms with 196 Ω and 2336 Ω load, respectively. The output waveform in LTspice simulation is similar to waveform in practical measurement.

According to these comparisons, the model fits with practical measurement results. Therefore, the proposed LTspice model of ballast R-140-1-TP and this modeling method based on magnetic circuit can be proved valid.

Proposed modeling method can be summarized in the following steps:

1. **Analysis magnetic flux paths in T12 EM ballast physical configuration;**
2. **Construct magnetic circuit model based on magnetic flux paths;**
3. **Measure ballast input resistance, output resistance and leakage inductance;**
4. **Build equivalent circuit in LTspice and adjust non-ideal components.**

By using this modeling method, LTspice models of other types ballasts can also be built because of their similar configurations and working principles. For example, the circuit configuration of dual-lamp ballast R-2S40-1-TP is shown in Fig 2.19. Obviously, it is similar to the circuit configuration of ballast R-140-1-TP as shown in Fig2.4. As a result, the aforementioned modeling method also works for this ballast or other types T12 EM ballast. For the sake of brevity, modeling of other types T12 EM ballast are not repeated here.

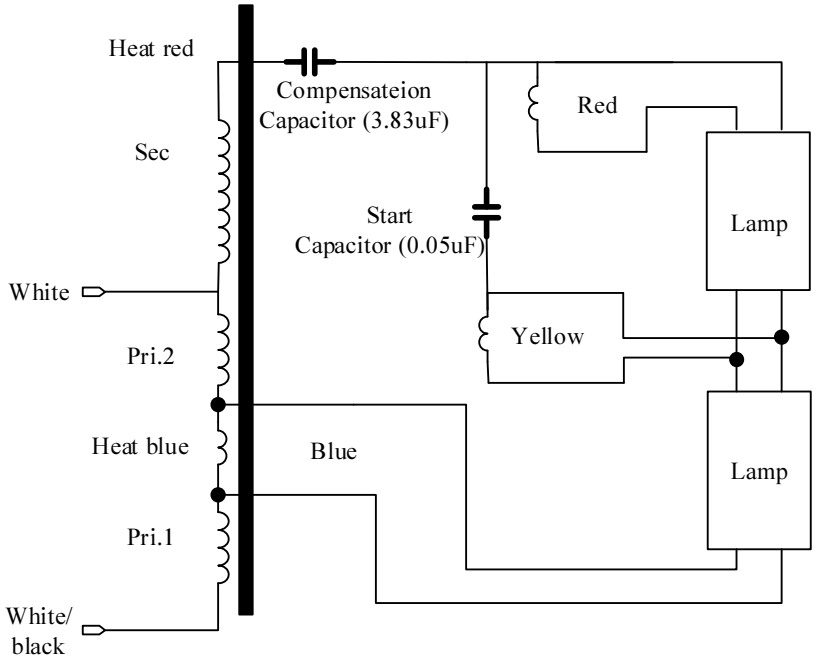

Fig2.19 Circuit configuration of dual-lamp ballast R-2S40-1-TP

2.3 Ballast measurement results and comparison

As the driver is designed to be compatible with different types of T12 EM ballast, it is essential to compare and analyze output characteristics of different ballast to determine driver design principle. In this project, ballast R140-1-TP, R2S40 and R3S34, are successively measured with a variable resistance load.

The Ballast R140-1-TP is a single-lamp ballast, its input and output characteristics with variable resistance load are list in Tab2.4 below.

The output voltage of ballast is a critical parameter for the driver design, because it is the input voltage of switching mode driver and has influence on the circuit topology choice. Therefore, some charts are drawn to illustrate R140-1-TP electrical characteristics curves within output voltage range, as shown in Fig2.20.

Load Resistance per lamp(Ω)	Iin (A)	Pin (W)	Vout per lamp (V)	Pout per lamp (W)
57	0.312	36	26.7	14.1
102	0.376	44	44.3	22.7
158	0.474	55.5	74.8	35.6
265	0.56	63.7	110	45.9
438	0.594	63.8	146.3	49
736	0.543	52.3	174	41.1
1020	0.5	44.3	187	34.3
1483	0.45	35.44	197.4	26.6
2004	0.42	29.1	203	20.8
2701	0.4	23.9	207	16
3370	0.39	20.8	209.3	13
Load Resistance per lamp(Ω)	**Ballast efficiency**	**THD (Iin)**	**Power Factor**	**Ballast Power loss per Lamp (W)**
57	39.2%	0.277	0.96	21.89
102	51.7%	0.217	0.975	21.25
158	64.1%	0.151	0.975	19.92
265	72%	0.107	0.95	17.84
438	76.7%	0.081	0.895	14.87
736	78.1%	0.087	0.81	11.45
1020	77.5%	0.1123	0.74	9.98
1483	75.1%	0.151	0.66	8.82
2004	71.5%	0.184	0.58	8.29
2701	66.7%	0.21	0.5	7.96
3370	62.5%	0.224	0.446	7.80

Tab2.4 input and output characteristics of ballast R140-1-TP

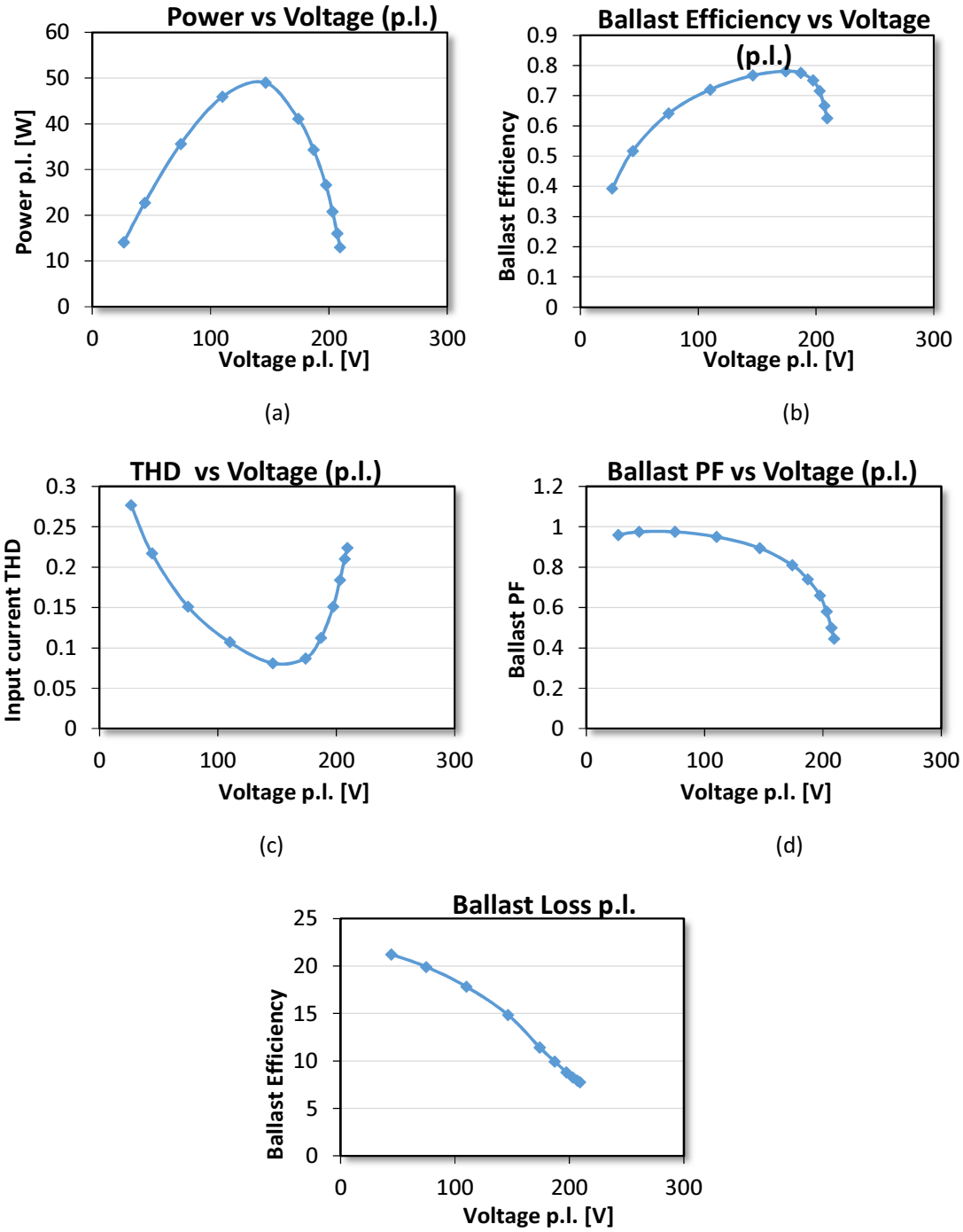

Fig2.20 R140-1-TP electrical characteristics curves within output voltage range: (a) power per lamp; (b) ballast efficiency per lamp; (c) THD; (d) power factor; (e) ballast loss per lamp.

Ballast R2S40 is a dual-lamp ballast, its input and output characteristics with variable resistance load are list in Tab2.5 below. R2S40 electrical characteristics curves are shown in Fig2.21.

Load Resistance per lamp(Ω)	Iin (A)	Pin (W)	Vout per lamp (V)	Pout per lamp (W)
25	0.56	42.1	16.4	10.8
50	0.61	54.2	28.9	16.7
100	0.665	70.7	51.3	26.3
150	0.7	80	69.2	31.9
200	0.71	83.5	82.2	33.8
290	0.69	81.6	99.6	34.2
400	0.64	74.8	110.8	30.7
610	0.54	60.5	122	24.4
800	0.483	51.4	127.4	20.3
1400	0.388	35.6	134	12.8
1800	0.36	30.3	135.3	10.2
Load Resistance per lamp(Ω)	**Ballast efficiency**	**THD (Iin)**	**Power Factor**	**Ballast Power loss per Lamp (W)**
25	51.1%	58.0%	0.62	10.29
50	61.6%	48.0%	0.745	10.40
100	74.4%	33.5%	0.89	9.03
150	79.8%	24.6%	0.95	8.08
200	80.9%	19.7%	0.98	7.97
290	83.8%	15.0%	0.985	6.59
400	82.1%	13.2%	0.98	6.71
610	80.7%	13.8%	0.93	5.85
800	78.9%	15.6%	0.89	5.41
1400	72.1%	21.2%	0.76	4.97
1800	67.1%	23.5%	0.7	4.98

Tab2.5 input and output characteristics of ballast R2S40

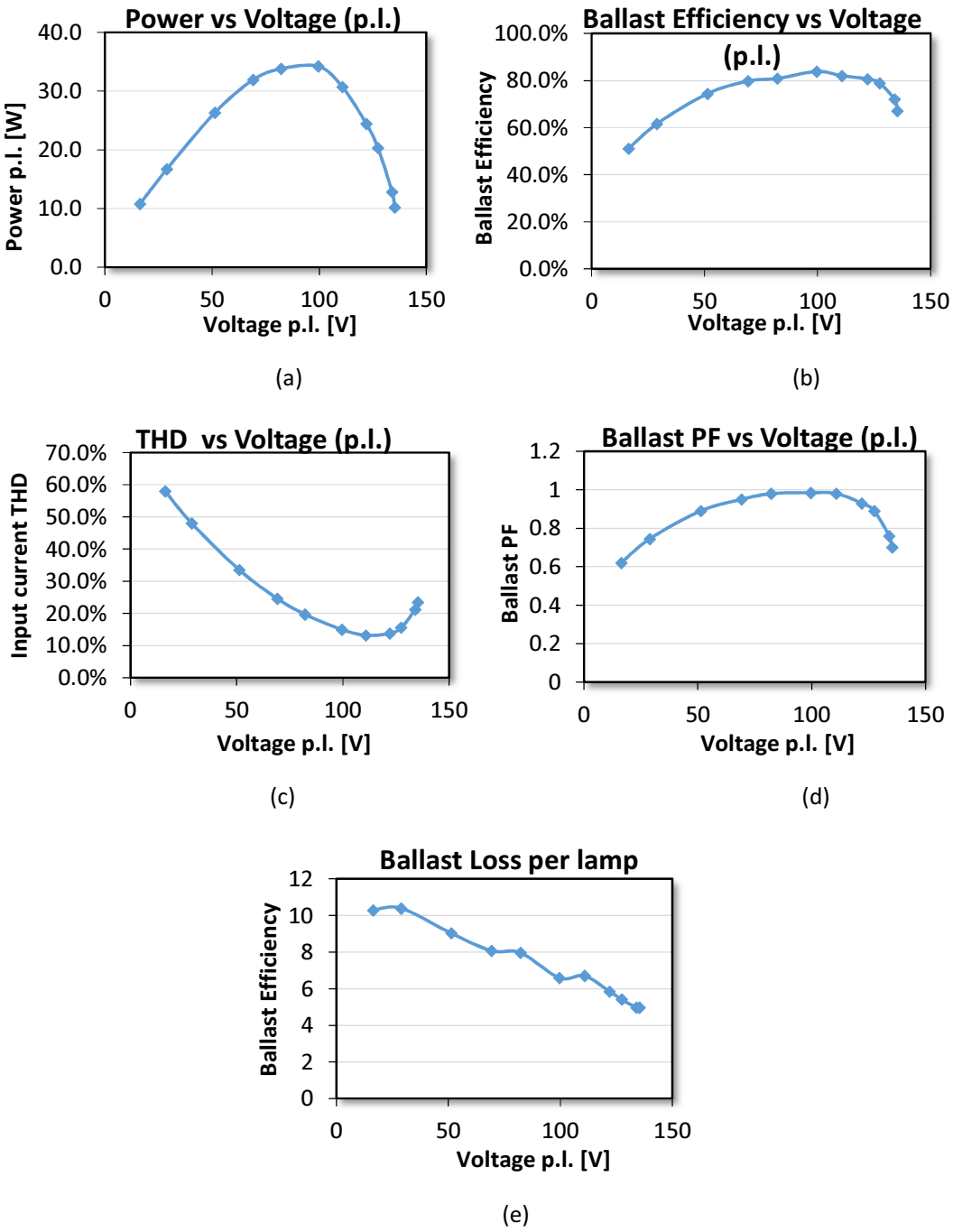

Fig2.21 R2S40 electrical characteristics curves within output voltage range: (a) power per lamp; (b) ballast efficiency per lamp; (c) THD; (d) power factor; (e) ballast loss per lamp.

Ballast R3S34 is a three-lamp ballast, its input and output characteristics with variable resistance load are list in Tab2.6 below. R3S34 electrical characteristics curves are shown in Fig2.22.

Load Resistance per lamp(Ω)	Iin (A)	Pin (W)	Vout per lamp (V)	Pout per lamp (W)
25	0.546	46	12.6	6.4
53	0.607	61.8	25.3	12.1
100	0.671	76.5	42.06	17.7
200	0.69	81	63.8	20.4
400	0.59	65	80.2	16.1
800	0.462	44.6	87.6	9.6
1000	0.432	39.2	89.6	8.0
Load Resistance per lamp(Ω)	**Ballast efficiency**	**THD (Iin)**	**Power Factor**	**Ballast Power loss per Lamp (W)**
25	41.4%	55.9%	0.7	8.98
53	58.6%	41.6%	0.85	8.52
100	69.4%	27.7%	0.95	7.81
200	75.4%	17.0%	0.98	6.65
400	74.2%	15.3%	0.92	5.59
800	64.5%	20.5%	0.802	5.27
1000	61.4%	22.5%	0.76	5.04

Tab2.6 input and output characteristics of ballast R3S34

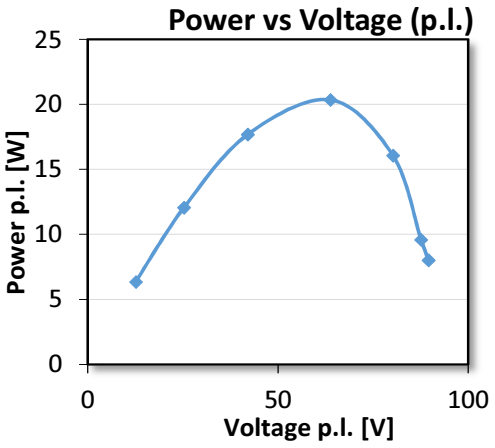

(a)

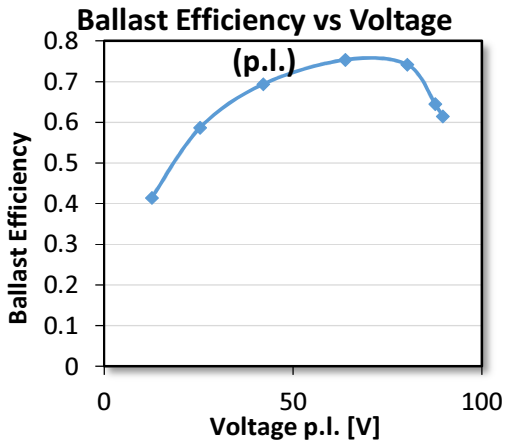

(b)

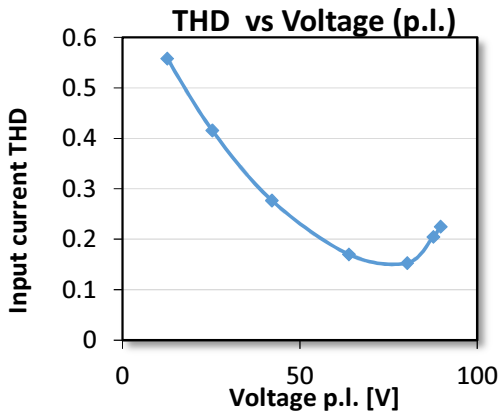

(c)

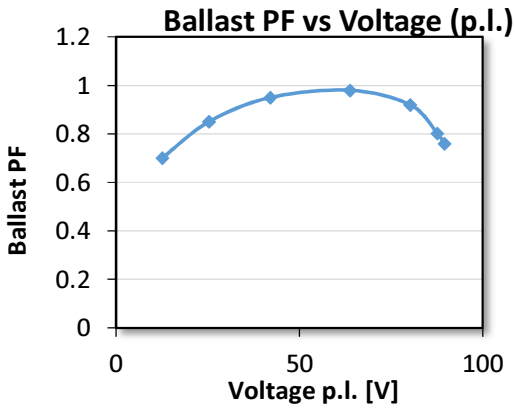

(d)

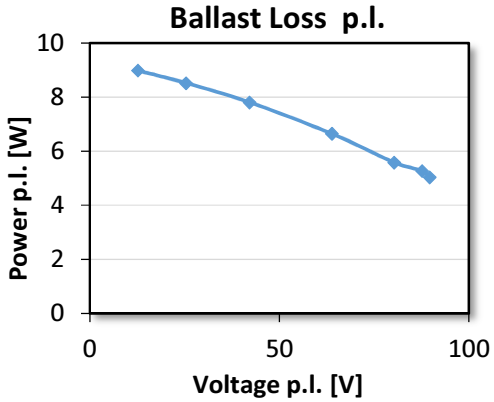

(e)

Fig2.22 R3S34 electrical characteristics curves within output voltage range: (a) power per lamp; (b) ballast efficiency per lamp; (c) THD; (d) power factor; (e) ballast loss per lamp.

It can be seen that all these three ballast have similar curves for each parameter even though their output voltage for per lamp are different. With output voltage increasing, all the output parameter curves except ballast power loss are parabolic. Output power, ballast efficiency and power factor increase with output voltage firstly, then begin to decrease after their peak values. On the contrary, ballast THD decreases as output voltage increases firstly, then begins to increase after its minimum value. Different from four aforementioned parameter curves, the ballast power loss for per lamp monotonously decreases with output voltage.

An output power comparison of these three ballast is shown in Fig 2.23. The mains voltage disturbance is considered in this comparison. The nominal main voltage is 120Vac, 60Hz. In the measurement, supply voltage applied on ballast are the nominal voltage and 10% plus or minus variation, namely 108V, 120V and 132V. For the same output power, single-lamp ballast has the highest output voltage per lamp while three-lamp ballast has the lowest output voltage per lamp.

As previous mentioned, their output power increase with output voltage firstly, then decrease with it. In this way, per lamp resistance also have the parabolic characteristic, as shown in Fig2.24, and this conclusion is helpful for the driver design. For a TLED driver, its operating point is determined by the LED lamp which has a constant input power. Therefore, for a LED lamp, there are two operating points

matching this constant LED power and the low output voltage point has higher current because of constant power. Under the influence of mains voltage disturbance, the output characteristic curves of these three ballast have overlap at low output voltage region. This overlap may cause serious problem in choosing operating point of driver design.

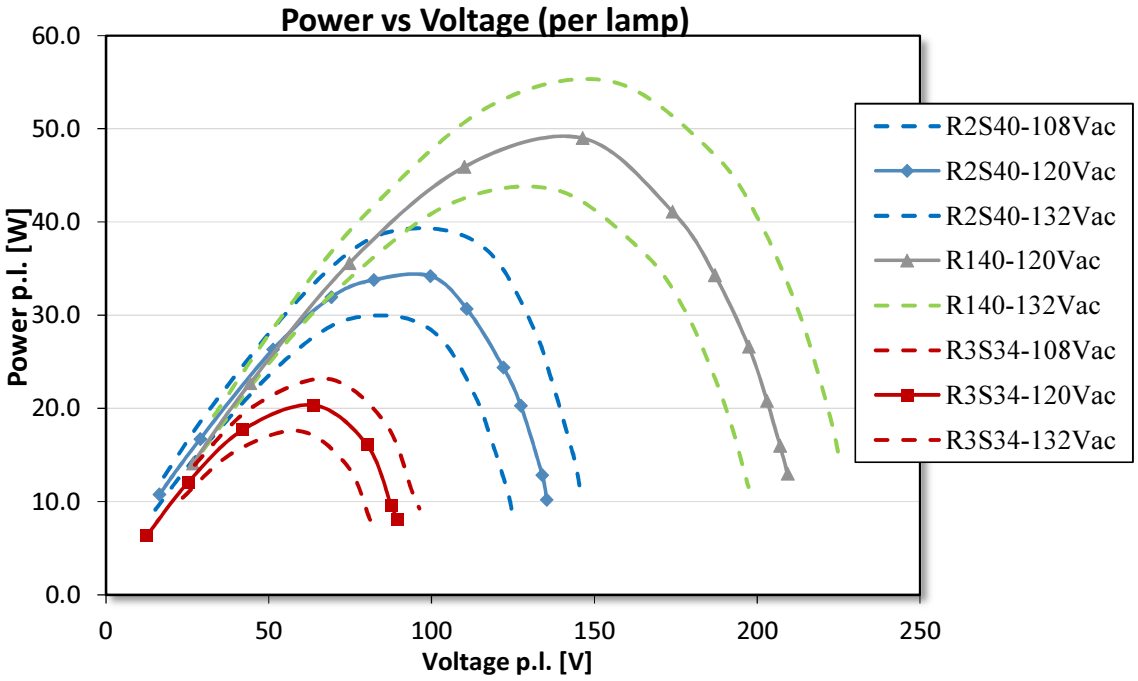

Fig2.23 Output power comparison of these three ballast with mains voltage disturbance

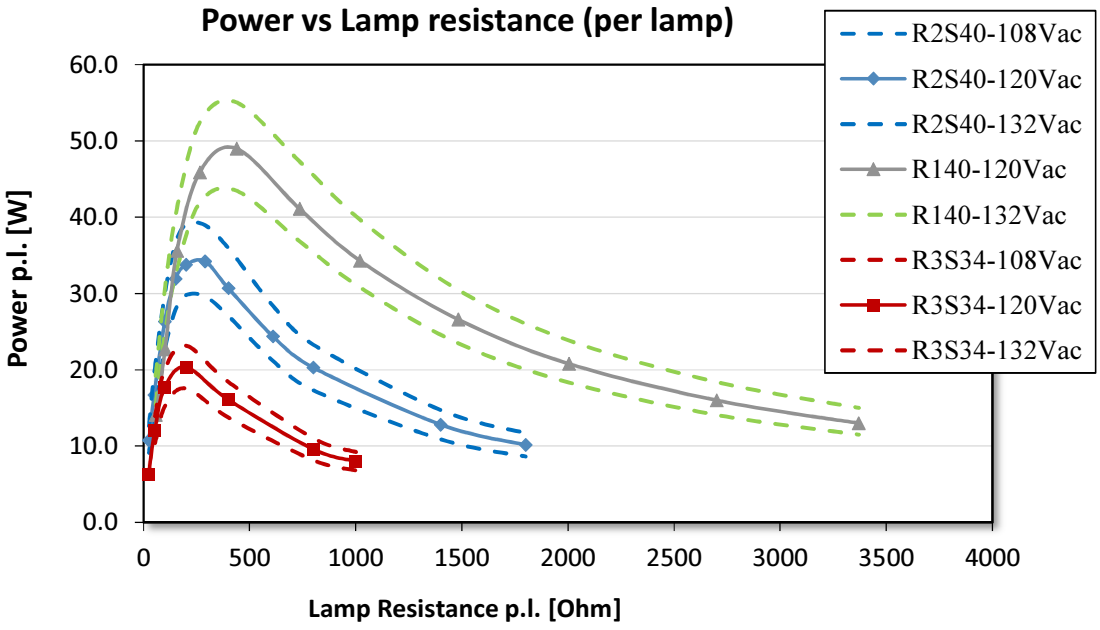

Fig2.24 Comparison of output voltage and resistance per lamp curves

It is a critical issue that choosing a driver circuit topology and selecting an operating point to make this driver be compatible with different types ballast based on these measurement results. For the driver design, it will be discussed in the next chapter.

2.4 Conclusion for ballast modeling and measurement

In this chapter, various T12 EM ballast and their structures are introduced. Fundamental electromagnetic laws are reviewed. Besides, magnetic core hysteresis characteristic and a hysteretic core model are introduced. Based on physical configuration and magnetic flux paths, a magnetic circuit model of T12 EM ballast R-140-1-TP is built. Then an equivalent electric circuit model of magnetic core is derived from this magnetic circuit model by using topological principle of duality. This equivalent electric circuit is simulated in LTspice, and simulation results match measurement results. The proposed ballast model and modeling method are valid.

Furthermore, different types T12 EM ballast are measured. Their input and output characteristics with variable resistance load are listed and compared. It is found that different ballasts have different output voltage for per lamp and have similar characteristic curves.

According to measurement results, it is possible to find out proper ballast operating points for different ballast. Based on input and output characteristics of ballast, driver operating point can be determined.

Based on these studies, a T12 EM ballast compatible TLED driver is designed and simulated in the next chapter.

3. Retrofit TLED driver design

In the previous chapter, physical structure, circuit configuration and input-output characteristics of T12 EM ballast were illustrated. An LTspice model of ballast R-140-1-TP has been built and the simulation results are basically accordant to the measurement results.

In this chapter, firstly, the operating point of driver will be determined. Then the driver's specification can be derived. Proper circuit topology and other electrical technics are adopted in the retrofit TLED driver. Driver working principle and design process are illustrated in this chapter. At last, simulation waveform of each circuit module is shown and explained.

3.1 Ballast operating point

The objective of this project is to develop a T12 retrofit TLED which is compatible with EM ballast in US market. Philips mid-power LED, whose luminous efficiency is 145 lumen per watt, is adopted in this project. As the designed LED lamp should have 2000 lumens, the driver output power can be determined, about 14W. To meet the system energy efficiency requirement, driver efficiency should be higher than 85% at least, so the driver input power also can be obtained, about 16W.

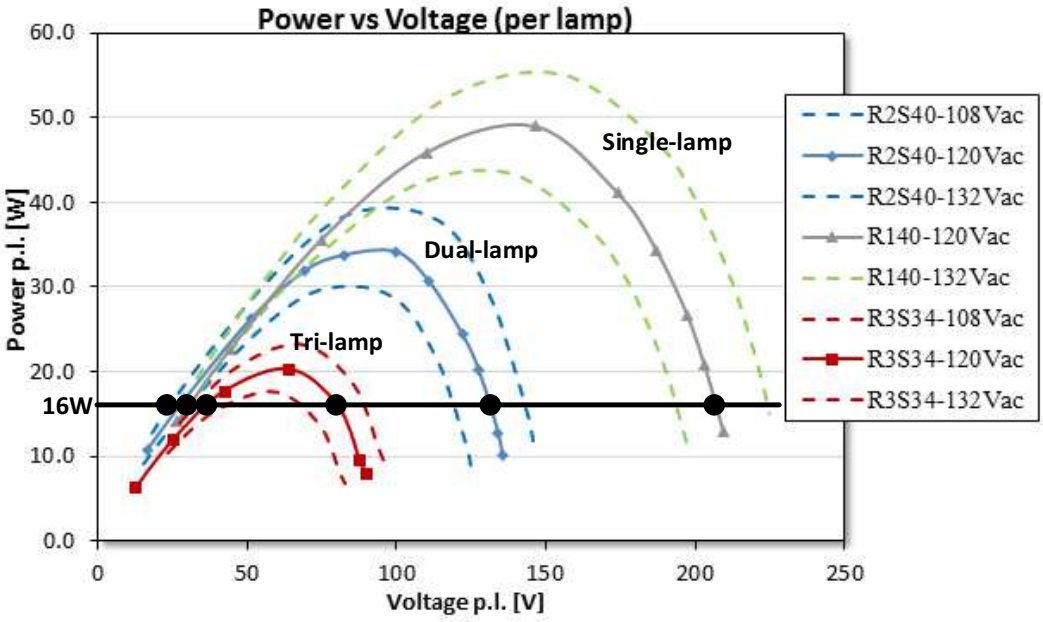

Fig 3.1 Driver operating point marked in ballast output characteristics curves

Combined with the ballast output characteristics curves, possible operating points and corresponding driver input voltage are located in Fig3.1. The black line in the figure indicates the 16W vertical coordinate, and its intersections with ballast output characteristics curves are marked by six black spots. As mentioned before, for the same power, each ballast has two operating point to provide the same output power with different input voltage. In the low voltage region, operating points of three ballast are contiguous, while in high voltage region, they are separated far apart.

Because power loss of the system is mainly caused by the ballast, ballast efficiency is the primary consideration in choosing operating point. For lower ballast power loss and higher efficiency, high

voltage region operating point should be selected due to its higher ballast efficiency, as shown in Fig2.20 (e), Fig2.21 (e) and Fig2.22 (e). In high voltage region, however, operating points of the three ballasts are far apart which will result in driver wide input voltage range. For the three-lamp ballast, 16W output power operating point is correspond to about 80V output voltage; as for the dual-lamp ballast, corresponding output voltage increase to about 130V; and for the single-lamp ballast, the corresponding output voltage is as high as about 205V.

3.2 Specification and functional modules of driver circuit

As discussed in the last section, the driver has a wide input voltage range, from 80V to 205V, while it must have the constant output voltage and power in three operating points. Deriver output voltage is determined by TLED string forward voltage. In this project, under the limits of conduction angle and voltage rating, TLED string forward voltage is determined to be 150V. However, each ballast output voltage of three aforementioned operating points is either higher or lower than 150V. Meanwhile, drivers are connected in series in dual-lamp or three-lamp ballast and have the same input current. For keeping good balance of power distribution between the lamps with a multi-lamp ballast, the driver is designed to have near-resistive input impedance. In conclusion, this chapter is aim to design a wide input voltage range near-resistive driver.

3.2.1 Circuit topology and working principle of buck-boost converter

For the voltage converting, a buck-boost converter is a suitable scenario. It is a DC-DC converter and combines step-up boost and step-down buck switching implementations. This converter satisfies the driver voltage converting requirement. The circuit topology of buck-boost converter is shown in Fig3.2 below. It consists of 4 components: a switch, an inductor, a capacitor and a diode.

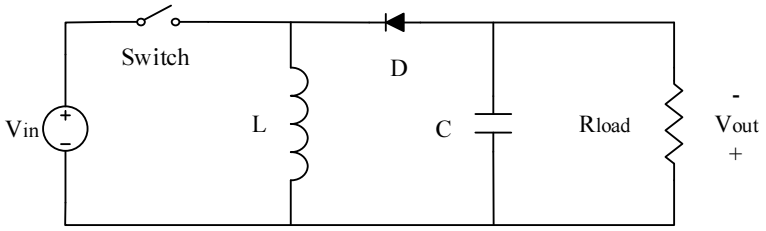

Fig3.2 Circuit topology of buck-boost converter

When the switch is on, as shown in Fig3.3 (a), the input voltage is isolated from output as a result of blocking diode. Input voltage is directly applied to the inductor. Current flow through the inductor results in accumulating energy in inductor. The current flow through the load resistor is provided by the capacitor at that stage.

When the switch is off, as shown in Fig3.3 (b), the input voltage is removed. Polarity of the inductor voltage is reversed and the inductor generates electromotive force to maintain current. This induced voltage in the inductor is the output voltage. Then capacitor is recharged by the inductor current and load resistor is also supplied by the inductor.

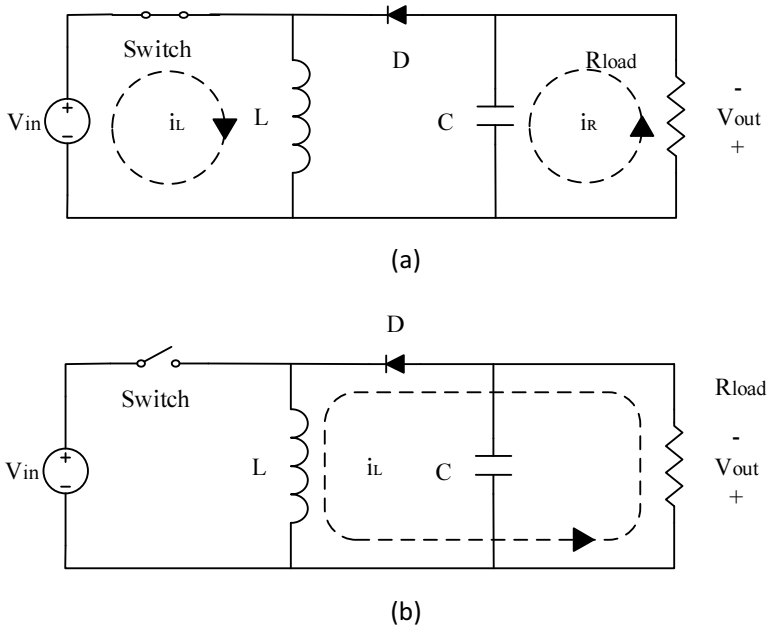

Fig3.3 Switch on (a) and switch off (b) states of buck-boost converter

Base on the state of inductor current, operating modes of the buck-boost can be classified into two: continuous conduction mode (CCM) and discontinuous conduction mode (DCM).

For the continuous conduction mode, the inductor never fall down to zero. In steady state, inductor voltage and current waveforms are shown in Fig3.4 below.

During on-state T_{on}, input voltage is applied on the inductor directly, and the increase of the inductor current is given by

$$\Delta I_1 = \int_0^{T_{on}} \frac{V_{in}}{L} dt = \frac{V_{in} \cdot T_{on}}{L} \quad [3.1]$$

, where the T_{on} is the on-time in one period and L is the inductance of the inductor.

During off-state T_{off}, reversed polarity voltage which is induced in inductor is applied on the load resistor and recharges the big capacitor as V_{out}. Decrease of inductor current is

$$\Delta I_2 = \int_0^{T_{off}} \frac{V_{out}}{L} dt = \frac{V_{out} \cdot T_{off}}{L} \quad [3.2]$$

As in steady state, increase inductor current magnitude is equal to decrease current magnitude in a cycle, then

$$\Delta I_1 = -\Delta I_2 = \frac{V_{in} \cdot T_{on}}{L} = \frac{-V_{out} \cdot T_{off}}{L} \quad [3.3]$$

$$\frac{V_{out}}{V_{in}} = -\frac{T_{on}}{T_{off}} \quad [3.4]$$

According to equation [3.4], ratio of output voltage and input voltage of buck-bust converter is determined by ratio of $T_{on}$and T_{off}. That's why the output voltage can be either higher or lower than the input voltage.

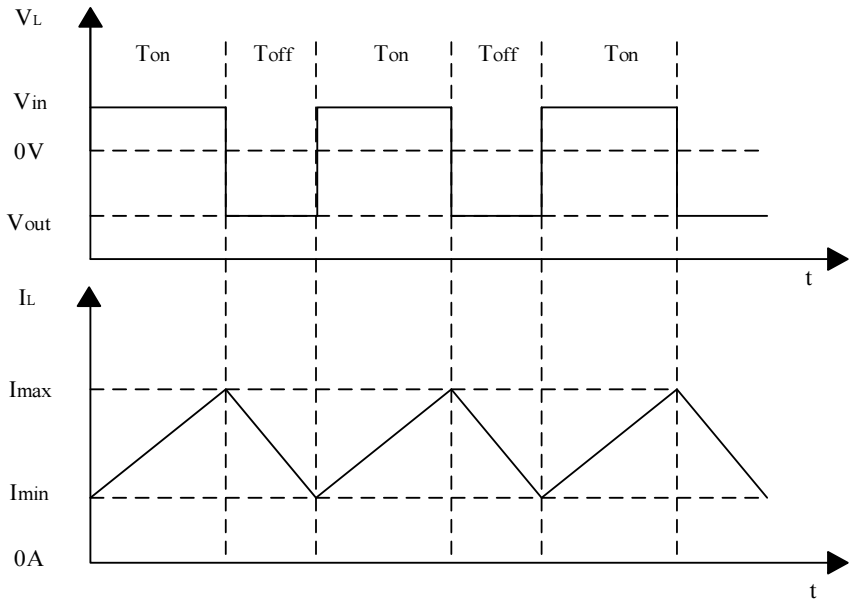

Fig3.4 Inductor voltage and current waveforms of buck-boost converter in CCM

In discontinuous conduction mode, the current through the inductor falls to zero during part of off-state. In steady state, inductor voltage and current waveforms are shown in Fig3.5 below.

During on-state T_{on}, input voltage is applied on the inductor directly, inductor current increase from zero to can be given by I_{max}, which can be given by

$$I_{max} = \int_0^{T_{on}} \frac{V_{in}}{L} dt = \frac{V_{in} \cdot T_{on}}{L} \quad [3.5]$$

The off-state has two separate sections. During the first section T_{off1}, the inductor current falls from I_{max} to zero. Inductor voltage reverses its polarity and supply the load resistor just like in CCM. During the second section T_{off2}, both inductor current and voltage are zero. This means that the inductor is completely discharged.

$$I_{max} + \frac{V_{out} \cdot T_{off1}}{L} = 0 \quad [3.6]$$

Followed from equation [3.5] and [3.6], T_{off1} is

$$T_{off1} = -\frac{V_{in} \cdot T_{on}}{V_{out}} \quad [3.7]$$

Meanwhile, the load current is provided by the inductor and big capacitor, its average value is

$$I_{out} = \frac{I_{max} \cdot T_{off1}}{2T} = -\frac{{V_{in}}^2 \cdot {T_{on}}^2}{2L \cdot T \cdot V_{out}} \quad [3.8]$$

Then relationship between input and output voltage can also be written as

$$\frac{V_{out}}{V_{in}} = -\frac{V_{in} \cdot {T_{on}}^2}{2L \cdot T \cdot I_{out}} \quad [3.9]$$

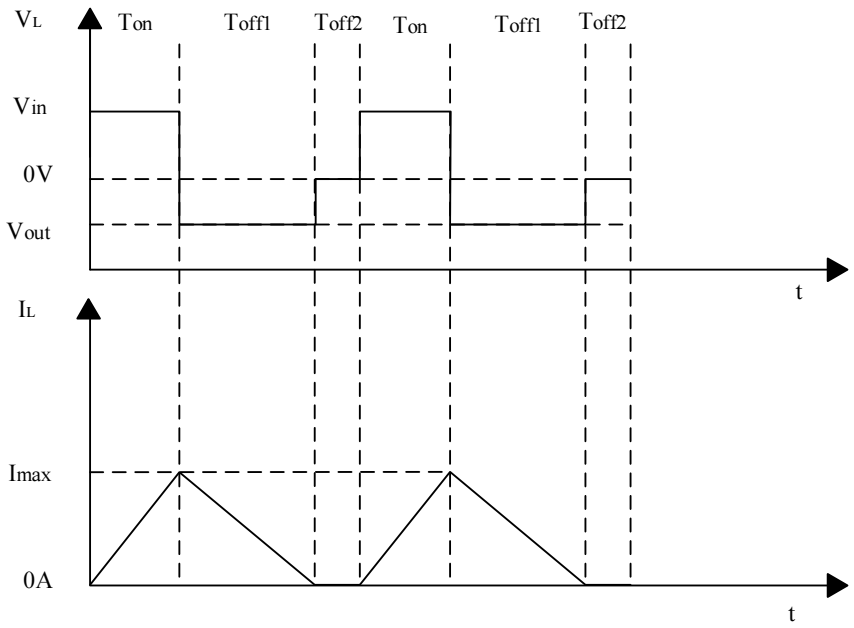

Fig3.5 Inductor voltage and current waveforms of buck-boost converter in DCM

For a constant input voltage, output voltage of buck-boost converter is determined by switch duty ratio. In this project, the driver input voltage is 60Hz AC voltage from EM ballast while buck-boost converter can only work with DC input voltage. To solve this problem, a rectifier is adopted in this driver circuit to rectify the input voltage. However, the input voltage is still not a constant DC voltage and one more control model is needed to provide the pulse-width modulation (PWM) signal to control the switch duty ration. As a solution to this issue, a self-oscillating buck-boost converter is employed and introduced in next section.

3.2.2 Ringing choke converter (RCC) module

The self-oscillating converter is often referred to as the ringing choke converter (RCC). It is popular in low-power and cost-sensitive devices because of its low component-count, circuit simplicity, output cross regulation and robustness. Compared with conventional PWM controlled buck-boost converter, which adopts a complicate PWM controller circuit, RCC only has very few discrete control components without loss of performance. This advantage can be attributed to self-oscillation, because it automatically limits input power by using feedforward control and constant current gain of power transistor. As a result, RCC has lower overall cost and smaller size than conventional buck-boost converter with PWM controller. [16] [17]

However, RCC is not suitable for high switching current or variable load devices. Because non-linear current gain of transistor varies with switching current and ambient temperature. When the input voltage or load change, the switching current will also change due to non-linearity and affect the voltage stabilization. Besides, other non-linear parameters, such as minority storage time, parasitic capacitors and leakage inductance also have influence on the oscillation cycle [17]. Therefore, peak current control mode is utilized as an open-loop control in RCC.

A buck-boost type RCC circuit topology is shown in Fig3.6 below. A transformer with primary winding L_p and secondary winding L_s is adopted to provide feedforward. And the primary winding works as the inductor in buck-boost converter. Obviously, primary winding L_p, diode D_1, big capacitor C_{big} and R_{load} formed the topology configuration of buck-boost converter as shown in

Fig3.2. Power bipolar junction transistor (BJT) Q_1 is driven by the secondary winding L_s which is connected in series with capacitor C_1 and driver resistor R_2. Diode D_2 is employed to provide a current loop for secondary winding L_s in off-state. Starting resistor R_1 is a big resistor and provides small base drive current before oscillation buildup.

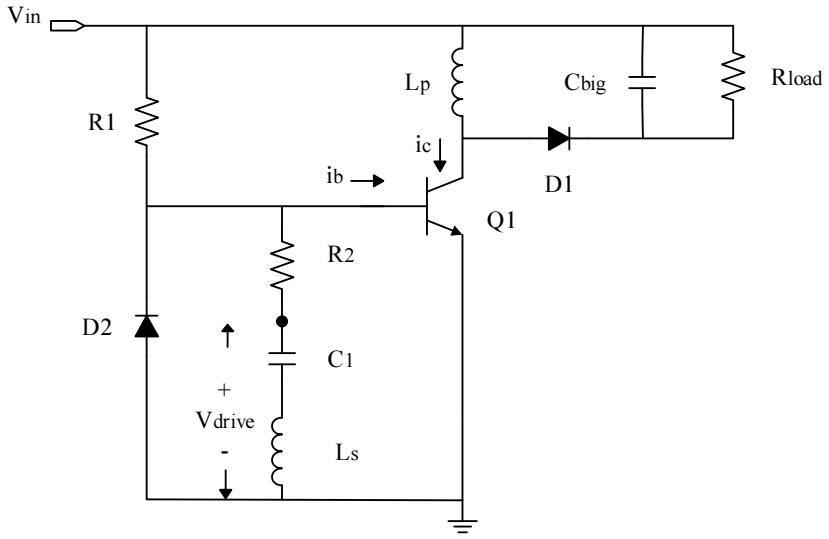

Fig3.6 Circuit topology of buck-boost type RCC

In steady state, self-oscillation of the RCC circuit can be divided into four sections as shown in Fig3.7.

From T_1 to T_2, it is the charging stage: input voltage V_{in} applied on the primary winding L_p. Primary winding current flow into power BJT and energy is accumulated and stored in primary winding. The collector current increase linearly and given by

$$i_c = \frac{V_{in}}{L_p} \cdot t \qquad [3.10]$$

The turns ratio of primary winding and secondary winding is N, so the induced voltage of secondary winding L_s is $\frac{V_{in}}{N}$ and applied the transistor base to provide driver current. Base driving voltage V_{driver} is determined by secondary winding voltage and capacitor C_1 voltage. Assuming that initial voltage of capacitor C_1 is U_o at T_1, then the capacitor C_1 voltage is

$$u_c(t) = U_o \cdot e^{-\frac{t}{\tau}} - (\frac{V_{in}}{N} - V_{R2} - V_{be}) \cdot (1 - e^{-\frac{t}{\tau}}) \qquad [3.11]$$

, where V_{be} is base-emitter drop voltage and V_{R2} is the voltage on R_2.

As the base driving current is provided by capacitor C_1, the base current can be given by

$$i_b(t) = -C_1 \cdot \frac{du_c(t)}{dt} = \frac{\frac{V_{in}}{N} - V_{R2} - V_{be} + U_o}{R_2} \cdot e^{-\frac{t}{\tau}} \qquad [3.12]$$

In this stage, collector current i_c is smaller than $\beta \cdot i_b$, which represents base current multiplied by current gain β of transistor Q_1. Then transistor operates at saturation region. Collector is conducted to ground and collector-emitter voltage V_{ce} is about 0V because of low resistance of BJT.

From T_2 to T_3, it is the transferring stage: With i_b decreasing and i_c increasing, loop gain is reduced to unity, which implies $\beta \cdot i_b$ is equal to i_c, and Q_1 comes to its active region of high resistance at T_2. As a result, the collector-emitter voltage V_{ce} start to increase. When the base current decrease to be low

enough, transistor will be cut off and current flow through primary winding is blocked by transistor. Due to decreasing magnetizing current, magnetomotive force is induced in primary winding. Then the voltage polarity of primary winding and secondary winding are reversed. Collector voltage become higher than input voltage while provide energy to big capacitor and load resistor. The negative direction base current comes from base minority carriers in cutting off process.

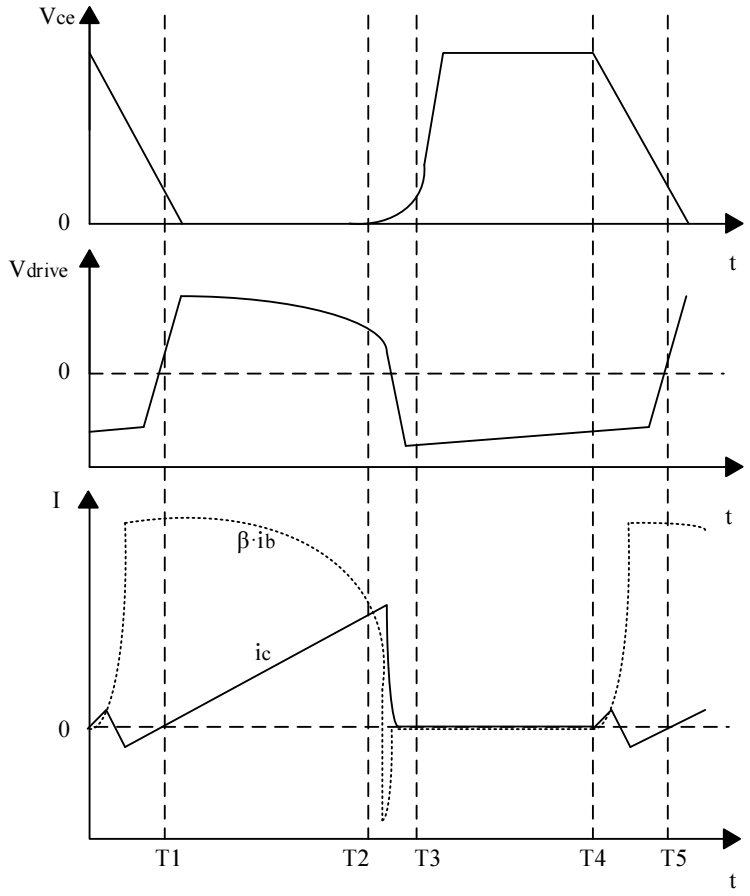

Fig3.7 Waveforms of RCC self-oscillation

From T_3 to T_4, it is the resetting stage: Primary winding induced voltage is output voltage V_{out} and secondary winding has polarity reversed voltage $\frac{V_{out}}{N}$. Assuming the primary winding current is i_{L1} and voltage of capacitor C_1 is U_1 at T_3. Then the primary winding current and capacitor voltage can be expressed as

$$i_L(t) = i_{L1} - \frac{V_{out}}{L_p} \cdot t \qquad [3.13]$$

$$u_c(t) = U_1 \cdot e^{-\frac{t}{\tau}} + (\frac{V_{out}}{N} - V_{R2} + V_{be}) \cdot (1 - e^{-\frac{t}{\tau}}) \qquad [3.14]$$

In this stage, the collector-emitter voltage V_{ce} is the sum of input voltage and output voltage. As the power BJT has been cut off, base current and collector current are near zero. Energy stored in primary winding is consumed by load resistor and capacitor recharging.

From T_4 to T_5, it is the recycling stage: When the energy stored in primary winding has been depleted, the magnetomotive force returns to zero. Energy stored in parasitic capacitor of BJT starts to resonate

with primary winding L_p. Assuming the cycle of resonance is T_r, the secondary winding voltage will reverse its polarity and saturates the BJT Q_1 after $\frac{T_r}{4}$. As a result, the RCC will return back to the charging stage again.

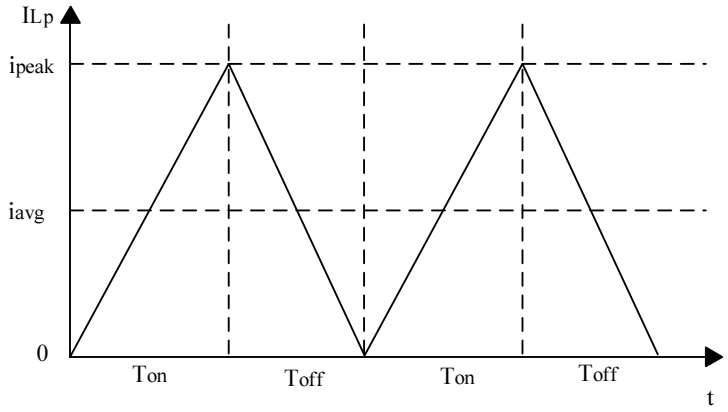

Fig3.8 Primary winding current in boundary conduction mode (CCM/DCM)

The RCC circuit operates at the boundary of continuous/discontinuous conduction mode (CCM/DCM). Primary winding current falls to zero and restart instantly in every self-oscillation cycle as shown in Fig3.8. Output power is determined by the current flow through primary winding. In each cycle, the energy stored in primary winding can be given by

$$W = \frac{1}{2} \cdot {i_{peak}}^2 \cdot L_p = \frac{{V_{in}}^2}{2 \cdot L_p} \cdot {T_{on}}^2 \qquad [3.15]$$

, where i_{peak} is the peak current of primary winding and T_{on} is power BJT conduction time.

Oscillation frequency is determined by inductance of primary winding L_p and input voltage. Higher input voltage and lower inductance result in higher oscillation frequency, which means larger switching energy loss in power transistor. For improving driver efficiency, oscillation should be set as low as possible. However, if the oscillation frequency lower than 20k Hz, driver will make high frequency noise. The lowest oscillation frequency is also limited by transformer size, which is a critical issue in product packaging. Therefore, a compromise have to be made in designing primary winding inductance.

In this project, as RCC circuit is supplied by rectified AC input voltage, this circuit has a variable switching frequency. To achieve constant output power under three different operating points, a peak current mode control module is adopted in this project.

3.2.3 Peak current mode control module

According to equation [3.15], output power is related to peak current and on-state time. Both of these two variables are determined by i_b, i_c and current gain of power BJT. It is possible to control the output power by blocking base current i_b. When the primary winding current reaches a reference value, an access between power transistor base and ground can be built to block the base driving current. Then the power BJT will be prematurely cut off and the output power become lower than that in automatically cut off RCC. As a result, the peak current i_{peak} and output power can be governed by the peak current controller.

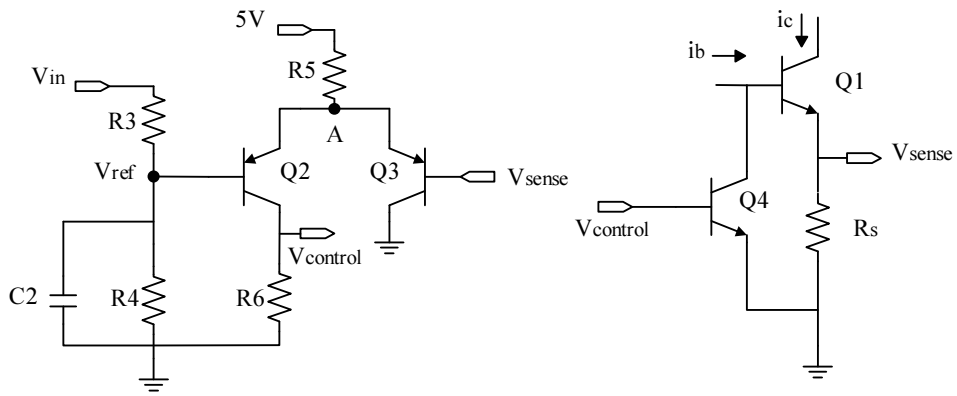

Fig3.9 Peak current mode control module

The peak current mode control module is shown in Fig 3.9. A NPN transistor Q_4 is placed between power transistor Q_1 base and ground to switch off Q_1. When $V_{control}$ is applied on the base of Q_4, Q_4 is switch on and Q_1 will be cut off in advance. The feedback signal $V_{control}$ is generated by a comparator which compare the sense voltage V_{sense} and reference voltage V_{ref}. Sense voltage V_{sense} is the voltage on the sense resistor R_s and represents the primary winding current. Reference voltage V_{ref} comes from the voltage divider, which consists of R_3 and R_4, and it is a fraction of input voltage V_{in}. Comparator is formed by a differential amplifier with two PNP transistors. A current source realized by 5V voltage source and R_5 provides current to these two PNP transistors. With the primary winding current i_c increasing, sense voltage V_{sense} also increases. At beginning, V_{sense} starts to increase from zero. The voltage at point A is equal to base-emitter junction voltage of Q_3, which is lower than V_{ref}. So transistor Q_2 is switch off and all the current from R_5 flow into Q_3. When V_{sense} increase to the same value as reference voltage V_{ref}, V_A is also increased to be high enough to turn on Q_2 and current begins to flow through R_6. Then control voltage $V_{control}$ is generated on R_6 and turn on Q_4. A small capacitor C_2 is connected in parallel with R_4 to filter out high frequency signal. The sense voltage V_{sense} and reference voltage V_{ref} can be briefly illustrated in Fig3.10. In each oscillation cycle, power transistor Q_1 is switched off immediately when V_{sense} increase to the value of V_{ref}. Hence, the peak current has the same envelop curve as input voltage. By employing this peak current mode control module, the peak current is regulated and can be given by

$$i_{peak} = \frac{R_4}{(R_3+R_4)\cdot R_s} \cdot V_{in} \qquad [3.16]$$

Combined with equation [3.1] and [3.2], then the switch time T_{on} and T_{off} can be derived,

$$i_{peak} = \frac{R_4}{(R_3+R_4)\cdot R_s} \cdot V_{in} = \frac{V_{in}\cdot T_{on}}{L} = \frac{V_{out}\cdot T_{off}}{L} \qquad [3.17]$$

$$T_{on} = \frac{R_4\cdot L}{(R_3+R_4)\cdot R_s} \qquad [3.18]$$

$$T_{off} = \frac{R_4\cdot L}{(R_3+R_4)\cdot R_s} \cdot \frac{V_{in}}{V_{out}} \qquad [3.19]$$

According to these equations, it is obvious that the current peak is proportional to the input voltage. On-state time is determined by peak control module resistors and primary winding inductance. Due to the constant output voltage determined by TLED lamp, off-state time is proportional to input voltage. Therefore, the oscillation frequency has lowest value in input voltage peak.

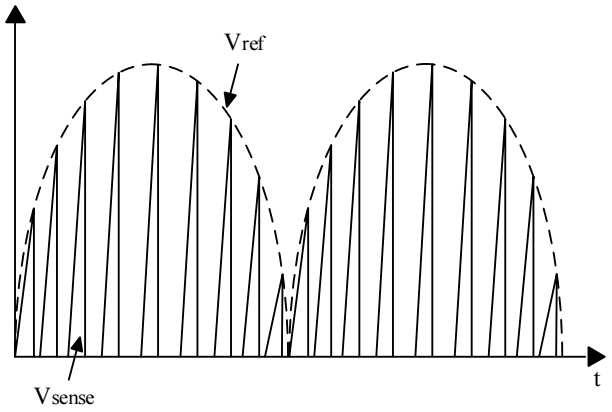

Fig3.10 Simplified waveforms of sense voltage V_{sense} (solid) and reference voltage V_{ref} (dashed)

Because the RCC circuit operates at the boundary of continuous/discontinuous conduction mode (CCM/DCM), average current of primary winding is close to the input voltage. As a result, impedance characteristic of RCC circuit with current peak mode control is near-resistive. Some research have demonstrated that this near-resistive driver can keep the power distribution balance in dual-lamp or three-lamp ballast series connection configuration. This can be explained by the simplified series connection system configuration shown in Fig3.11. For an example, when voltage disturbance occur in this system, driver1 voltage u_1 increase and driver2 voltage u_2 decrease. If the driver is resistive, driver1 current i_1 will increase with voltage u_1. Due to constant total current i_{total}, the current flowing in capacitor1 will be reduced and the voltage on driver1 u_1 will be pulled back to balance point. On the contrary, constant power driver, which has negative differential resistive characteristics, can be seen as a counterexample in this situation. Different from resistive driver, driver1 current i_1 will decrease for keeping driver constant power and u_1 will further increase. As a result of this regenerative feedback, the voltage u_1 will continuously increase and driver2 will be turned off. That's why this driver is designed to be near-resistive rather than a constant power load.

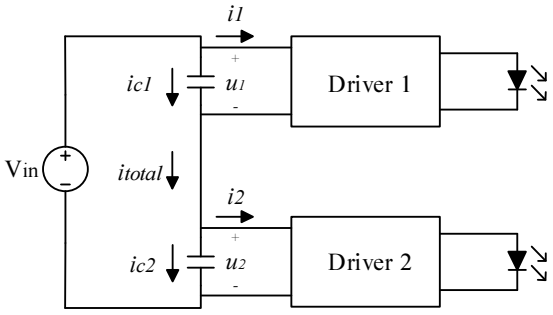

Fig3.11 Simplified series connection system configuration

As peak current mode control belongs to open loop control, line regulation performance of this driver is not so satisfactory. One possible solution is adding DC voltage component to reference voltage to improve line regulation performance while driver input power factor will decrease as compromise.

For three different ballast operating points, reference voltage V_{ref} should be altered to achieve constant output power under different input voltages. This can be done by changing the reference resistor R_4 due to the relation between i_{peak} and R_4 as shown in equation [3.16]. For single-lamp ballast, which outputs high voltage for driver, the reference resistor R_4 should be set with low

resistance to limit peak current. On the other hand, for three-lamp ballast, which outputs low voltage for per driver, the reference resistor R_4 should be set with high resistance to increase the peak current. Therefore, the driver designed in this project have three operating modes, each of them corresponds to a ballast operating point. Operating mode is selected by a detection module and realized by altering reference resistor R_4. The detection module is not included in this master project but is a subproject belonging to the Philips T12 retrofit TLED project. Its function is detecting type of ballast and switching reference resistor R_4.

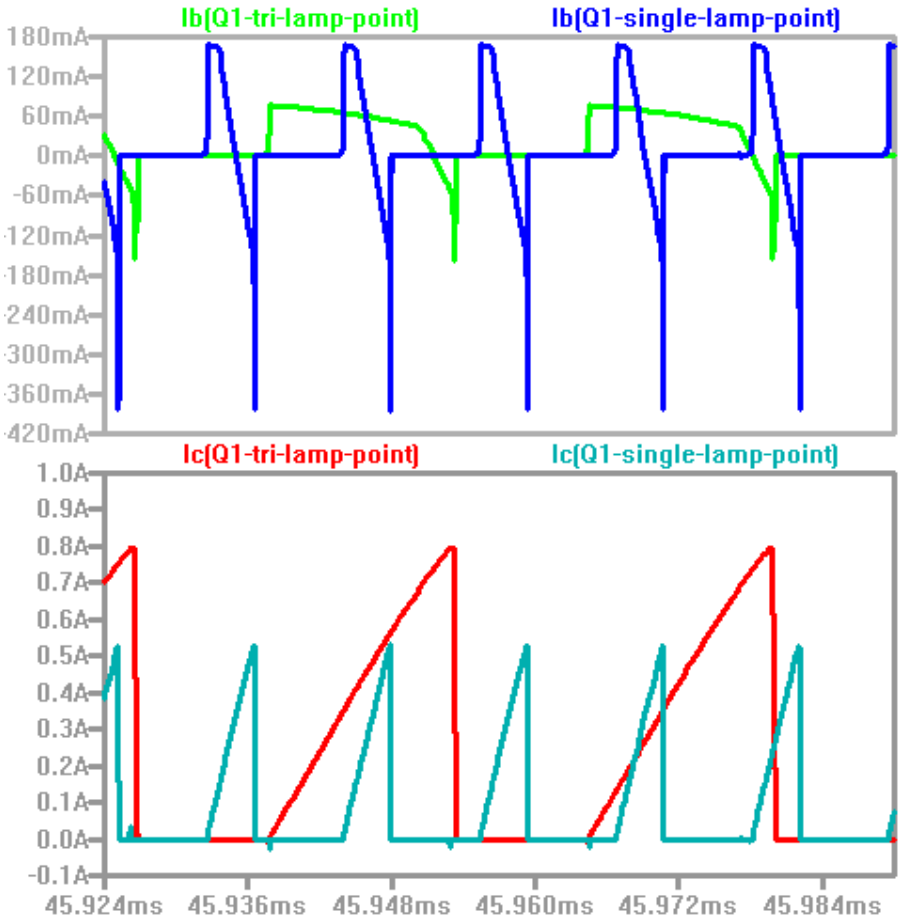

Fig3.12 Peak current and driving current waveforms in LTspice simulation

According to equation [3.12], driving current $i_b$is proportional to input voltage. However, for achieving constant output power, primary winding peak current operating in single-lamp ballast should be lower than that in three-lamp ballast. Obviously, for the three ballast operating points, high driving current is linked to low peak current, while low driving current is linked to high peak current. LTspice simulation of RCC with current peak mode control illustrates this negative correlation between peak current and driving current in Fig3.12. In the simulation, by altering resistor R_4, RCC driver outputs the constant power (14W) under 80V and 205V input voltage separately. Fig3.12 shows simulation results of base current and collector current. The blue waveform and green waveform represent the base current of power transistor Q_1 operating in single-lamp ballast point and in three-lamp ballast points, respectively. The peak value of green waveform is about 80mA while the blue waveform has a peak value about 170mA. So the power transistor has higher driving base current in single-lamp ballast operating point as previous explained. On the contrary, the power transistor collector current in

single-lamp ballast operating point, which is indicated by cyan waveform and has about 0.5A peak value, is lower than that in three-lamp ballast operating point as shown by the red waveform.

For the driver design, some problems are caused by this negative correlation. When the driver operates at single-lamp ballast point, excess driving current i_b leads the power transistor Q_1 into deep saturation and extends its switching off time. This over drive problem destructs the function of peak current mode control module. Meanwhile, excess driving current means power loss. Both of these two problems have bad effects on driver efficiency.

3.2.4 Emitter switching and proportional drive techniques

To solve these problems caused by negative correlation, emitter switching and proportional drive techniques are employed in the driver.

Besides aforementioned components in RCC circuit, a low voltage transistor Q_4 is added in the emitter of the power transistor Q_1 to form a cascade configuration as shown in Fig3.13. The power transistor Q_1 is controlled by the low voltage transistor Q_5. When Q_5 is switch on, the current in Q_1 flows from collector to emitter as the blue arrows indicated in Fig3.13. When Q_5 is switched off, the Q_1 emitter current is cut-off and all the collector current is diverted to the Q_1 base as the red arrow indicated in Fig3.13. The power transistor Q_1 and the low voltage transistor Q_5 are respectively driven by a high-voltage base driving circuit and a low-voltage base driving circuit. [18]

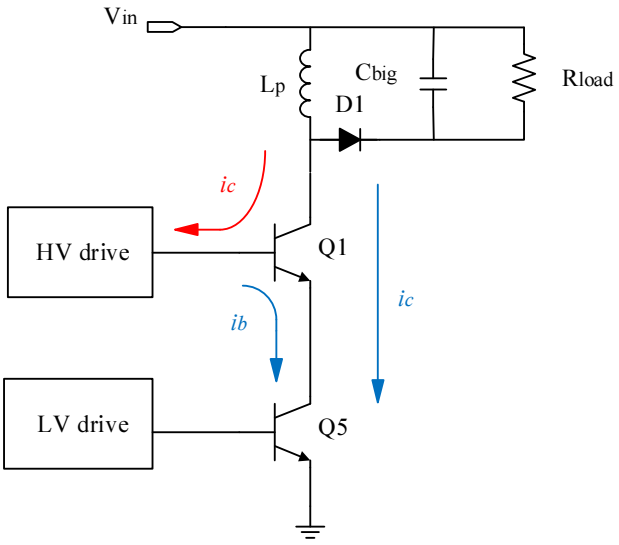

Fig 3.13 Emitter switching configuration

Emitter switching technique is an effective technique to decrease the storage time and switching power loss of the power transistor. This permit can be explained by bipolar junction transistor switching characteristics and switch-off mechanism of emitter switching. As a switch, BJT operates at saturation region and cut-off region. Minority carrier distributions of the NPN bipolar transistor operating in cut-off and in saturation are shown in Fig3.14. In this figure, thermal-equilibrium minority carrier concentrations in the emitter, base, and collector are indicated by dash lines with parameters p_{E0}, n_{B0} and p_{C0}, respectively. The steady-state minority carrier concentrations in the emitter, base and collector are expressed by functions $p_E(x)$, $n_B(x)$ and $p_C(x)$ and denoted with solid lines, respectively.

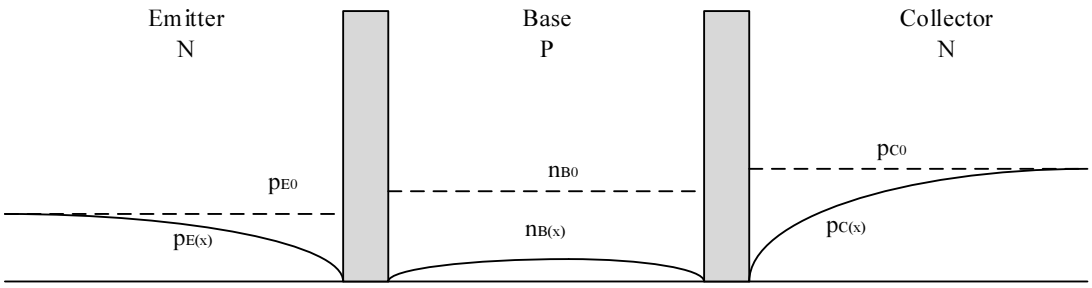

(a)

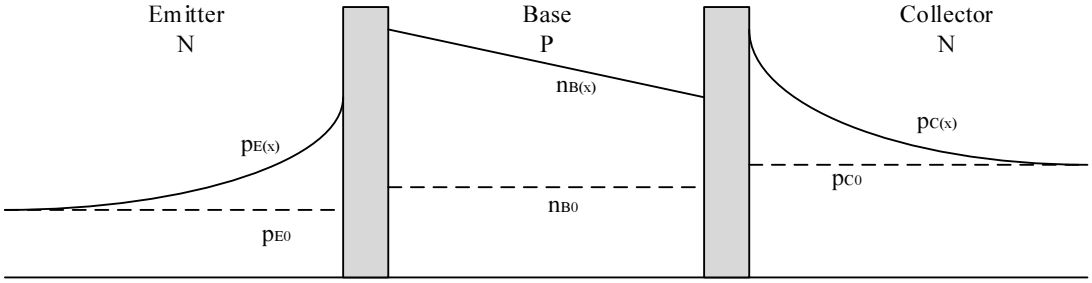

(b)

Fig3.14 Minority carrier distribution of the NPN bipolar transistor operating in (a) cut-off

(b) saturation

The concentrations of minority carrier at the edge of each space charge region can be given by

Right side of B-E junction: $$p_E(x) = p_{E0} \cdot \exp(\frac{q \cdot V_{EB}}{kT}) \quad [3.20]$$

Left side of B-E junction: $$n_B(x) = n_{B0} \cdot \exp(\frac{q \cdot V_{EB}}{kT}) \quad [3.21]$$

Right side of B-C junction: $$n_B(x) = n_{B0} \cdot \exp(\frac{q \cdot V_{CB}}{kT}) \quad [3.22]$$

Left side of B-C junction: $$p_C(x) = p_{C0} \cdot \exp(\frac{q \cdot V_{CB}}{kT}) \quad [3.23]$$

, where $k = 1.38 \times 10^{-23} J/K$ is the Boltzmann constant, T is the absolute temperature, and $q = 1.6 \times 10^{-19} C$ is the charge of electron. Junction voltage V_{EB} and V_{CB} can be positive or negative. As the base width x_B is small enough compared with the minority carrier diffusion length L_B, is short enough, minority concentration in the base can be expressed by linear approximation. [19] Obviously, base minority carrier concentration in saturation are much higher than that in cut-off. These extra charges stored in saturated transistor results in switching time delay.

In regular transit switching process, as shown in Fig3.15, switching-on and switching-off have some time delay. During T_0 to T_1, the transistor switches from cut-off region to saturation region. Base current supplies charge to bring the B-E junction from reverse bias to forward bias. Then carriers are injected into the base so that the gradient of the minority carrier electron concentration in the base increases, causing the collector current to increase. After T_1, the transistor operates in saturation region and this means it has been switched on. During T_2 to T_3, the base current reverses its direction to remove extra stored carriers from the emitter and base regions. Initially, the collector current doesn't change significantly, because both the B-C junction and B-E junction are forward biased and the gradient of the minority carrier concentration in the base does not change instantaneously.

Collector current decrease significantly when base extra minority carriers are removed by reverse direction base current and B-C junction is reverse biased. The delay time between T_2 and T_3 is called storage time which is usually the most important parameter in the switching speed of the bipolar transistor. During T_3 to T_4, excess carriers in the base are still being removed and collector current falls to zero. [19]

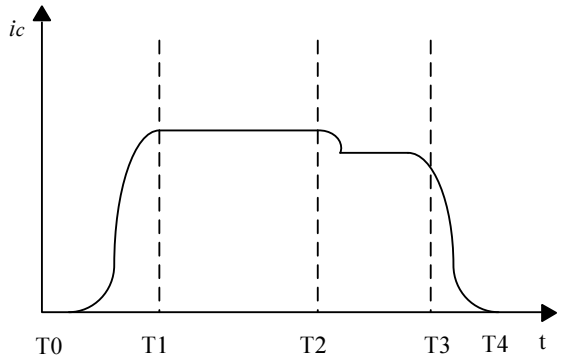

Fig3.15 Collector current versus time during transistor switching

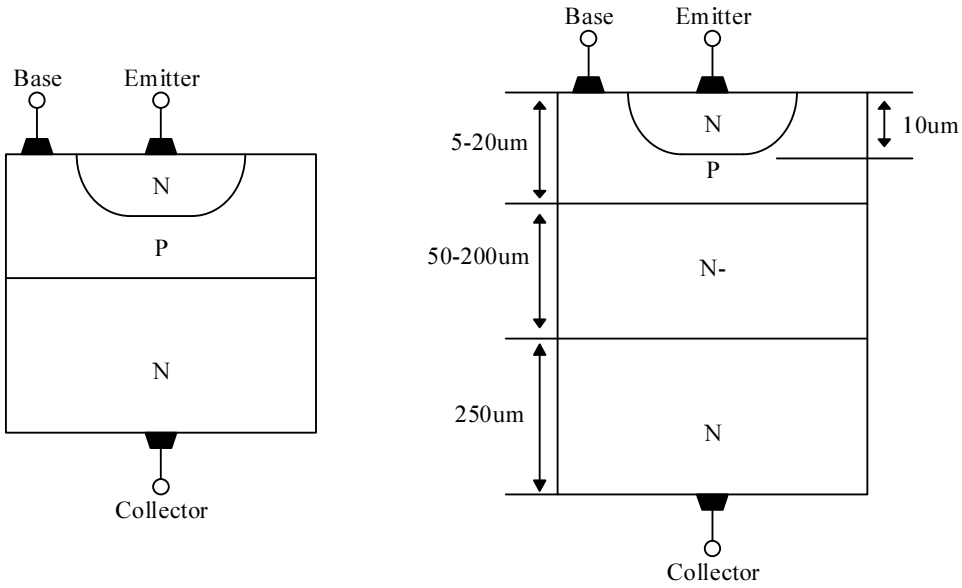

(a) (b)

Fig3.16 Simplified low voltage bipolar transistor (a) and power bipolar transistor (b) structures

Compared with regular low voltage bipolar transistor, power bipolar transistor has longer storage time due to its special structure. The simplified low voltage bipolar transistor and power bipolar transistor structures are shown in Fig3.16, respectively. To obtain larger breaking voltage, a lightly doped layer called the collector drift region is added between base layer and collector layer. Meanwhile, base width of power bipolar transistor is extended to accommodate collect-base depletion region under high voltage. Due to wider base and additional collector drift region, operating in saturation region, power bipolar transistor stores more extra minority carriers compare with low voltage transistor. As previous explained, these additional extra minority carriers result in longer storage time of power bipolar transistor.

The reason why emitter switching technique can effectively reduce transistor storage time is that the negative base current is provided by the collector current. When Q_5 is switched off, the collector current of Q_1 is diverted to the Q_1 base and remove all the charges stored in the base. As collector current is much larger than base current, emitter switching removes extra minority carriers more quickly than regular transistor and shortens the storage time of power transistor. In this way, both of the fall time and the switching power loss of power transistor Q_1 are reduced. Difference in reverse base current can be illustrated in the LTspice simulation result as shown in Fig3.17. Under the same input voltage and output power condition, reverse base current in emitter switching, as indicated by blue waveform, has much higher peak value than that in regular RCC circuit, which is represented by red waveform. Meanwhile, the collector current in emitter switching is also simulated and shown by green waveform. The reverse base current peak value is close to the collector current peak value. This demonstrates that the reverse base current is provided by the collector current.

As the power transistor switching-off power loss can be simply given by

$$W_{loss}(switching-off) = \frac{1}{6} \cdot V_{CE} \cdot I_{peak} \cdot T_{off} \quad [3.24]$$

, where T_{off} is switching-off time and I_{peak} is the peak value power transistor collector current. Stronger reverse base current means shorter switching-off time and less switching power loss.

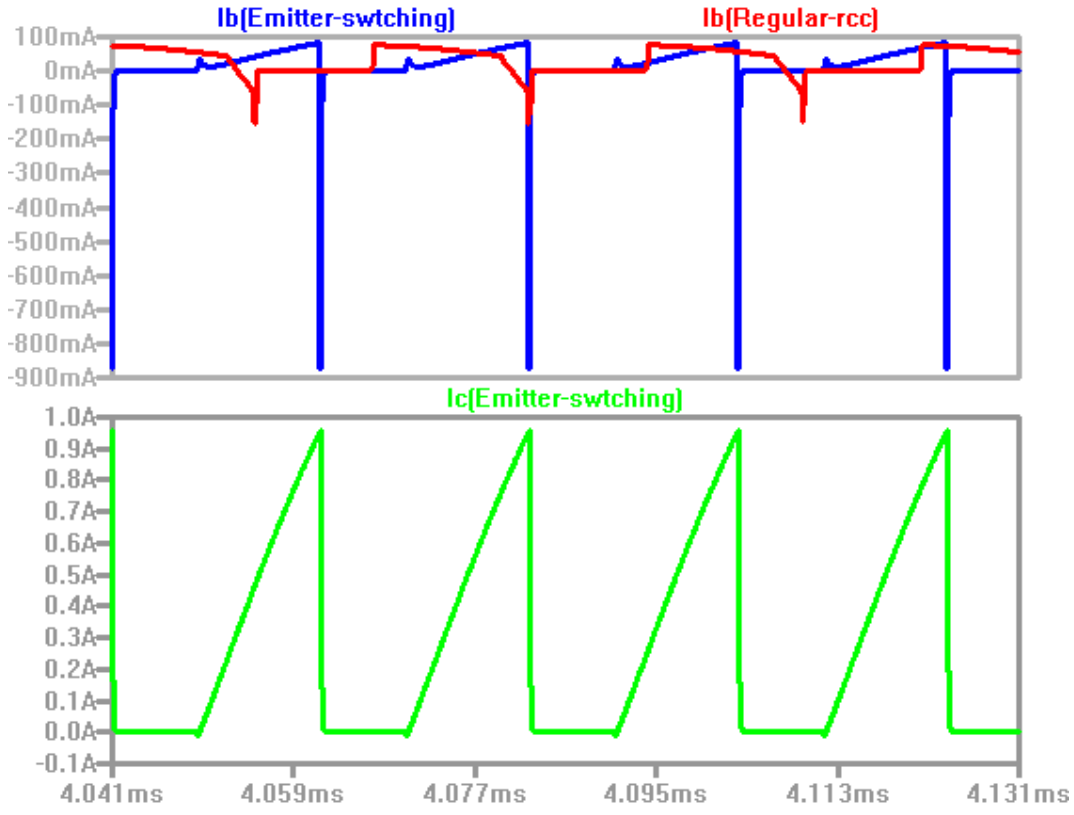

Fig 3.17 Reverse base current simulation of emitter-switching and regular RCC in LTspice

As a low voltage transistor, Q_5 has short storage time and low switching power loss. Although the low voltage transistor Q_5 itself also has some power loss and storage time, these defects can be counteracted by merits it brought. Compared with the performance improving in power transistor Q_1, delay time and power loss caused by Q_5 are acceptable.

Another merit brought by emitter switching is high breakdown voltage. Power bipolar transistor has higher breakdown voltage in emitter switching than in regular RCC circuit. This can be explained by transistor avalanche breakdown mechanism. Fig3.18 illustrates transistor configuration and saturation current with emitter open (a) and base open (b). When the emitter is left open and a reverse bias voltage applied on base-collector junction, as shown in Fig3.18 (a), the current flow through the transistor is the reverse junction current I_{CBO}. Assuming the base-collector breakdown voltage is BV_{CBO}, when reverse bias voltage increases to BV_{CBO} and avalanche breakdown occurs, saturation current will increase to $M \cdot I_{CBO}$. The M is multiplication factor and can be given by an empirical approximation,

$$M = \frac{1}{1-\left(\frac{V_{CB}}{BV_{CBO}}\right)^n} \qquad [3.25]$$

, where n is an empirical constant, usually between 3 and 6.

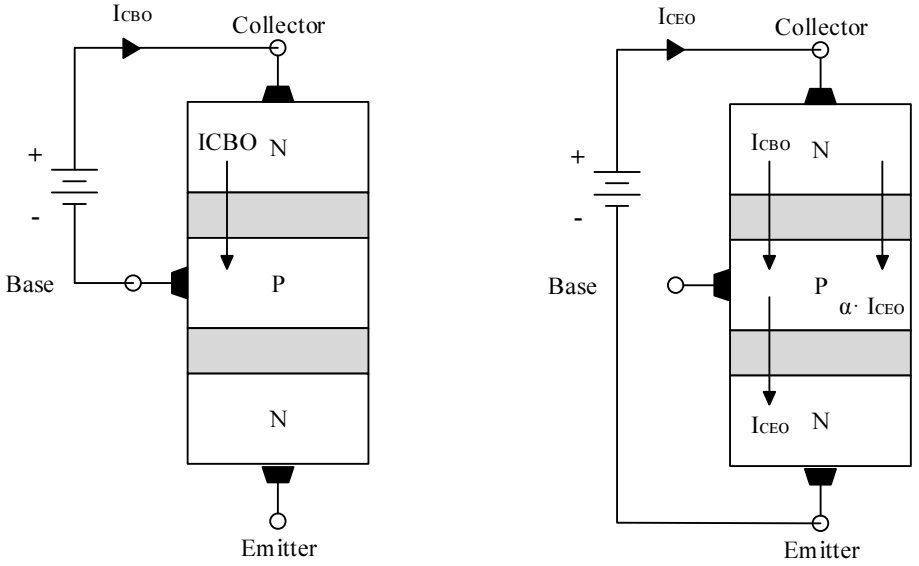

Fig3.18 Transistor configuration and saturation current with emitter open (a) and base open (b)

When the base is left open and the voltage is applied on collector-emitter junction, as shown in Fig3.18 (b), the current flowing in this connection configuration is I_{CEO}. In this situation, base-collector junction reverse biased and normal reverse-biased current I_{CBO} flows from collector to base. Part of this current I_{CBO} belongs to the flow of minority carrier holes from collector across the base-collector space charge region into the base. These injected holes make the base positive with respect to the emitter, and the base-emitter junction becomes forward biased. Then minority carrier electrons in emitter are injected into base and diffuse across the base toward the base-collector junction. After recombination processes in base, the electrons reach the base-collector junction and this current component is $\alpha \cdot I_{CEO}$. Coefficient α is the common base current gain, its relation with the common emitter current gain β can be given by

$$\alpha = \frac{\beta}{1+\beta} = \frac{I_C}{I_E} \qquad [3.26]$$

And reverse-based current I_{CEO} and I_{CBO} can be written as

$$I_{CEO} = \alpha \cdot I_{CEO} + I_{CBO} = \frac{I_{CBO}}{1-\alpha} \approx \beta \cdot I_{CBO} \quad [3.27]$$

When the avalanche breakdown occurs in this connection configuration, the current in the base-collector junction are multiplied, therefore,

$$I_{CEO} = M(\alpha \cdot I_{CEO} + I_{CBO}) \quad [3.28]$$

$$I_{CEO} = \frac{M \cdot I_{CBO}}{1-\alpha M} \quad [3.29]$$

For avalanche breakdown, corresponding condition is

$$\alpha M = 1 \quad [3.30]$$

Assuming the collector-emitter voltage is BV_{CEO} at avalanche breakdown, and primarily applied on the reverse biased base-collector junction. Then have $V_{CB} \approx V_{CE}$ and

$$M = \frac{1}{1-\left(\frac{BV_{CEO}}{BV_{CBO}}\right)^n} = \frac{1}{\alpha} \quad [3.31]$$

$$\frac{BV_{CEO}}{BV_{CBO}} = \sqrt[n]{1-\alpha} \quad [3.32]$$

According to equation [3.26], obtain $1 - \alpha = \frac{1}{1+\beta} \approx \frac{1}{\beta}$, equation [3.32] can also be written as

$$\frac{BV_{CEO}}{BV_{CBO}} = \frac{1}{\sqrt[n]{\beta}} \quad [3.33]$$

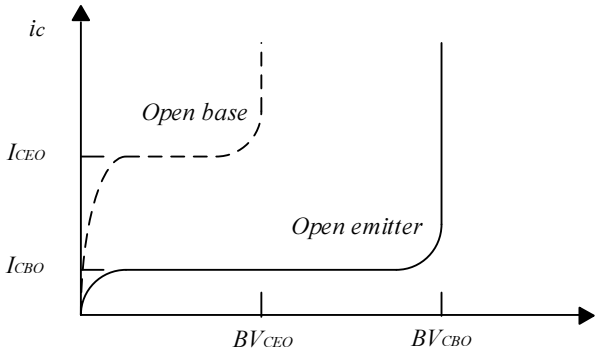

Fig 3.19 Relative breakdown voltages and saturation currents of the open base and open emitter configurations [19]

The breakdown voltage in the open-base configuration is smaller, by the factor $\sqrt[n]{\beta}$, than the break voltage in the open-emitter configuration. This characteristic is shown in Fig3.19. [19]

Due to this breakdown voltage characteristic, power transistor in emitter switching connection configuration withstands higher voltage. In switching off process, power transistor in emitter switching leaves its emitter open and input voltage applies on base-collector junction. So the highest input voltage is determined by BV_{CBO} of the power transistor. For regular RCC circuit, the highest input voltage is BV_{CEO} of the power transistor because of open base connection configuration in switching off.

In conclusion, emitter switching technique not only shortens power transistor storage time but also improves power transistor capability of withstanding high input voltage.

Besides emitter switching technique, proportional drive technique is also employed in this driver for solving the over-drive problem caused by negative correlation between primary winding peak current and base driving current. In this project, proportional drive technique is realized by a current transformer, as shown in Fig3.20, which couples primary winding L_{cp} and secondary winding L_{cs} together. Turns of current transformer are coiled around a small ringcore and turns ratio of primary winding L_{cp} to secondary winding L_{cs} is $\frac{N_1}{N_2}$. Then the current ratio can be given by

$$\frac{i_{LCP}}{i_{LCS}} = \frac{V_{LCS}}{V_{LCP}} = \frac{N_2}{N_1} \quad [3.34]$$

, where $N_1 < N_2$. Diode D_3 and resistor R_7 are added and parallel to L_{cp} to absorb over shoot voltage caused by the leakage inductance of the current transformer. A Schottky diode is connected with L_{cs} in series to rectify the current direction.

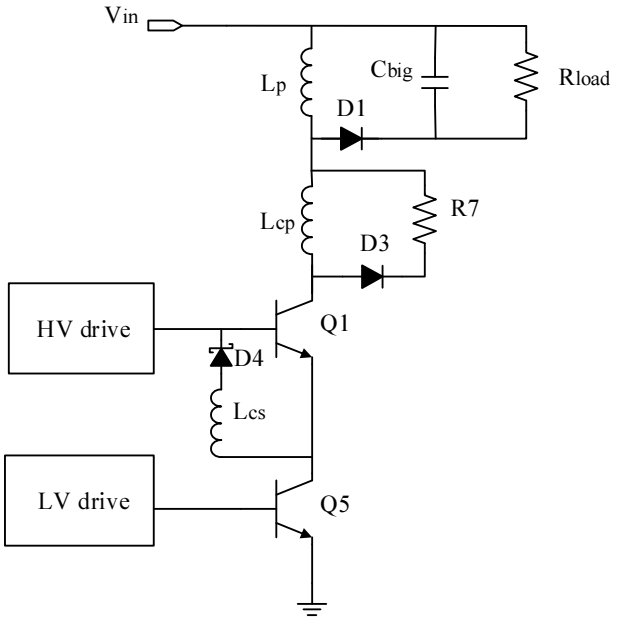

Fig3.20 Proportional drive technique realized by current transformer

In this driver, current flow through L_{cp} , which only has few turns and small inductance, is same to the collector current of power transistor Q_1. Meanwhile, compared with regular RCC circuit, a large proportion of the base driving current is provided by L_{cs} rather than base driving circuit. Therefore, the base driving current is proportional to collector current of power transistor Q_1 and can be determined by current transformer turns ratio. In LTspice simulation, a current transformer, with 10 turns ratio, is implemented in the emitter switching circuit to provide proportional base current. The simulation result of base current and collector current are indicated by blue waveform and green waveform in Fig3.21, respectively. Obviously, base current value multiplied by 10 is close to the value of collector current, so it is demonstrated that base current is proportional to and determined by collector current. By adopting this current transformer, the over-drive problem caused by negative correlation can be solved.

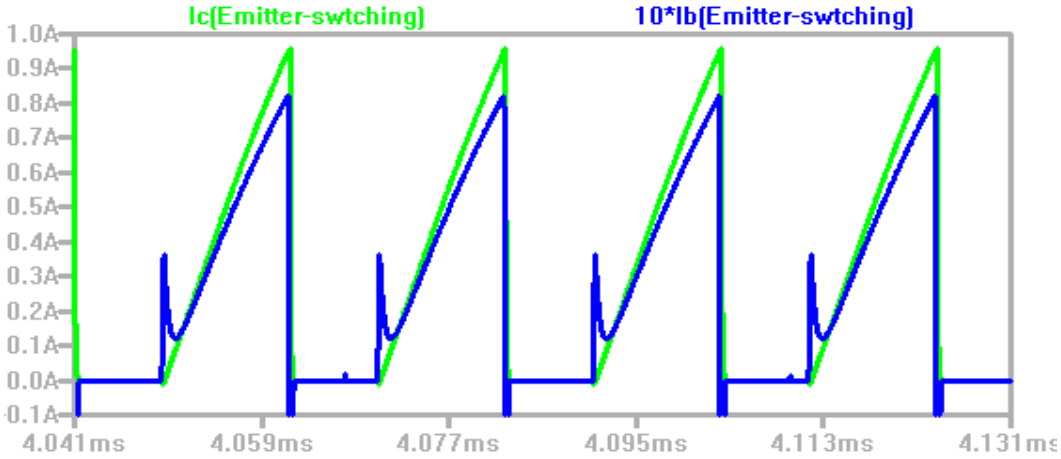

Fig 3.21 Proportional base current (blue) and collector current (green) in LTspice simulation

3.2.5 High-voltage and low-voltage base driving circuits

With the help of emitter switching and proportional drive techniques, the switching power loss and switching performance of power transistor can be optimized. A high-voltage base driving circuit and a low-voltage base driving circuit are designed to drive power transistor Q_1 and low voltage transistor Q_5, respectively. As power transistor Q_1 can be switched off by low voltage transistor Q_5 in emitter switching configuration, the peak current control is realized through controlling on-off state of Q_5. The low-voltage base driving circuit outputs logic control signal based on $V_{control}$ signal, which is generated from the current peak mode control module, and controls low voltage transistor Q_5. After both of Q_1 and Q_5 have been switched on, a large proportion of the base driving current is provided by L_{cs} rather than high-voltage drive circuit. So the high-voltage base driving circuit only needs to generate a small driving pulse current to turn on Q_1 at the beginning of each cycle. Meanwhile, a start-up circuit is designed to provide current to turn on Q_1 and Q_5. The high-voltage and low-voltage base driving circuits combined with start-up circuit are drawn and illustrated in Fig3.22 below.

The start-up circuit is circled by blue dash line. Before self-oscillation built up, capacitor C_3 voltage is zero and Q_6 base voltage is equal to the Zener diode breakdown voltage 15V. Then high voltage transistor Q_6 is switched on and charges capacitor C_3. After the self-oscillation has been built, capacitor C_3 can be charged by the reverse base current from power transistor Q_1. So the voltage on capacitor C_3 become higher than 15V due to forward drop voltage of D_8, and transistor Q_6 is switched off. Owing to strong current driving capability of bipolar transistor, driver have enough current to turn on Q_1 and Q_5 and start up self-oscillation quickly. Compared with the starting resistor used in regular RCC circuit, start-up circuit is able to switch off automatically after self-oscillation has been built up, which means less energy loss and better efficiency. In parameters setting, R_{12} is much larger than R_{13} because of current gain of the transistor.

As for the high-voltage base driving circuit, which is circled by red dash line, it has a small capacitor connected with voltage transformer secondary winding L_s. At the beginning of each oscillation cycle, this small capacitor C_5 generates a small driving pulse current to turn on Q_1. Meanwhile, this small driving pulse current is regulated by the resistor R_{10}. After this, as previous mentioned, the base current is mainly provided by the secondary winding of the current transformer. And the base driving current is not affected by input voltage anymore. When Q_1 is switching off, reverse base current is equal to collector current. The diode D_7 diverts this reverse base current to capacitor C_3. Resistor R_{11} is used to provide initial current in start-up process.

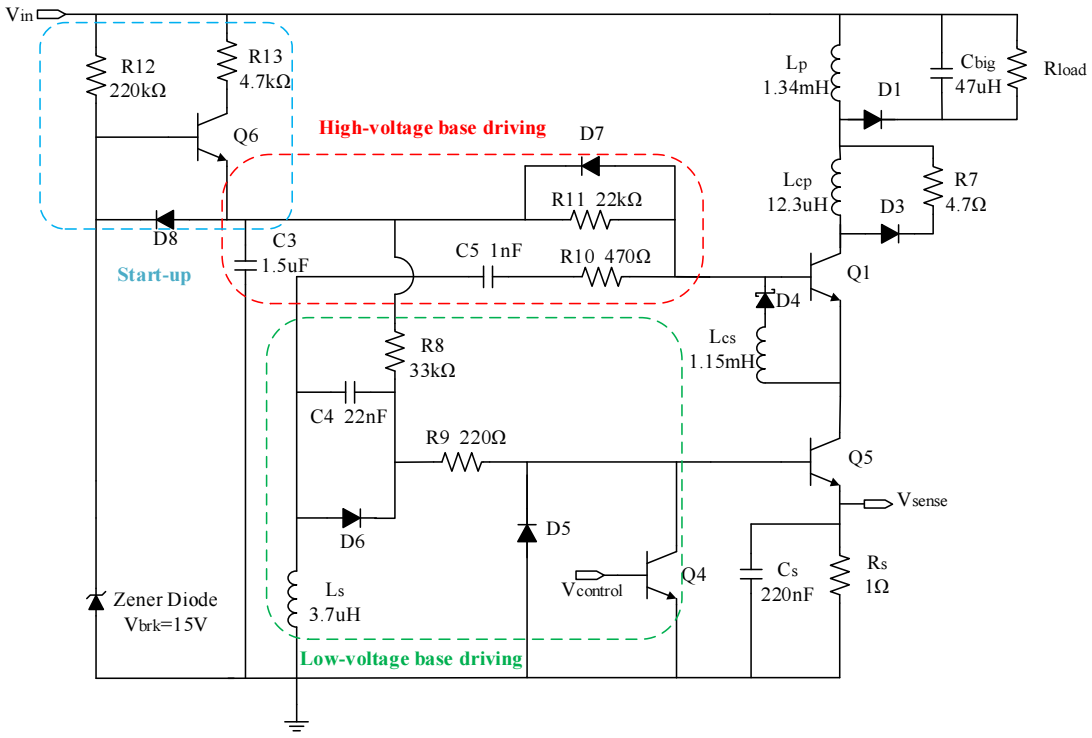

Fig3.22 high-voltage and low-voltage base driving circuits combined with start-up circuit

Low-voltage base driving circuit is controlled by signal from peak current mode control module. The control method is by using transistor Q_4 to pull down Q_5 base voltage, which is same to that in regular RCC circuit shown in Fig3.9. Base driving current of Q_5 is provided and regulated by R_9. Similar to high voltage base drive module, a driving pulse current is generated by capacitor C_4 to turn on Q_5. No matter in start-up or in steady oscillation, Q_1 should be turned on prior to Q_5. So the starting resistor R_8 has higher resistance than R_{11} and time constant of R_9 and C_4 is larger than time constant of R_{10} and C_5 to make sure switching on of Q_5 lags Q_1.

As stated earlier, primary winding current is sensed by resistor R_s. For keeping the pull down capability of Q_4 during switching off process, a small capacitor C_s is added in parallel with R_s. This small capacitor extends the voltage stepping down time in R_s.

3.2.6 5V regulator realized by TL431

In steady state, capacitor C_3 is charged by reverse direction base current from power transistor while doesn't have any access to discharge due to high resistance of R_{11}. So the voltage on C_3 will continuously increase until Zener diode clamping C_3 voltage and building a path for C_3 to discharge. For utilizing the energy stored in C_3, a 5V regulator realized by TL431, as shown in Fig3.23, is connected to C_3. In this regulator, TL431 chip is adopted to generate 2.5V reference voltage and apply this reference voltage on the middle of a voltage divider, which consists of R_{15} and R_{16}. Due to the same resistance of R_{15} and R_{16}, output voltage is double reference voltage, namely 5V. Capacitor C_6 and C_7 are employed to reduce ripple in reference voltage and 5V output voltage, respectively. This generated 5V constant voltage can be used in aforementioned peak current mode control module. [20]

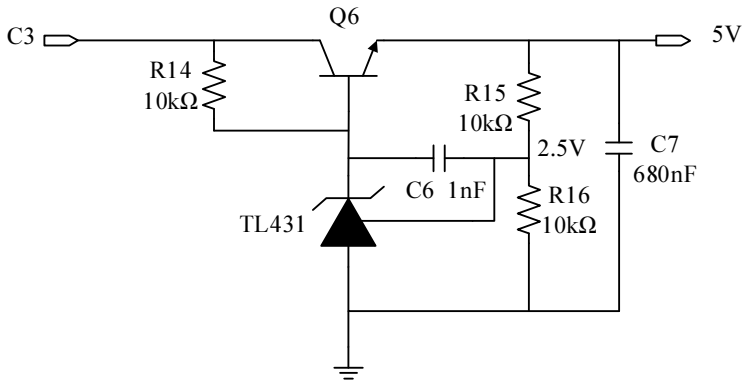

Fig3.23 5V regulator realized by TL431

3.3 Block diagram and simulation of designed driver circuit

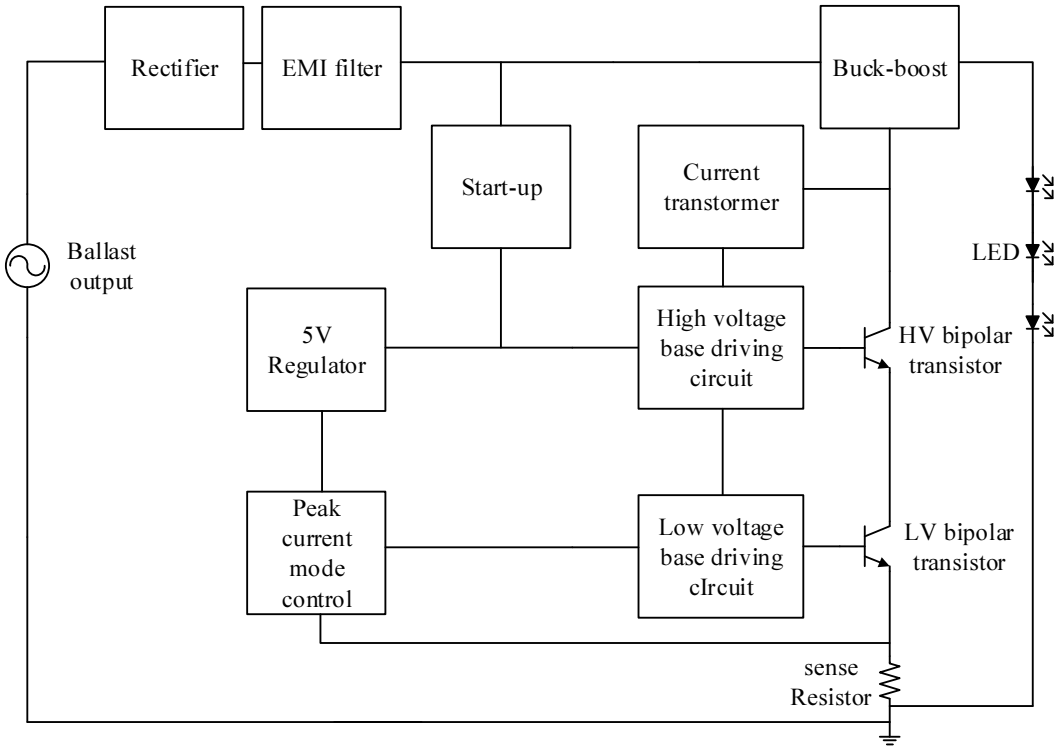

Fig3.24 Block diagram of designed driver circuit

Functional modules have been introduced in last section. By adopting these functional modules, a wide input voltage range driver is realized and tested compatible with different T12 EM ballasts. The block diagram of this driver is illustrated in Fig3.24.

The rectifier module and EMI filter module in block diagram are employed to rectify driver input voltage and filter out high-frequency component. Output voltage of buck-boost is determined by the LED forward voltage, whose value is about 150V in this project. Peak current mode control module senses the voltage on sense resistor and controls low-voltage base driving module. The 5V regulator module supplies the peak current mode module. Other modules and operating principles have been explained in previous sections.

Modules have been separately simulated in LTspice and their principles have been proven. For demonstrating the whole designed driver operating principle, the designed driver circuit is built in LTspice and simulated with different input voltage. The circuit built in LTspice is shown below in Fig3.25.

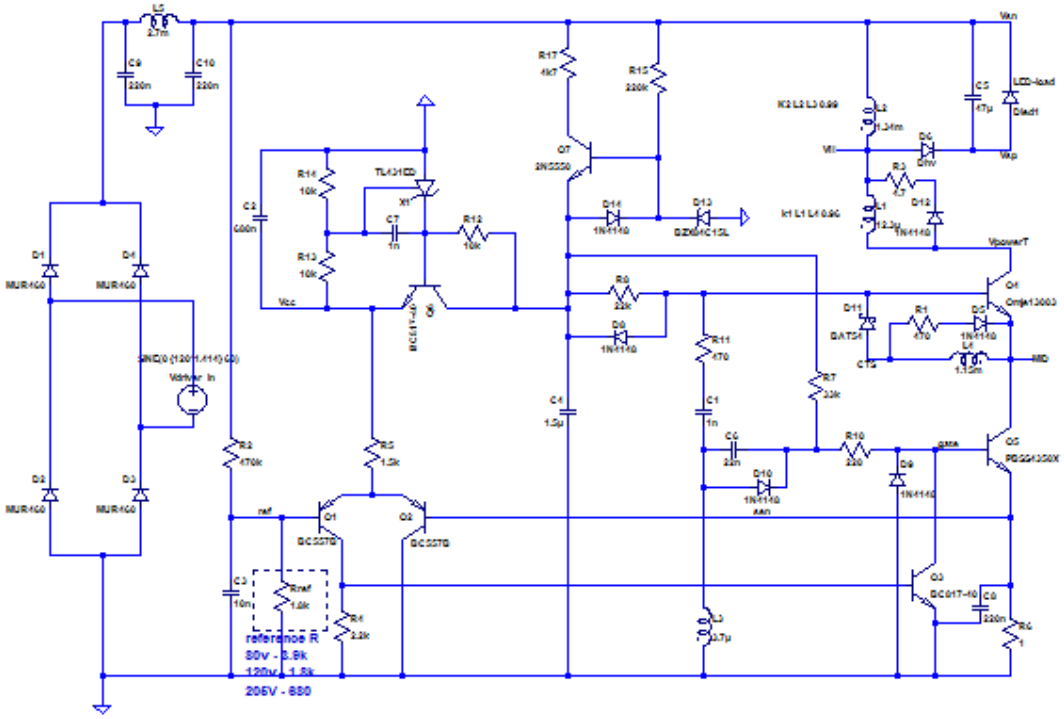

Fig3.25 Driver circuit built in LTspice

Simulation results of whole driver circuit under 80V, 130V and 205V are illustrated in Fig 3.26 separately. By altering the reference resistor, designed driver is able to output constant power to LED load, about 14W. The buck-boost module operates in peak current control mode. Because the envelop curve of the sense voltage follows the reference voltage, it is proven that the peak current mode control module switch off power transistor timely without over shoot. Meanwhile, negative correlation between input voltage and primary winding peak current is also illustrated in these simulation results. This negative correlation simulation result has been explained in previous section.

LTspice simulation results prove that designed driver can work properly in three ballast operating points and output constant power for the LED load.

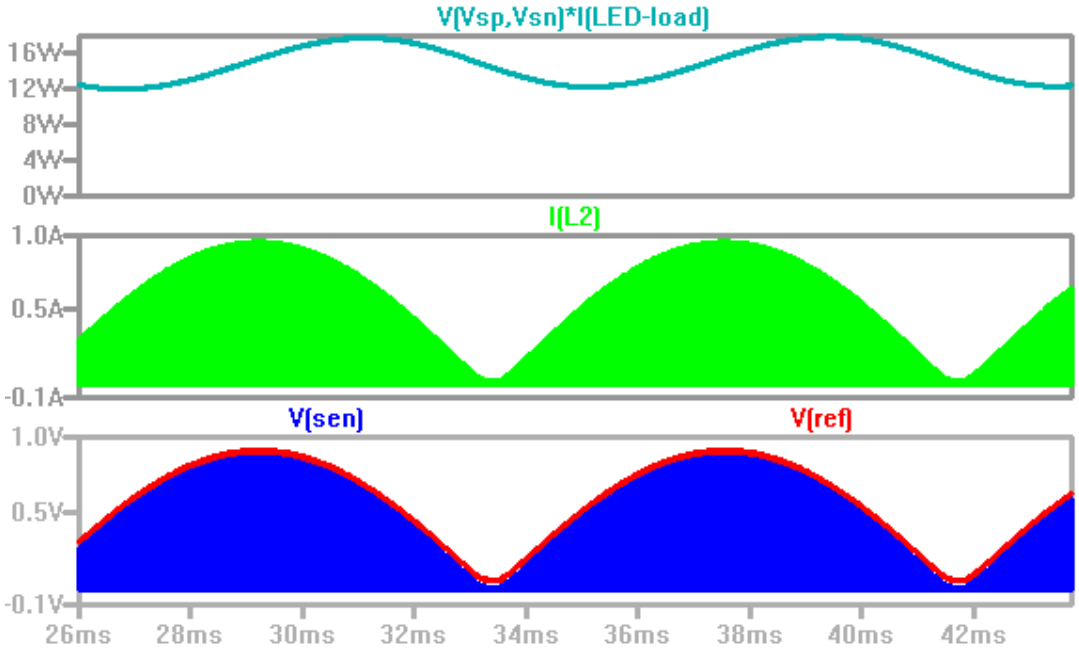

(a) 80V input voltage

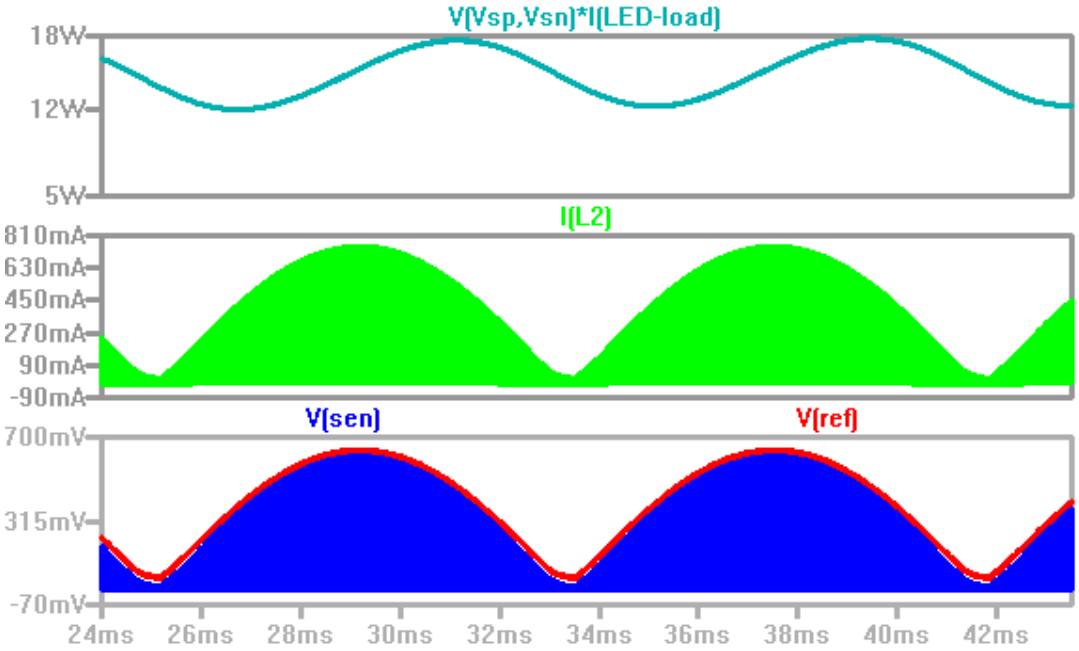

(b) 130V input voltage

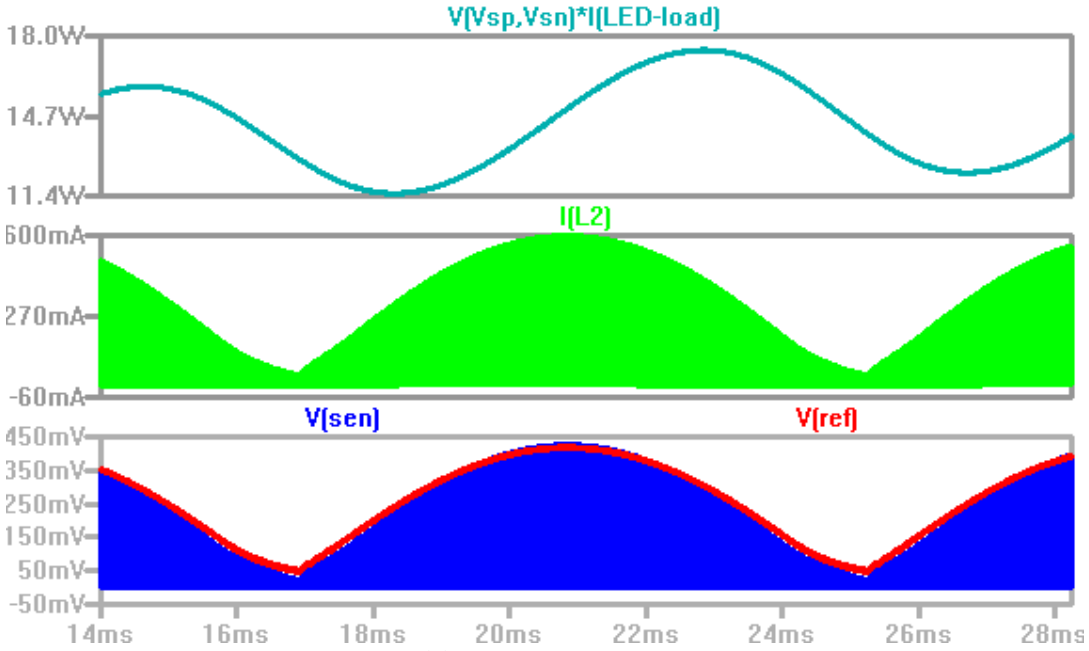

(c) 205V input voltage

Fig3.26 Complete driver simulation results under different input voltage: LED load power (cyan), primary winding current (green), sense voltage (blue) and reference voltage (red)

3.4 Conclusion for retrofit TLED driver design

In this chapter, a T12 EM ballast compatible driver has been designed and simulated. This driver adopts buck-boost topology configuration with modulated peak current mode control. A differential amplifier compares the reference voltage and the sense voltage to generate a control signal to realized peak current mode control. Emitter switching technique is employed to shorten storage time and increase withstanding voltage of the power transistor. For solving the over drive problem caused by negative correlation between the base driving current and the lamp input voltage, proportional drive technique realized by a current transformer is adopted to provide proportional base driving current. Simulation results proved operating principle of these modules.

The proposed driver is built and simulated in LTspice. Under different input voltages of the three ballast operating points, the driver outputs constant power to the LED load. Its near-resistive impedance is guaranteed by good performance of peak current mode control, so power distribution balance in series connection can be achieved. Based on these simulation results, it is proven that designed driver can work with different T12 EM ballasts.

This designed driver is realized on breadboard and measured. Then measurement results of each module and the whole system performance will be presented and explained in the next chapter.

4. Driver prototype demonstration and test results

To verify the proposed driver, three driver prototypes are realized on breadboard and tested, as shown in Fig4.1. Functionality of each module is demonstrated under three ballast operating voltage supplied by an AC voltage source. In system test, driver is successively connected to single-lamp ballast, dual-lamp ballast and three-lamp ballast. By changing reference resistor, driver operates in three different ballast operating points and outputs the same power to LED load under different input voltage. After that, driver performance is measured in single-lamp system, dual-lamp system and three-lamp system. Meanwhile, the ballast loss power and ballast input power factor as important design specifications are measured in this experiment.

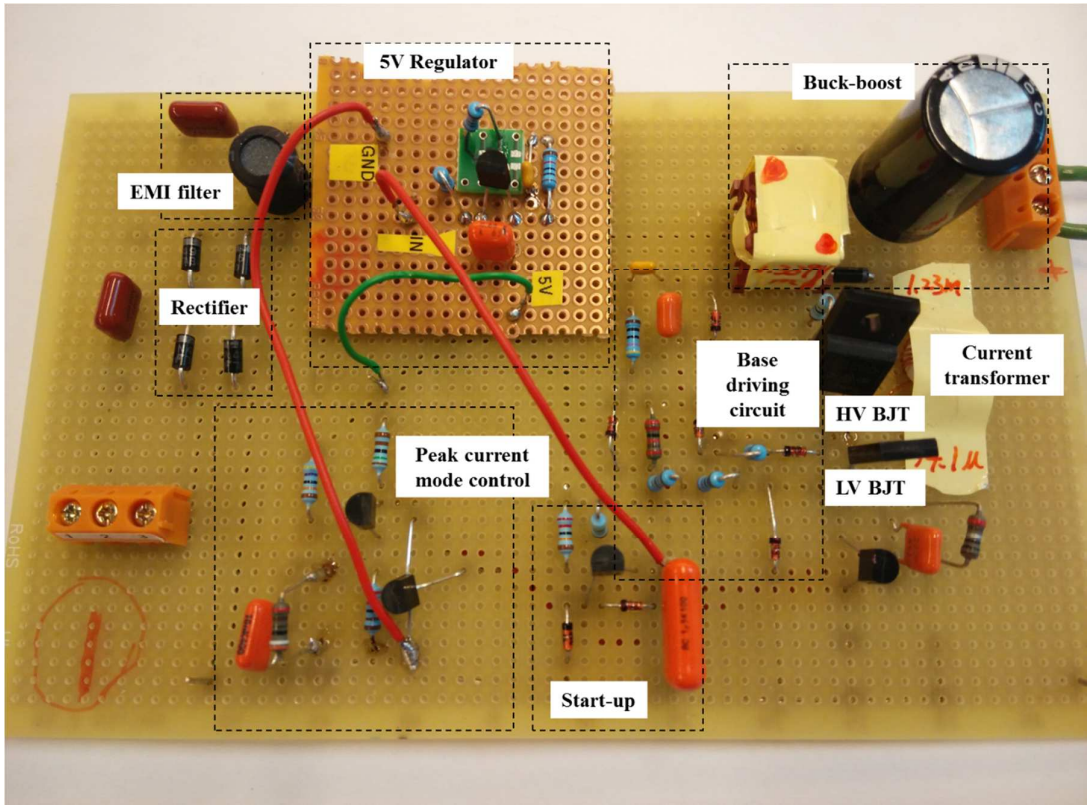

Fig4.1 Driver prototype realized on breadboard

4.1 Functional modules test and verification

The driver is tested under three input voltage corresponding to three ballast operating points: 80V, 130V and 205V. In module test, all modules are expected to work properly from 80V to 205V input voltage. For demonstrating that this driver has wide input voltage range, each module performance are measured under 80V and 205V input voltage.

4.1.1 Peak current mode control module test

In the test of peak current mode control module, the reference voltage and the sense voltage are measured and shown in Fig4.2. Obviously, no matter under 80V input voltage or 205V input voltage, envelop curve of the sense voltage is equal to the reference voltage. For constant output power, reference voltage in 205V input voltage is lower than that in 80V input voltage. Peak current mode control module instantaneously turn on transistor Q_4 to switch Q_5 off when the sense voltage

increase to the same value of the reference voltage. Due to storage time of Q_4 and Q_5, the sense voltage has some over shoot in 205V input voltage situation. This over shoot is acceptable and doesn't have effect on the Q_5 switching off behavior. Meanwhile, switching frequency of inductor is also shown in sense voltage waveform. At the peak point of 80V input voltage, switching frequency is 43.792 kHz; at the peak point of 205V input voltage, switching frequency is 83.26 kHz. This means that power transistor has larger switching power loss with high input voltage due to higher switching frequency.

As a result, the function of peak current mode control module is validated. Reference voltage, sense voltage and switching frequency are close to their LTspice simulation results.

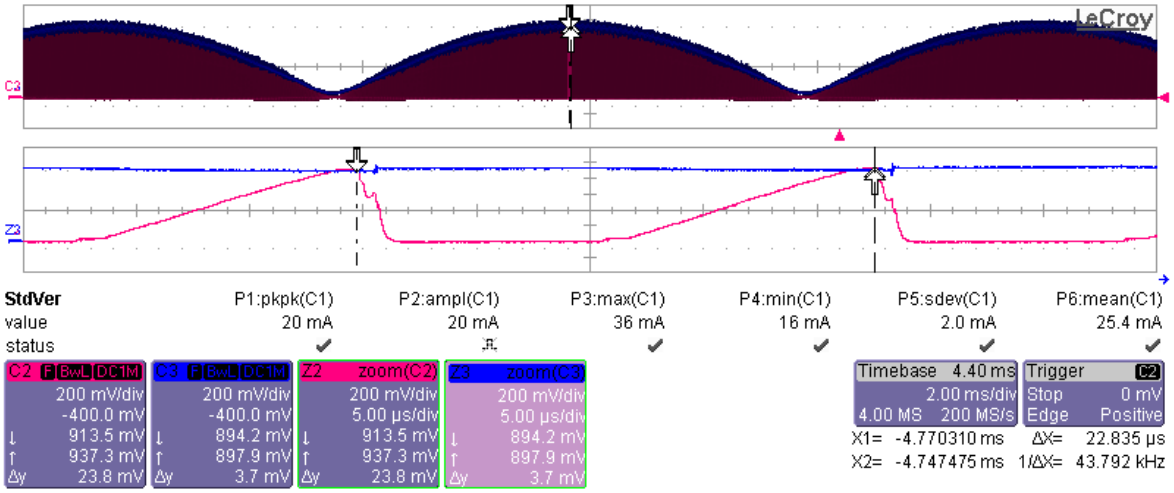

(a) 80V input voltage

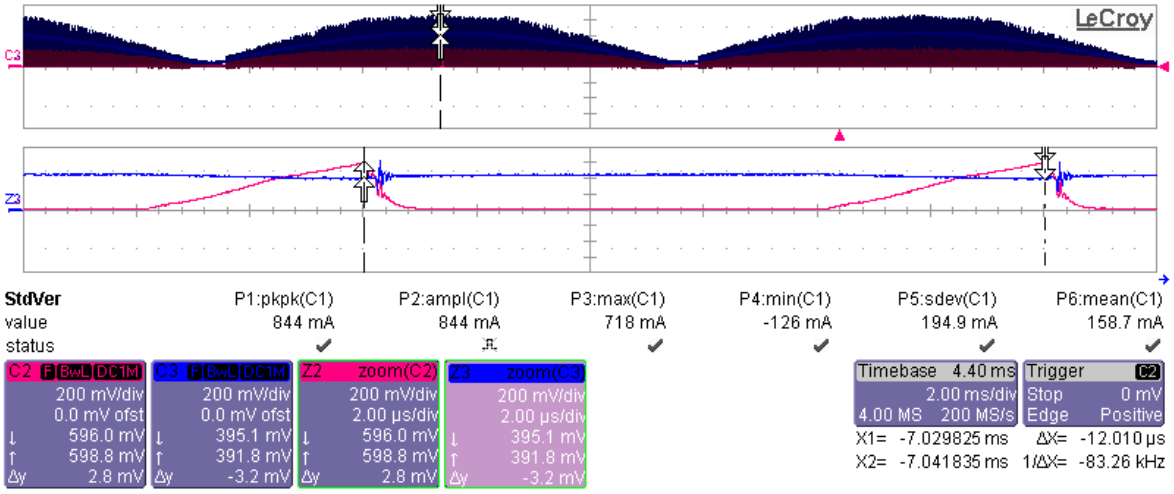

(b) 205V input voltage

Fig4.2 Reference voltage (blue) and sense voltage (pink) under 80V (a) and 205V (pink)

4.1.2 Emitter switching module test

By adopting emitter switching, storage time of power transistor Q_1 is shorten. Because the reverse base current is provided by the collector current. This can be observed in this experiment, as shown

in Fig4.3. Peak value of the reverse base current is much larger than the peak value of forward base current and almost equal to the collector current.

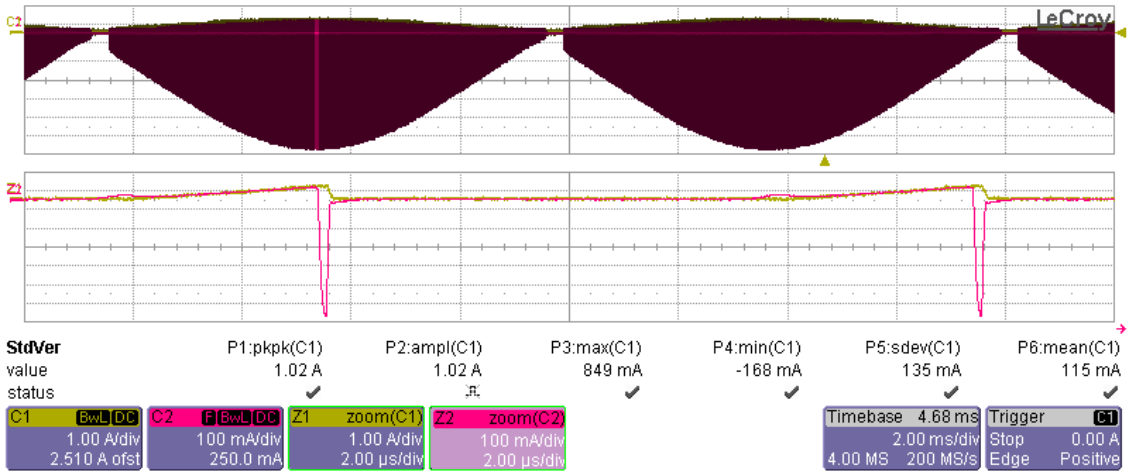

Fig4.3 Base current (pink) and collector current (yellow) under 205V input voltage

Due to stronger reverse base current, minority carriers stored in base can be removed more quickly and power transistor storage time will be reduced. Practical experiment results demonstrate that power transistor switching off time is shortened by the emitter switching technique. Fig4.4 illustrates the power transistor collector current fall time in regular RCC circuit (a) and emitter switching circuit (b), respectively. In regular RCC circuit power transistor switching-off process, fall time of collector current is about 310ns, while fall time decreases to 166ns in emitter switching circuit. When Q_1 switches off, collector current decreases and V_{CE} increases. According to equation [3.24], switching-off power loss is mainly determined by collector current fall time. Owing to shorter storage time, power transistor switching-off power loss is effectively reduced by adopting emitter switching technique.

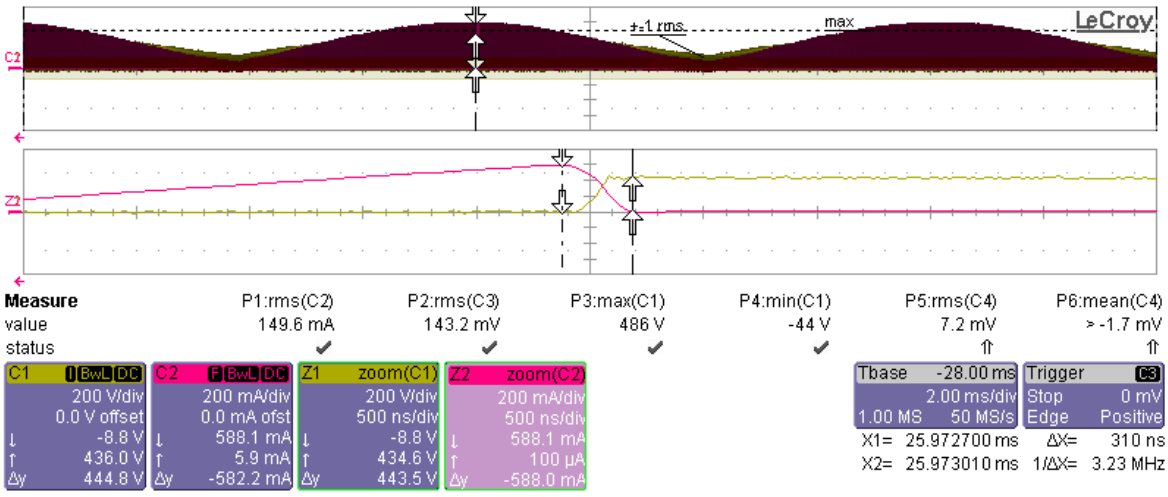

Fig4.4 (a) Power transistor switching-off collector current (pink) and V_{CE} (yellow) in regular RCC circuit

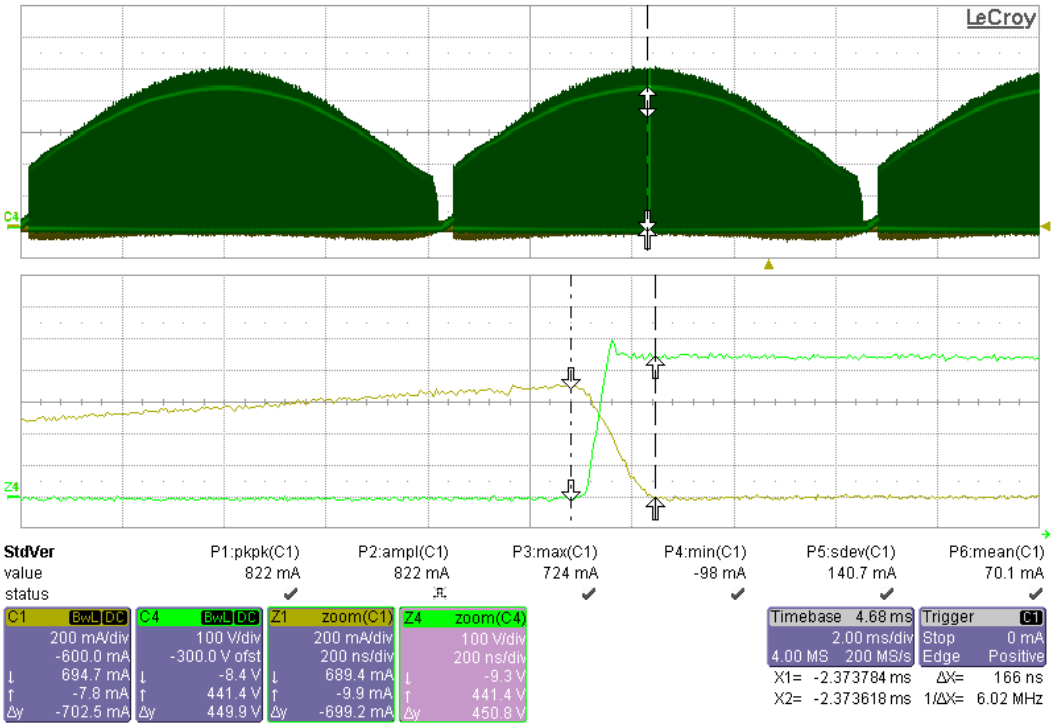

Fig4.4 (b) Power transistor switching-off collector current (yellow) and V_{CE} (green) in emitter switching circuit

4.1.3 Proportional drive module test

In this project, proportional drive technique is realized by a current transformer as shown in Fig4.5. Ferroxcube TN9/6/3-3E25 ferrite core is adopted in this prototype as current transformer ringcore. This type ringcore has high permeability, so the turns number and current transformer sized can be reduced to fit in TL tubes. The primary winding has 3 turns and secondary winding has 27 turns coiled around ringcore. Current transformer primary winding inductance is 1.23mH, and the secondary winding inductance is 14.1uH. As a result, current ratio is about 9.34, which means the base current provided by current transformer is about one-ninth of collector current.

Fig4.5 Current transformer

The current flow through primary winding and secondary winding of current transformer are measured and shown in Fig4.6. The secondary winding current multiplied by 10 is almost equal to primary winding current as shown by the overlap waveforms.

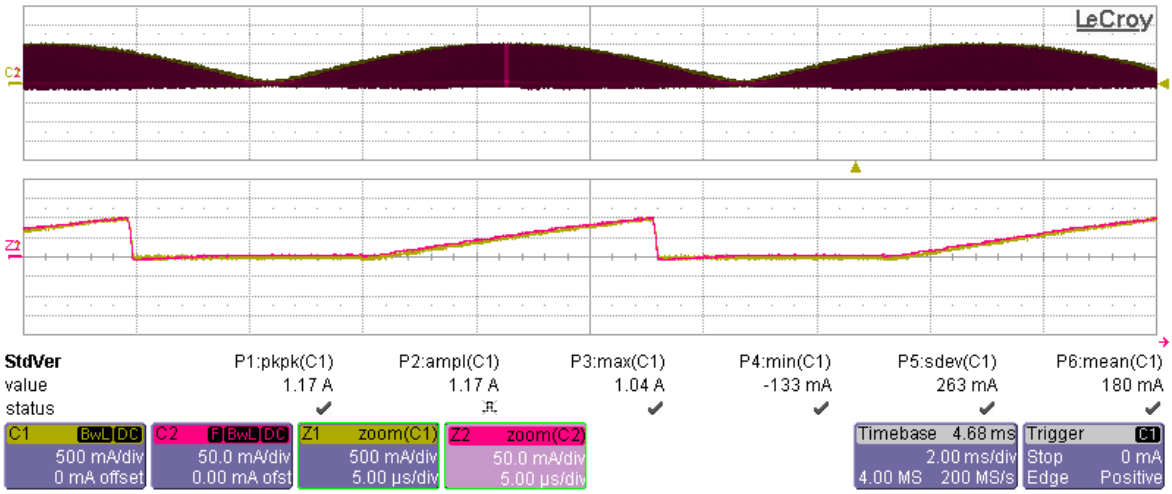

Fig4.6 Current transformer primary winding current (yellow) and secondary winding current (pink)

Because the primary winding current of current transformer is equal to the collector current of the power transistor Q_1 and proportional to the secondary winding current, the secondary winding current can be used as proportional base driving current. The base current and current transformer secondary winding current are measured together and shown in Fig4.7. A large proportion of base current is provided by the secondary winding current. A small current pulse occurred in beginning of each oscillation cycle to turn on Q_1. It is generated by capacitor C_5 as illustrated in base driving circuit section.

In conclusion, current transformer provides a proportional current to drive power transistor Q_1. Proportional drive technique is realized by this current transformer.

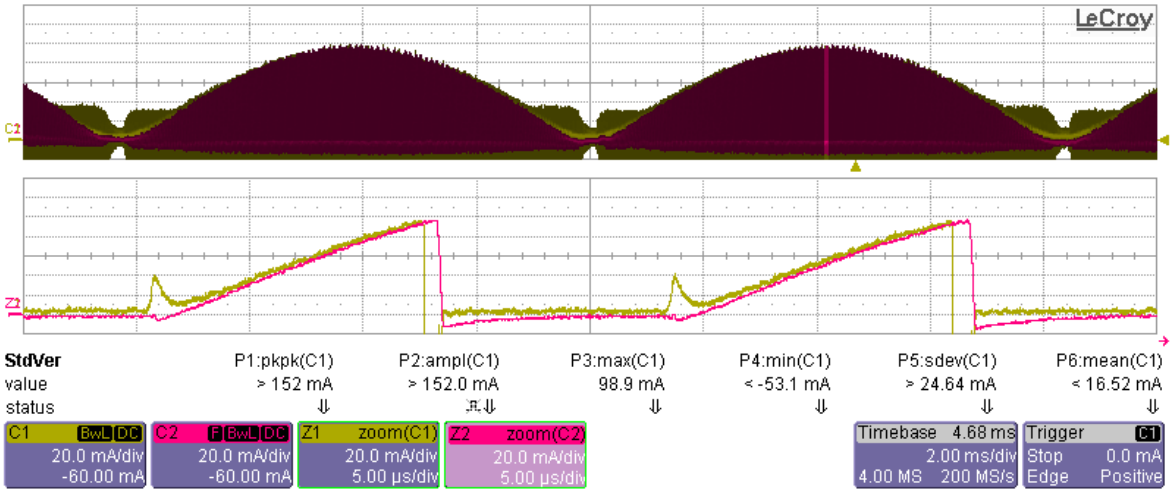

Fig4.7 (a) 80V input voltage: secondary winding current (pink) and base current (yellow)

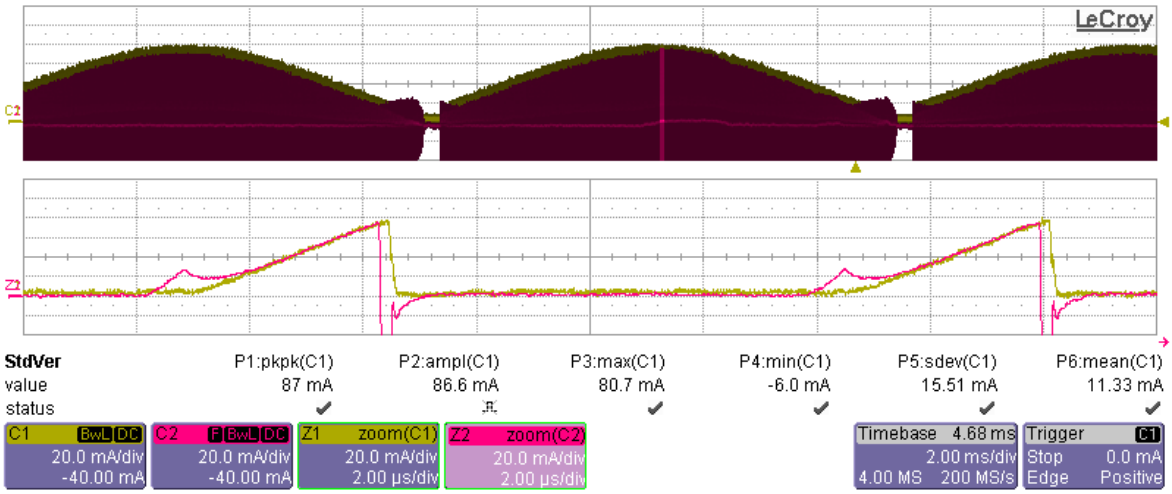

Fig4.7 (b) 205V input voltage: secondary winding current (yellow) and base current (pink)

4.2 Compatibility and system performance test

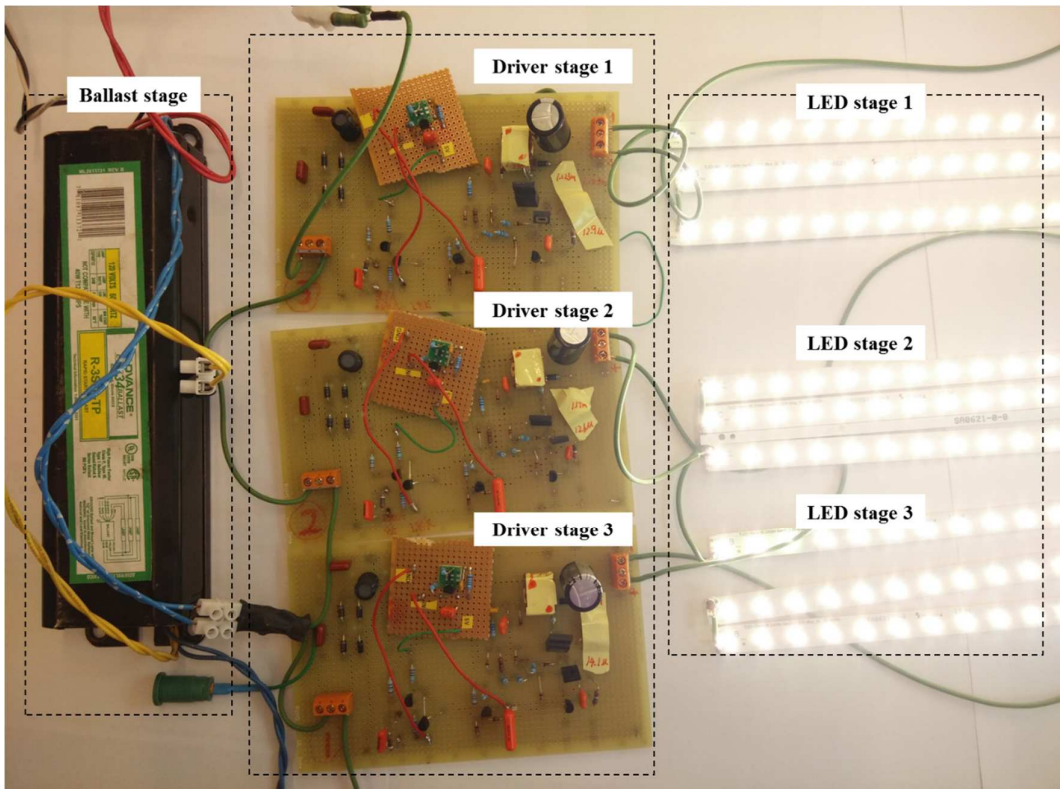

Fig4.8 System performance and compatibility test

Each functional module has been demonstrated under 80V and 205V input voltage. In this section, driver compatibility with ballast is tested by connecting drivers to different ballasts. Meanwhile, both driver performance and system performance are measured in this experiment to judge whether up to standards. Input power of LED load is about 14W and forward voltage is about 150V. For achieving 14W constant output power, reference resistor R_4 is altered to corresponding value: $3.9k\Omega$ for single-lamp ballast, $1.8k\Omega$ for dual-lamp ballast and 680Ω for three-lamp ballast. For estimating driver performance, input power, output power and efficiency are measured under different ballast systems.

In terms of system performance, power loss, input power factor and total harmonic distortion of input current are important specifications.

4.2.1 Compatibility test

For demonstrating that designed driver is compatible with three type ballasts, the drivers are successively connected to sing-lamp ballast, dual-lamp ballast and three-lamp ballast. There are three stages in whole system: ballast stage, driver stage and LED load stage. Ballast stage is connected to 120V/60Hz mains and supplies the driver stage, while the driver stage provides power to the LED load stage, as shown in Fig4.8.

The proposed driver has near-resistive impedance for keeping power distribution balance. Driver input current and input voltage have the same phase as shown in Fig4.9. Installed after rectifier, an EMI filter is employed to filter out high frequency, so the driver input current is the inductor current filtered by EMI filter. Because of peak current mode control, inductor current envelop curve should follow input voltage. The inductor current and driver input voltage are measured and illustrated in Fig4.10. Measurement result shows that driver input voltage is not typical sinusoidal but with some distortion. This distortion is caused by ballast saturation as explained in chapter 2.

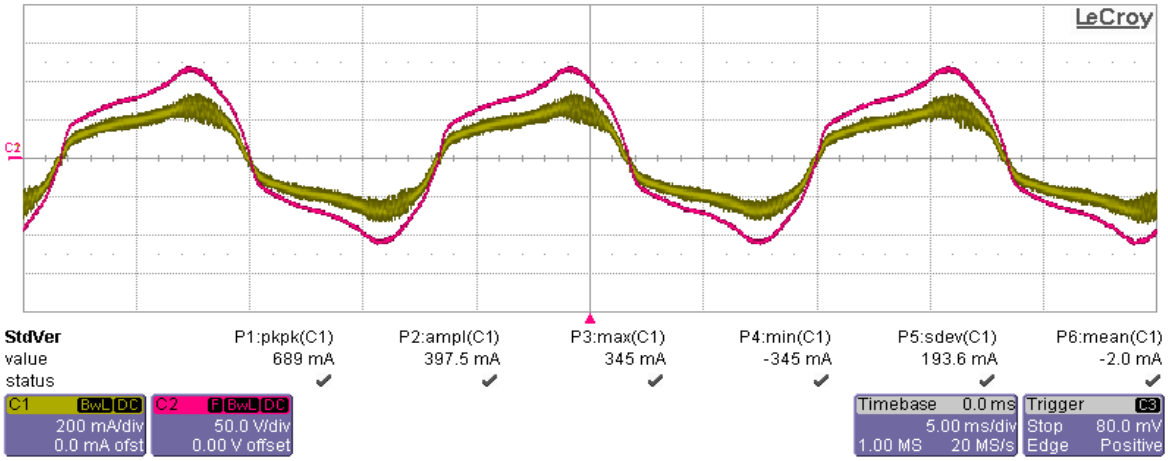

Fig4.9 Driver input current and input power

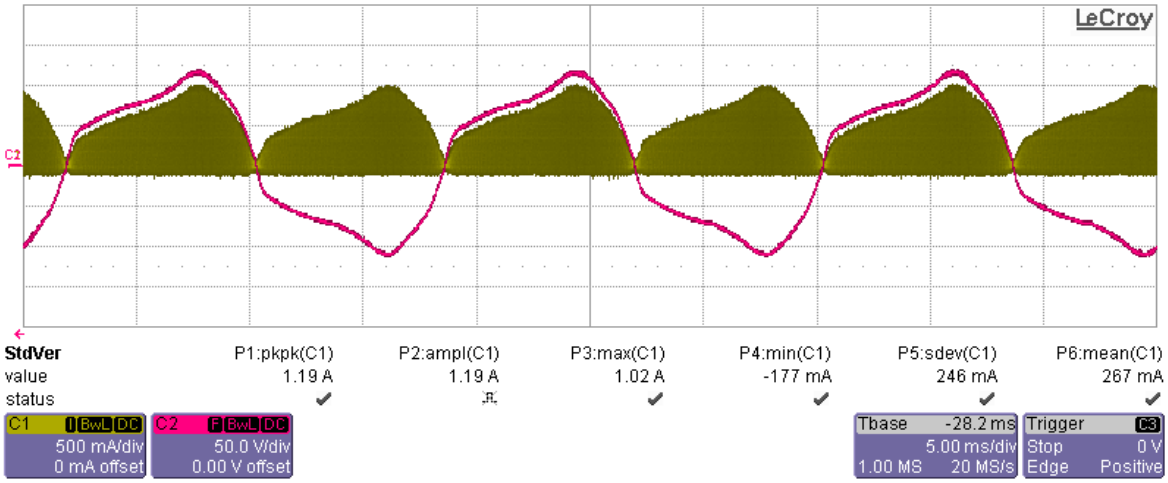

Fig4.10 Inductor current and driver input voltage

According to the measurement results, designed driver has near-resistive impedance and envelop curve of inductor current follows driver input voltage. Compatibility of the driver is demonstrated.

When two drivers are connected in series, they should simultaneously start up and have almost the same input voltage. Starting up process of two drivers are shown in Fig4.11. Experiment results demonstrate that the drivers have matched input voltage and equally share the ballast output power. This means that driver is compatible with multi-lamp ballast and is able to keep power distribution balance.

System starting up process is shown in Fig4.12. Driver input voltage, inductor current, big capacitor voltage and LED load current are illustrated in this measurement. LED filter capacitor voltage begins to increase after oscillation has been built up. When this voltage increase to LED load forward voltage, LED current starts to increase. The starting-up process duration time is about 60ms.Based on these test results, a conclusion can be drawn that proposed driver is compatible with T12 EM ballast and able to operate stably in series connection.

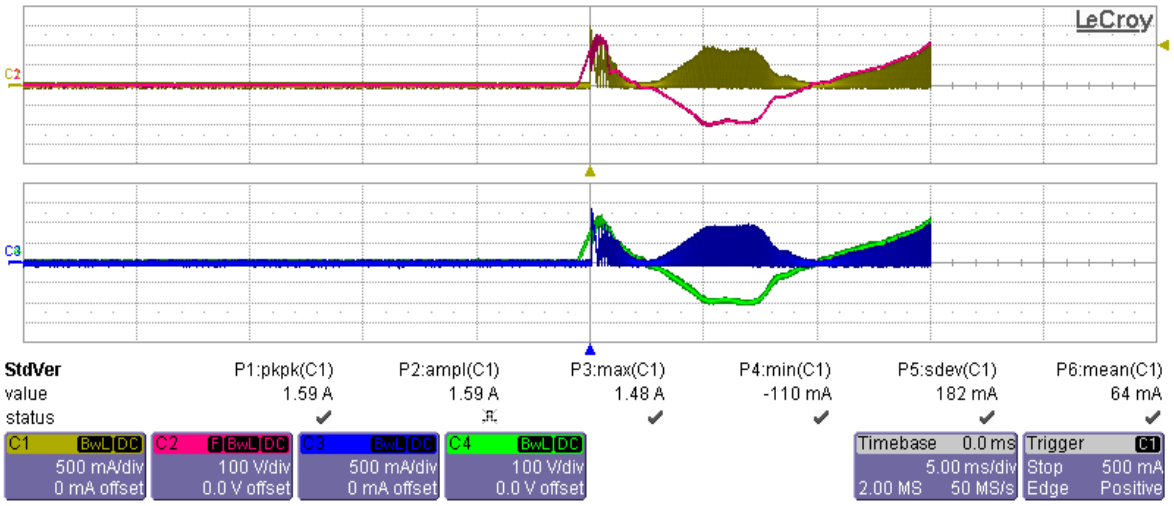

Fig 4.11 Input voltage (pink for driver 1, green for driver 2) and inductor current

(yellow for driver 1, blue for driver 2) of two Driver in series connecting

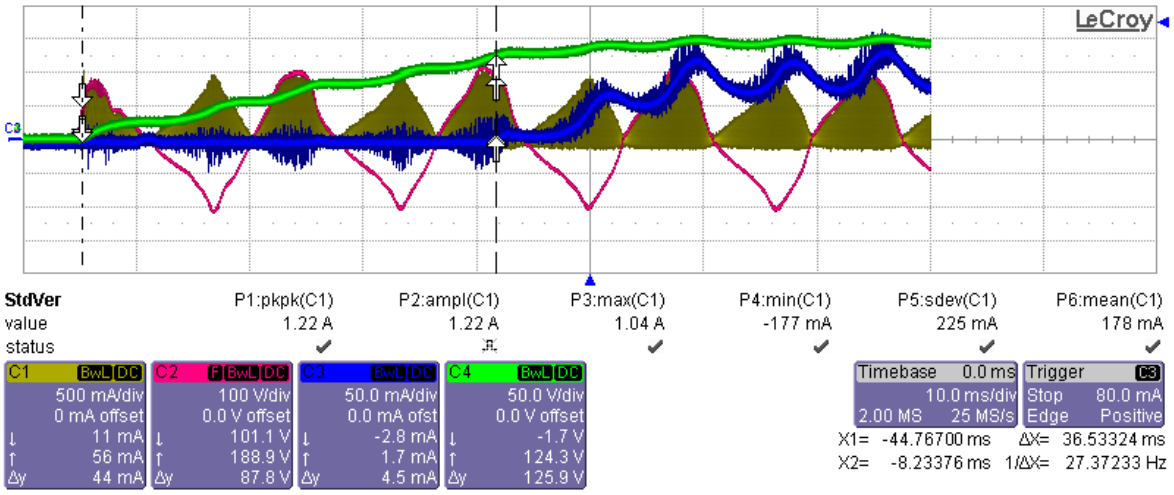

Fig4.12 Driver input voltage (pink), inductor current (yellow), big capacitor voltage (green) and LED load current (blue) in starting up process

4.2.2 Driver and ballast performance measurement in different systems

The driver and ballast performance are measured and their specifications are list below in Tab4.1 (a), Tab (b), Tab4.2 and Tab4.3, which correspond to low power factor single-lamp ballast (L-140F), high power factor single-lamp ballast (R-140-1), dual-lamp ballast (R-2S40-1) and three-lamp ballast (R-3S34-1).

L-140F	Ballast stage	Driver stage	LED stage	System
Input Voltage (V)	120	204.5	140.1	120
Input current (mA)	191.8	76.4	94.3	191.8
Input power (W)	19.53	15.32	13.05	19.53
Power factor	0.847	0.981	-	0.847
THD	15.57%	5.57%	-	15.57%
Power loss	4.21	2.27	-	6.48
Power Efficiency	78.44%	85.21%	-	66.82%

Tab4.1 (a) Each stage and system performance in low PF sing-lamp ballast system

R-140-1	Ballast stage	Driver stage	LED stage	System
Input Voltage (V)	120	208.6	142.7	120
Input current (mA)	368.8	80.6	102.8	368.8
Input power (W)	23.84	16.22	14.36	23.84
Power factor	0.537	0.964	-	0.537
THD	29%	27.95%	-	29%
Power loss	7.62	1.86	-	9.48
Power Efficiency	68.04%	88.53%	-	60.23%

Tab4.1 (b) Each stage and system performance in high PF sing-lamp ballast system

R-2S40-1	Ballast stage	Driver stage 1	Driver stage 2	LED stage 1	LED stage 2	System
Input Voltage (V)	120	124.9	130.8	142.1	142.8	120
Input current (mA)	419.8	124.1	123.1	98.3	102.6	419.8
Input power (W)	42.43	15.44	16.02	13.8	14.48	42.43
Power factor	0.842	0.996	0.995	-	-	0.842
THD	20.06%	27.95%	27.95%	-	-	20.06%
Power loss	10.97	1.64	1.54	-	-	14.15
Power Efficiency	74.15%	89.38%	90.39%	-	-	66.70%

Tab4.2 Each stage and system performance in dual-lamp ballast system

R-3S34-1	Ballast stage	Driver stage 1	Driver stage 2	Driver stage 3	LED stage 1	LED stage 2	LED stage 3	System
Input Voltage (V)	120	76.94	79.46	82.13	140.7	141.3	141.7	120
Input current (mA)	575.6	195.2	195.1	195.6	91.9	94.8	98.2	575.6
Input power (W)	63.77	14.97	15.47	16.05	12.85	13.31	13.82	63.77
Power factor	0.923	0.997	0.998	0.999	-	-	-	0.923
THD	15.65%	22.28%	22.26%	22.67%	-	-	-	15.65%
Power loss	17.28	2.12	2.16	2.23	-	-	-	23.79
Power Efficiency	72.90%	85.84%	86.04%	86.11%	-	-	-	62.70%

Tab4.3 Each stage and system performance in three-lamp ballast system

Another important specification is the line regulation. Line regulation is the system capability to maintain a constant LED voltage despite changes to the mains voltage. It can by indicated by the LED current variation amplitude with 10% disturbance in mains voltage. In different ballast system, line regulation performance are list below in Tab 4.4.

	LED current (120V mains)	LED current (108V mains)	LED current (132V mains)
R-140F	94.3mA/100%	78.7mA/83.46%	108.5mA/115.06%
R-140-1	102.8mA/100%	88.8mA/86.38%	114.1mA/110.99%
R-2S40-1	98.3mA/100%	84.9mA/90.03%	109.3mA/111.19%
R-3S34-1	91.9mA/100%	79.9mA/86.94%	104.1mA/113.28%

Tab4.4 Line regulation performance of different ballast system

According to these measurements results, driver compatibility with T12 EM ballast has been demonstrated. Because the driver is designed to be near-resistive, driver input voltage is nearly the same to the output voltage of ballast measured with resistor load shown in Fig3.1. For single lamp ballast, driver input voltage is about 205V; for dual-lamp ballast, driver input voltage decreases to about 125V; for three-lamp ballast, driver has the lowest input voltage, about 80V. In different T12 EM ballast systems, driver power efficiency are higher than 85% and the power loss in driver is acceptable, about 2W. Due to open loop control, the line regulation performance of designed driver may not be ideal. As mentioned earlier, one possible approach to increase line regulation performance is adding a DC component to reference voltage. Mains voltage changes won't affect the DC component of reference voltage so that line regulation performance can be improved. However, driver power factor will be compromised by this DC component. As system power loss is mainly caused by the ballast, choosing higher input resistance driver is an effective method to reduce ballast power loss as illustrated in previous sections.

To estimate the energy saving brought by retrofit LED lamp system, a comparison between conventional fluorescent lamp system and proposed retrofit LED lamp system has been made and list below in Tab4.5.

Ballast type	Lamp type	System power	Power Factor	Input current THD	Line regulation (90% input voltage)	Line regulation (110% input voltage)
LPF single-lamp ballast (L-140F)	**LED lamp**	19.53W	0.847	15.57%	83.46%	115.06%
	Fluorescent lamp	44W	0.527	10.16%	80.11%	122.76%
HPF single-lamp ballast (R-140-1)	**LED lamp**	23.84W	0.537	29%	86.38%	110.99%
	Fluorescent lamp	53.11W	0.975	8.22%	93.29%	106.23%
Dual lamp ballast (R-2S40-1)	**LED lamp**	42.43W	0.842	20.06%	90.03%	111.19%
	Fluorescent lamp	91.61W	0.988	15.10%	92.99%	106.64%

Tab4.5 Performance comparison between proposed retrofit LED and fluorescent lamp system.

Obviously, proposed retrofit LED lamp significantly improved system energy efficiency. By adopting this retrofit LED lamp, system energy consumption is reduced by 55% for single-lamp ballast system and 54% for dual-lamp ballast, respectively. System retrofit LED system input power factor is lower than fluorescent lamp system except in low power factor ballast case. Near-resistive LED driver causes some current phase delay because of the compensation capacitor in high power factor ballast. Meanwhile, high frequency component existing in driver current results in high frequency harmonic component of ballast input current, so the total harmonic distortion in LED system is higher than that in fluorescent lamp system. As for line regulation, LED lamp has better performance in low power factor ballast but worse in high power factor ballast.

4.3 Conclusion for driver prototype test

In this chapter, a driver prototype is realized by discrete components on a breadboard. Each functional module is tested and measured with an AC power source. Test results show that all functional modules are working properly. By altering reference resistor, driver outputs constant power in three different ballast operating points.

System test and measurements are conducted by connecting drivers to different T12 EM ballasts. The driver compatibility with T12 EM ballast is demonstrated. According to measurement results, the driver has a power efficiency above 85%. Compared with conventional fluorescent lamp system, proposed retrofit LED system has remarkable energy saving performance. Power consumption is lowered by more than 55% with the LED lamp. System power factor and line regulation performance are improved with low power factor ballast, which doesn't have compensation capacitor, while become worse with high power factor ballast. Higher system total harmonic distortion is caused by high frequency components in TLED driver.

In a word, the compatibility of proposed driver with T12 EM ballast has been shown. Compared with conventional fluorescent lamp system, retrofit LED lamps significantly improved power efficiency.

5. Conclusion

As a subproject of Philips T12 retrofit TLED project, this project proposed a T12 EM ballast modeling method. A model of high power factor single-lamp ballast has been constructed in LTspice as an example. Various T12 EM ballasts characteristics were measured and illustrated. A compatible TLED driver was designed and realized on a breadboard.

T12 EM ballast classification and physical configuration have been illustrated. A magnetic circuit model was derived from physical circuit configuration of the T12 EM ballast R-140-1 based on fundamental magnetic laws and magnetic characteristics. Then an equivalent circuit was built in LTspice for simulation. Simulation results of the proposed model match practical T12 EM ballast measurement results. For other types of T12 EM ballasts, because of similar physical configurations, their LTspice models can be derived from their magnetic circuit model. Therefore, a general modeling method for T12 EM ballast has been developed in this project. Furthermore, ballast input and output characteristics, such as output voltage, power factor, were measured with a variable power resistor for finding out proper operating points for the TLED.

A TLED driver was designed to be compatible with various T12 EM ballasts. Firstly, the ballast operating points were determined by the LED load power, aiming for as low as possible ballast power loss. For the selected ballast operating points of the three T12 EM ballast types, they have different output voltages for per driver. Buck-boost topology configuration and RCC circuit were adopted to provide constant output current for the LED load. This driver was designed to be near-resistive for the sake of power distribution balance in series connection of the lamps. So a modulated current peak mode control module, which is realized by a differential comparator, was adopted in this driver to realize that the envelop of the primary winding peak current follows the driver input voltage. However, because of the negative correlation between the driver input voltage and the primary winding peak current, over driving of the base current causes long storage time of the power transistor, which leads to inaccurate output current and low efficiency. To solve that problem, proportional drive and emitter switching techniques were introduced. In this project, proportional drive was realized by a current transformer. A large proportion of base current was provided by this current transformer rather than secondary winding as in a regular RCC circuit. Then the base current was almost proportional to collector current and the over driving issue can be solved. Meanwhile, by employing emitter switching technique, power transistor storage time was shortened and its withstanding voltage is boosted. A circuit has been built in LTspice. Each module simulation and the whole driver simulation results shown that all the modules were working properly and the driver can provide constant output power for LED load in different ballast operating points.

At last, a prototype of proposed driver was realized with discrete components on a breadboard. Supplied by an AC voltage source, each functional module has been tested. In system performance test and measurement, the driver was shown compatible with different T12 EM ballasts and has a power efficiency above 85%. Compared with conventional fluorescent lamp system, proposed retrofit LED lamp has remarkable energy saving performance of over 50%. However, higher system total harmonic distortion was brought by the switching mode driver inside the lamp. Power factor reduces slightly with high power factor ballast with the LED lamp because of the compensation capacitor; on the contrary, low power factor ballast has increased higher power factor with the LED lamp.

As a part of TLED product developing project, a lot of compromises have to be made. Each component cost should be taken into consideration in driver designing. Line regulation can be improved by adding a DC component to reference voltage while power factor will be compromised. Meanwhile, if the LED lamp has higher power, both ballast power efficiency and power factor can be increased. For reducing switching power loss of power transistor, the oscillation frequency should be as low as possible. But when the oscillation frequency is lower than 20k Hz, driver will produce audible noise and the size of transformer may be too big to fit in TL tubes.

A detection module for altering reference resistor is not included in this project but very important. This part work belongs to Philips T12 retrofit TLED project and can be done in the future based on results of this project.

In a word, a T12 EM ballast LTspice model and a general modeling approach have been developed in this project. Based on measurement results of various T12 EM ballasts, a retrofit TLED driver has been designed and demonstrated with an experimental prototype. Thus, by adopting the proposed driver, a new TLED lamp can be developed to replace T12 fluorescent lamp in the US market.

Reference

[1] “Fluorescent ballasts”, E Source Company, http://bizenergyadvisor.com/BEA1/PA/PA_Lighting/PA-12

[2] “Lighting ballasts”, electric light sources, discover Lighting, http://www.ies.org/lighting/sources/lighting-ballasts.cfm

[3] “Electrical ballast”, Wikipedia, http://en.wikipedia.org/wiki/Electrical_ballast

[4] Chung, HS-H., et al. "Comparison of dimmable electromagnetic and electronic ballast systems—An assessment on energy efficiency and lifetime." Industrial Electronics, IEEE Transactions on 54.6 (2007): 3145-3154.

[5] Gil-de-Castro, A., et al. "Study of harmonic generated by electromagnetic and electronic ballast used in street lighting." Industrial Electronics (ISIE), 2011 IEEE International Symposium on. IEEE, 2011.

[6] “Ballast types”, occu-smart, http://www.occu-smart.com/pdf/Ballast_types.pdf

[7] “Light-emitting diode”, Wikipedia, http://en.wikipedia.org/wiki/Light-emitting_diode

[8] “p-n junction”, Wikipedia, http://en.wikipedia.org/wiki/P%E2%80%93n_junction

[9] Mottier, Patrick. LED for lighting applications. Vol. 134. John Wiley & Sons, 2010.

[10] “LED lamp”, Wikipedia, http://en.wikipedia.org/wiki/LED_lamp

[11] Boyce, Peter, and Peter Raynham. "SLL Lighting Handbook." (2009).

[12] Erickson R W, Maksimovic D. Fundamentals of power electronics[M]. Springer Science & Business Media, 2001.

[13] Witulski A F. Introduction to modeling of transformers and coupled inductors[J]. Power Electronics, IEEE Transactions on, 1995, 10(3): 349-357.

[14] Chan J H, Vladimirescu A, Gao X C, et al. Nonlinear transformer model for circuit simulation[J]. Computer-Aided Design of Integrated Circuits and Systems, IEEE Transactions on, 1991, 10(4): 476-482.

[15] Slemon G R. Equivalent circuits for transformers and machines including non-linear effects[J]. Proceedings of the IEE-Part IV: Institution Monographs, 1953, 100(5): 129-143.

[16] Irving B T, Jovanovic M M. Analysis and design of self-oscillating flyback converter[C]//Applied Power Electronics Conference and Exposition, 2002. APEC 2002. Seventeenth Annual IEEE. IEEE, 2002, 2: 897-903.

[17] Yang Y R. Analysis of winding capacitance effects on ringing choke converters[C]//Industrial Electronics Society, 2004. IECON 2004. 30th Annual Conference of IEEE. IEEE, 2004, 2: 1008-1013.

[18] Ronsisvalle C, Enea V. The ESBT (R)(Emitter-Switched Bipolar Transistor): a new monolithic power actuator technology devoted to high voltage and high frequency applications[C]//Integrated Power Systems (CIPS), 2008 5th International Conference on. VDE, 2008: 1-5.

[19] Neamen D A, Pevzner B. Semiconductor physics and devices: basic principles[M]. New York: McGraw-Hill, 2003.

[20] Basso C P. Switch-mode power supply SPICE cookbook[M]. McGraw-Hill, 2001.